NASA
Technical Paper 1324

AVRADCOM
Technical Report 78-45

Low-Speed Aerodynamic Characteristics of a 16-Percent-Thick Variable-Geometry Airfoil Designed for General Aviation Applications

Richard W. Barnwell, Kevin W. Noonan,
and Robert J. McGhee

DECEMBER 1978

NASA

U.S. ARMY
AVRADCOM

Low-Speed Aerodynamic Characteristics of a 16-Percent-Thick Variable-Geometry Airfoil Designed for General Aviation Applications

Richard W. Barnwell
Langley Research Center, Hampton, Virginia

Kevin W. Noonan
Structures Laboratory, AVRADCOM Research and Technology Laboratories
Langley Research Center, Hampton, Virginia

Robert J. McGhee
Langley Research Center, Hampton, Virginia

SUMMARY

Tests were conducted in the Langley low-turbulence pressure tunnel to determine the aerodynamic characteristics of climb, cruise, and landing configurations of a 16-percent-thick variable-geometry airfoil designed for general aviation applications (NASA GA(PC)-1). These tests were conducted over a Mach number range from 0.10 to 0.35, a chord Reynolds number range from 2.0×10^6 to 20.0×10^6, and an angle-of-attack range from $-8°$ to $20°$. Test results show that the maximum section lift coefficients increased in the Reynolds number range from 2.0×10^6 to 9.0×10^6 and reached values of approximately 2.1, 1.8, and 1.5 for the landing, climb, and cruise configurations, respectively. Stall characteristics, although of the trailing-edge type, were abrupt. The section lift-drag ratio of the climb configuration with fixed transition near the leading edge was about 78 at a lift coefficient of 0.9, a Mach number of 0.15, and a Reynolds number of 4.0×10^6. Design lift coefficients of 0.9 and 0.4 for the climb and cruise configurations were obtained at the same angle of attack, about $6°$, as intended. Generally, good agreement was obtained between experimental results and the predictions of a viscous, attached-flow theoretical method.

INTRODUCTION

Research on advanced low-speed aerodynamic technology airfoils has been conducted over the last several years at the NASA Langley Research Center. Aerodynamic characteristics were reported in reference 1 for the first of these airfoils, a 17-percent-thick fixed-geometry airfoil which has been designated the General Aviation (Whitcomb)-number one airfoil (NASA GA(W)-1). In references 2 and 3, results were reported for this airfoil with a Fowler flap system and with a spoiler system, respectively. Aerodynamic characteristics are presented in reference 4 for 13- and 21-percent-thick airfoils which were derived from the NASA GA(W)-1 airfoil by using the same camber line and scaling the thickness distribution. The 13-percent-thick airfoil has been designated the NASA GA(W)-2 airfoil. Aerodynamic characteristics for this airfoil with an aileron, slotted flap, Fowler flap, and spoiler system are presented in reference 5.

Aerodynamic characteristics are reported in reference 6 for wing-body combinations with two advanced rectangular NASA GA(PC)-1 and NASA GA(W)-1 wings having aspect ratios of nine. Section drag polars and some chordwise pressure distributions are also given for each of three configurations of the NASA GA(PC)-1 airfoil. These data were obtained at approximately midspan of the NASA GA(PC)-1 wing-body combination and are for the relatively low chord Reynolds number of 1.72×10^6.

In this report, low-speed aerodynamic characteristics are presented for three configurations of a 16-percent-thick variable-geometry airfoil which has been designated the General Aviation (Peterson-Chen)-number one airfoil

(NASA GA(PC)-1). The climb configuration of the NASA GA(PC)-1 airfoil was designed to have minimum drag at the design climb lift coefficient of 0.9. The boundary layer was assumed to be turbulent over most of the airfoil. The cruise configuration, which is obtained by deflecting the trailing-edge flap upward, was designed so that the design cruise lift coefficient of 0.4 would be attained at the same angle of attack at which the climb configuration attains the design climb lift coefficient. As a result, the fuselage drag can be minimized for both the climb and cruise configurations. The airfoil also has a landing configuration which is obtained by deflecting the trailing-edge flap downward.

This investigation was performed in the Langley low-turbulence pressure tunnel over a Mach number range from 0.10 to 0.35 and Reynolds number range from 2.0×10^6 to 20.0×10^6 for angles of attack from $-8°$ to $20°$.

SYMBOLS

Values are given in both SI and U.S. Customary Units. The measurements and calculations were made in U.S. Customary Units.

c_p pressure coefficient, $\dfrac{p - p_\infty}{q_\infty}$

c chord of airfoil, cm (in.)

c_c section chord-force coefficient, $\displaystyle\oint c_p \, d\!\left(\frac{z}{c}\right)$

c_d section profile-drag coefficient determined from wake measurements, $\displaystyle\int_{wake} c_d{}' \, d\!\left(\frac{h}{c}\right)$

$c_d{}'$ point drag coefficient,

$$2\left(\frac{p}{p_\infty}\right)^{6/7}\left[\frac{\left(\dfrac{p_t}{p}\right)^{2/7} - 1}{\left(\dfrac{p_{t\infty}}{p_\infty}\right)^{2/7} - 1}\right]^{1/2}\left\{\left(\frac{p_t}{p_{t\infty}}\right)^{1/7} - \left[\frac{\left(\dfrac{p_t}{p_\infty}\right)^{2/7} - 1}{\left(\dfrac{p_{t\infty}}{p_\infty}\right)^{2/7} - 1}\right]^{1/2}\right\}$$

c_l section lift coefficient, $c_n(\cos \alpha) - c_c(\sin \alpha)$

c_m section pitching-moment coefficient about quarter-chord point,

$$-\oint c_p \left(\frac{x}{c} - 0.25\right) d\left(\frac{x}{c}\right) + \oint c_p \frac{z}{c} d\left(\frac{z}{c}\right)$$

c_n section normal-force coefficient, $-\oint c_p \, d\left(\frac{x}{c}\right)$

h vertical distance in wake profile, cm (in.)

l/d section lift-drag ratio, c_l/c_d

M free-stream Mach number

p static pressure, Pa (lb/ft^2)

p_t total pressure, Pa (lb/ft^2)

q dynamic pressure, Pa (lb/ft^2)

R Reynolds number based on free-stream conditions and airfoil chord

x airfoil abscissa, cm (in.)

z airfoil ordinate, cm (in.)

z_c mean-line ordinate, cm (in.)

z_t mean thickness, cm (in.)

α angle of attack, deg

Subscripts:

max   maximum

∞ free-stream conditions

Abbreviations:

GA(PC)-1   General Aviation (Peterson-Chen)-number one

GA(W)-1   General Aviation (Whitcomb)-number one

GA(W)-2   General Aviation (Whitcomb)-number two

The airfoil section used in these investigations was developed for use in general aviation by John B. Peterson, Jr., and Allen W. Chen and, hence, was designated the NASA GA(PC)-1 airfoil. Descriptions of the design procedures for this airfoil have been given by Chen in reference 7 and by Peterson and Chen in reference 8. The design objectives were to obtain low drag at the climb and cruise design conditions with an airfoil which would not be difficult to manufacture. The design criteria used to achieve these objectives include specifications that the profile drag of the upper surface of the airfoil be a minimum, that a flap be used in such a manner that the angle of attack for the climb and cruise design conditions would be the same, and that the segments of the lower surface be either flat or convex. The angles of attack for the climb and cruise design conditions had to be the same so that the fuselage drag increments for the two conditions would be about the same and, hence, could be minimized by the aircraft designer. The boundary layer was considered to be turbulent on both the upper and lower surfaces downstream of the 0.1c position, because boundary-layer transition usually occurs near the leading edge of wings on general-aviation aircraft. The design section lift coefficients for the climb and cruise conditions were specified to be $c_l = 0.9$ and $c_l = 0.4$, respectively.

The procedure for designing the airfoil section involved two basic steps. In the first step, Peterson iteratively determined the upper-surface pressure distribution with minimum profile drag. This distribution was determined from a family of pressure distributions which had the pressure prescribed at five points along the chord. The upper-surface profile drag coefficient $c_{d,u}$ for these computations was determined from the approximate equation

$$c_{d,u} = \frac{2\theta}{c}\left\{\left(\frac{u_e}{U_\infty}\right)^2 + \frac{\delta^*}{\theta}\left[\left(\frac{u_e}{U_\infty}\right)^2 - \frac{u_e}{U_\infty}\right]\right\}$$

where U_∞ is the free-stream velocity, u_e is the boundary-layer edge velocity at the trailing edge, c is the airfoil chord, and θ and δ^* are the momentum thickness and displacement thickness, respectively, at the trailing edge. Peterson obtained this equation from the more general equation of Betz (ref. 9) after assuming that the static pressure and the hypothetical inviscid velocity u_l' in the Betz equation are constant across the boundary layer. Values for the momentum thickness θ and the displacement thickness δ^* for the different pressure distributions were determined with the method of Truckenbrodt (ref. 9).

In the second step of the design procedure, Chen determined an airfoil shape which had the optimum upper-surface pressure distribution and which satisfied the geometric constraints at the design climb lift coefficient. This airfoil shape was obtained iteratively with the method of Ormsbee and Chen (ref. 10). It was found that the requirement that the angle of attack be the same for the design climb and cruise conditions could be satisfied if the flap

had a width of 0.2c and was deflected upward 10° for cruise. The lower surface of the flap and a considerable part of the lower surface ahead of the flap were constrained to be flat to minimize manufacturing costs. The lower surface immediately ahead of the flap was contoured so that the slope would be continuous across the airfoil/flap juncture in the cruise configuration. The flap pivot point was located at the airfoil/flap juncture on the lower surface.

The NASA GA(PC)-1 airfoil is depicted in figure 1. Note that there is a landing configuration in addition to the climb and cruise configurations, which are the design configurations of the airfoil. The landing configuration is obtained by deflecting the flap downward 10° from the setting for the climb configuration. The thickness distribution and the mean camber lines for the three configurations are shown in figure 2.

MODEL, APPARATUS, AND PROCEDURE

Model

The aft portion of the airfoil model is a detachable flap. Various airfoil configurations are obtained by using flush brackets to position this flap relative to the rest of the model. The model has a span of 91.44 cm (36.00 in.), and the climb configuration of the model, which is the basic design configuration, has a chord of 60.96 cm (24.00 in.). The chords of the cruise and landing configurations differ slightly from that of the climb configuration. The model is equipped with orifices along the midspan station on both the upper and lower surfaces. The locations of these orifices are given in table I (all of the entries in the table, except those for the trailing edge, are orifice locations). Figure 3 is a photograph of the climb configuration of the model.

The airfoil model was machined from an aluminum billet. Grooves were machined in the surface of the aluminum, and pressure tubing was routed through the grooves to the various orifice locations. The tubes were potted in plastic resin, and orifices were drilled through the plastic into the tubing. The plastic was then machined to reform the original surface. The airfoil surface was sanded by hand in the chordwise direction with number 400 dry silicon-carbide paper to provide a smooth aerodynamic finish.

Wind Tunnel

The Langley low-turbulence pressure tunnel (ref. 11) is a closed-throat, single-return tunnel which can be operated at stagnation pressures from 1 to 10 atmospheres with tunnel-empty test-section Mach numbers up to 0.42 and 0.22, respectively. The maximum unit Reynolds number is about 49×10^6 per meter (15×10^6 per foot) at a Mach number of about 0.22. The tunnel test section is 91.44 cm (3.00 ft) wide by 228.6 cm (7.50 ft) high.

Hydraulically actuated circular plates provide positioning and attachment for the two-dimensional model. The plates are 101.6 cm (40.00 in.) in diameter, rotate with the airfoil, and are flush with the tunnel wall. The airfoil ends

5

are attached to rectangular model-attachment plates as shown in figure 4, and the airfoil is mounted so that the center of rotation of the circular plates is at 0.25c on the model reference line. The air gaps at the tunnel walls between the rectangular plates and the circular plates are sealed with flexible sliding metal seals (fig. 4).

Wake Survey Rake

A fixed, wake survey rake (fig. 5) at the model semispan is mounted perpendicular to the airfoil trailing edge on supports cantilevered from the tunnel sidewall at a distance of one chord behind the airfoil trailing edge. The wake survey rake has 91 total-pressure tubes which are 0.1524 cm (0.060 in.) in diameter and 6 static-pressure tubes which are 0.3175 cm (0.125 in.) in diameter. The total-pressure tubes have been flattened to 0.1016 cm (0.040 in.) for a distance of 0.6096 cm (0.240 in.) from the tip of the tube. The static pressure tubes each have four flush orifices drilled 90° apart and located eight tube diameters from the tip of the tube in the measurement plane of the total-pressure tubes.

Instrumentation

Measurements of the static pressures on the airfoil surface and of the wake-rake pressures are made with an automatic pressure-scanning system which uses precision variable-capacitance transducers. Basic tunnel pressures are measured with precision quartz manometers. Angle of attack is measured with a calibrated digital shaft encoder operated by a pinion gear and rack attached to one of the circular plates. Data are obtained on a high-speed acquisition system and recorded on magnetic tape.

TESTS AND METHODS

The climb and cruise configurations of the airfoil were tested at Mach numbers from 0.10 to 0.35 and Reynolds numbers, based on airfoil chord, from approximately 2.0×10^6 to 20.0×10^6 in the angle-of-attack range from approximately -8° to 20°. The landing configuration was tested at Mach numbers from 0.10 to 0.20 and Reynolds numbers based on chord from approximately 2.0×10^6 to 12.0×10^6 in the same angle-of-attack range. The angle of attack was varied from zero to the maximum value and then from zero to the minimum value. The airfoil was tested both smooth (natural transition) and with roughness strips located on the upper and lower surfaces at 0.05c. These strips were 0.127 cm (0.05 in.) wide and consisted of sparsely distributed granular material attached to the model with clear lacquer. The size of the granular material was determined by the technique described in reference 12. For Reynolds numbers of 2.0×10^6, 4.0×10^6, and 6.0×10^6, the commercial grits used were number 60, number 100, and number 120, respectively. For comparative purposes, the landing configuration of the airfoil was tested with the NACA standard roughness (number 60 grains distributed over both surfaces from the leading edge to 0.08c).

6

The static-pressure measurements at the airfoil surface were reduced to standard pressure coefficients which were numerically integrated to obtain section normal-force coefficients, section chord-force coefficients, and section pitching-moment coefficients about the quarter chord. The section lift coefficients were obtained from the section chord-force and normal-force coefficients. The section profile-drag coefficients were computed from the wake-rake total and static pressures by the method of Jones described in reference 13.

PRESENTATION OF DATA

The results of this investigation are presented as follows:

Results	Airfoil	Config.	M	R	Transition	Variable	Figure
Pressure distribution	GA(PC)-1	Climb	0.15	4.0×10^6	Fixed	α	6
	GA(PC)-1	Cruise	.15	6.0	Fixed	α	7
	GA(PC)-1	Landing	.15	4.0	Fixed	α	8
	GA(PC)-1	Climb	.15	4.0	Fixed	} Airfoil	9
	GA(W)-1	-------	.15	4.0	Fixed		
α, c_d, and c_m against c_l	GA(PC)-1	Climb	0.15	Varied	Natural	R	10(a)
	GA(PC)-1	Climb	.20	Varied	Natural	R	10(b)
	GA(PC)-1	Climb	.28	Varied	Natural	R	10(c)
	GA(PC)-1	Climb	Varied	4.0×10^6	Natural	M	11
	GA(PC)-1	Climb	.15	Varied	Fixed	R	12
	GA(PC)-1	Climb	Varied	4.0	Fixed	M	13
	GA(PC)-1	Climb	.15	2.1	Varied	Transition	14(a)
	GA(PC)-1	Climb	.15	4.0	Varied	Transition	14(b)
	GA(PC)-1	Climb	.15	6.0	Varied	Transition	14(c)
	GA(PC)-1	Cruise	.15	Varied	Natural	R	15(a)
	GA(PC)-1	Cruise	.20	Varied	Natural	R	15(b)
	GA(PC)-1	Cruise	.28	Varied	Natural	R	15(c)
	GA(PC)-1	Cruise	Varied	6.0	Natural	M	16
	GA(PC)-1	Cruise	.15	Varied	Fixed	R	17
	GA(PC)-1	Cruise	Varied	6.0	Fixed	M	18
	GA(PC)-1	Cruise	.15	2.0	Varied	Transition	19(a)
	GA(PC)-1	Cruise	.15	4.0	Varied	Transition	19(b)
	GA(PC)-1	Cruise	.15	6.0	Varied	Transition	19(c)
	GA(PC)-1	Landing	.10	Varied	Natural	R	20(a)
	GA(PC)-1	Landing	.15	Varied	Natural	R	20(b)
	GA(PC)-1	Landing	Varied	4.0	Natural	M	21
	GA(PC)-1	Landing	Varied	4.0	Fixed	M	22
	GA(PC)-1	Landing	.15	4.0	Varied	Transition	23
	GA(PC)-1	Landing	.15	6.0	Varied	Transition	23
	GA(PC)-1	Climb	.15	2.0	Fixed	} Airfoil	24(a)
	GA(PC)-1	Cruise	.15	2.0	Fixed		
	GA(W)-1	-------	.15	2.0	Fixed		

Results	Airfoil	Config.	M	R	Transition	Variable	Figure
α, c_d, and c_m against c_l	GA(PC)-1	Climb	0.15	4.0×10^6	Fixed	Airfoil	24(b)
	GA(PC)-1	Cruise	.15	4.0	Fixed		
	GA(PC)-1	Landing	.15	4.0	Fixed		
	GA(W)-1	-------	.15	4.0	Fixed		
	GA(PC)-1	Climb	.15	6.0	Fixed	Airfoil	24(c)
	GA(PC)-1	Cruise	.15	6.0	Fixed		
	GA(W)-1	------	.15	6.0	Fixed		
$c_{l,max}$ against R	GA(PC)-1	Climb	0.15	Varied	Varied	R, Transition	25(a)
	GA(PC)-1	Cruise	.15	Varied	Varied	R, Transition	25(a)
	GA(PC)-1	Landing	.15	Varied	Varied	R, Transition	25(a)
	GA(W)-1	-------	.15	Varied	Varied	R, Transition	25(a)
	GA(W)-2	-------	.15	Varied	Varied	R, Transition	25(a)
	GA(PC)-1	Climb	.20	Varied	Natural	R	25(b)
	GA(PC)-1	Cruise	.20	Varied	Natural	R	25(b)
	GA(PC)-1	Climb	.28	Varied	Natural	R	25(c)
	GA(PC)-1	Cruise	.28	Varied	Natural	R	25(c)
$c_{l,max}$ against M	GA(PC)-1	Climb	Varied	4.0×10^6	Varied	M, Transition	26(a)
	GA(PC)-1	Landing	Varied	4.0	Varied	M, Transition	26(a)
	GA(PC)-1	Cruise	Varied	6.0	Varied	M, Transition	26(b)
c_d at climb c_l against R; c_d at cruise c_l against R	GA(PC)-1	Climb	0.15	Varied	Fixed	Airfoil	27(a)
	GA(W)-1	-----	.15	Varied	Fixed		
	GA(W)-2	-----	.15	Varied	Fixed		
	GA(PC)-1	Climb	.15	Varied	Fixed	Airfoil	27(b)
	GA(PC)-1	Cruise	.15	Varied	Fixed		
	GA(W)-1	------	.15	Varied	Fixed		
	GA(W)-2	------	.15	Varied	Fixed		
l/d at climb c_l against R; l/d at cruise c_l against R	GA(PC)-1	Climb	0.15	Varied	Fixed	Airfoil	28(a)
	GA(W)-1	-----	.15	Varied	Fixed		
	GA(W)-2	-----	.15	Varied	Fixed		
	GA(PC)-1	Climb	.15	Varied	Fixed	Airfoil	28(b)
	GA(PC)-1	Cruise	.15	Varied	Fixed		
	GA(W)-1	------	.15	Varied	Fixed		
	GA(W)-2	------	.15	Varied	Fixed		
l/d against c_l	GA(PC)-1	Climb	0.15	2.0×10^6	Fixed	Airfoil	29(a)
	GA(PC)-1	Cruise	.15	2.0	Fixed		
	GA(W)-1	------	.15	2.0	Fixed		
	GA(W)-2	------	.15	2.0	Fixed		
	GA(PC)-1	Climb	.15	4.0	Fixed	Airfoil	29(b)
	GA(PC)-1	Cruise	.15	4.0	Fixed		
	GA(W)-1	------	.15	4.0	Fixed		
	GA(W)-2	------	.15	4.0	Fixed		
	GA(PC)-1	Climb	.15	6.0	Fixed	Airfoil	29(c)
	GA(PC)-1	Cruise	.15	6.0	Fixed		
	GA(W)-1	------	.15	6.0	Fixed		
	GA(W)-2	------	.15	6.0	Fixed		

Results	Airfoil	Config.	M	R	Transition	Variable	Figure
Pressure distribution, theory/experiment	GA(PC)-1 GA(PC)-1	Climb Cruise	0.15 .15	4.0×10^6 6.0	Fixed Fixed	Type of data Type of data	30(a) 30(b)
α, c_d, and c_m against c_l, theory/experiment	GA(PC)-1	Climb	0.15	4.0×10^6	Fixed	Type of data	31

DISCUSSION OF RESULTS

Experimental Results

Pressure distributions.- The effects of angle of attack on the chordwise pressure distributions for the climb, cruise, and landing configurations are shown in figures 6, 7, and 8, respectively. Transition is fixed at $x/c = 0.05$, the Mach number is 0.15, and the Reynolds number is approximately 4.0×10^6 for the climb and landing configurations and approximately 6.0×10^6 for the cruise configuration.

Most of the load is carried on the forward portion of the airfoil, and the peak pressure coefficient at the nose does not exceed -5.5 for any of the three configurations. This peak value is less than those for the 13-percent-thick and 17-percent-thick general-aviation airfoils and about the same as that for the 21-percent-thick airfoil. (See ref. 4.) A small positive load is carried on the flap of the climb configuration, as shown in figure 6. In general, turbulent trailing-edge separation is indicated by a region of nearly constant pressure upstream of the airfoil trailing edge. The results of the figure show that the flow on the upper surface of the climb configuration is separated for angles of attack greater than about 12°. A small negative load is carried on the flap of the cruise configuration near the design angle of attack ($\alpha = 6°$), and virtually no load is carried on the flap and rear portion of the rest of the airfoil for larger angles of attack. (See fig. 7.) The flap of the landing configuration carries more load than that of the climb configuration, and the flow near the trailing edge of the upper surface is separated for angles of attack greater than about 0°. (See fig. 8.)

A comparison of the pressure distributions for the climb configuration of the NASA GA(PC)-1 airfoil and the NASA GA(W)-1 airfoil is shown in figure 9 for lift coefficients near the design climb lift coefficient for the NASA GA(PC)-1 airfoil. The data show somewhat higher upper-surface negative pressure peaks near the nose of the NASA GA(PC)-1 airfoil. The NASA GA(PC)-1 airfoil carries most of its load on the forward portion, while the NASA GA(W)-1 airfoil distributes the load over the chord. Both airfoils are free of flow separation at this lift coefficient. The recovery portion of the upper-surface pressure distribution for the NASA GA(PC)-1 airfoil is of the concave type, which usually yields low-drag, abrupt-stall behavior (ref. 14). The upper-surface pressure distribu-

9

tion of the NASA GA(W)-1 airfoil exhibits a reduced pressure gradient in the mid-chord region which is followed by a nearly linear pressure recovery. This type of pressure distribution results in soft stall behavior at higher angles of attack (ref. 1).

Lift.- Shown in figures 10, 15, and 20 are the effects of Reynolds number on the relationship between the section lift coefficient c_l and the angle of attack α for the smooth (natural boundary-layer transition) climb, cruise, and landing configurations, respectively, at several Mach numbers. In general, the dependence of c_l on α is linear over most of the angle-of-attack range prior to stall. The deviations from linearity in the prestall range are small when they do occur, and the stall is abrupt. In figures 10(a) and 15(a) (M = 0.15), the lift-curve slope for the climb and cruise configurations varies from about 0.11 per degree to 0.12 per degree as the Reynolds number changes from approximately 2.0×10^6 to 9.0×10^6. The slope is unchanged by further increases. Over the same range of Reynolds numbers, the maximum section lift coefficients for these two configurations increase about 0.3 and the angles of attack at which maximum lift occurs increase about 2° as the Reynolds number is increased. Figures 10(b) and 15(b) (M = 0.20) illustrate that increasing the Reynolds number above 9.0×10^6 does not appreciably affect the lift-curve slope, the maximum lift coefficient, or the angle of attack at which maximum lift occurs. As shown in figure 20(b) (M = 0.15), the lift-curve slope for the landing configuration varies from about 0.10 per degree to about 0.11 per degree as the Reynolds number varies from approximately 2.0×10^6 to 9.0×10^6, and the slope is unchanged by further increases. The maximum section lift coefficient for the landing configuration increases about 0.4 and the angle of attack at which maximum lift occurs increases about 3° as the Reynolds number is increased over this range.

In figures 11, 16, and 21, the effects of Mach number on the curves of c_l against α for the smooth climb, cruise, and landing configurations are shown. Only for the largest Mach number tested, M = 0.35, is the effect of Mach number significant. For this Mach number, the lift-curve slope and the maximum lift coefficient are increased slightly, and the angle at which maximum lift occurs is decreased about 1°.

The effects of Reynolds number on the relationship of c_l to α are shown for the climb (fig. 12) and cruise (fig. 17) configurations with roughness strips applied at x/c = 0.05. These effects are essentially the same as those with the model smooth. This conclusion can also be drawn from the results shown in figures 14 and 19, where the effects of roughness on the Reynolds number trends for the climb and cruise configurations are compared. Effects of roughness on $c_{l,max}$, shown in figure 25(a), are configuration dependent as well as Reynolds number dependent. The greatest effect of roughness on $c_{l,max}$ occurs for the climb and cruise configurations at low Reynolds numbers.

The effects of Mach number on the lift curves for the climb, cruise, and landing configurations with transition fixed at x/c = 0.05 are shown in figures 13, 18, and 22, respectively. These effects differ very little from those observed for the smooth configurations.

10

In figure 23, the effects of roughness on the landing configuration are shown. In addition to the data obtained with a roughness strip at $x/c = 0.05$, data are shown which were obtained with the standard NACA roughness (number 60 grit distributed between the leading edge and $x/c = 0.08$ on the upper and lower surfaces). The effect of the roughness strip is small, but the effect of the standard NACA roughness is appreciable. The latter roughness reduced the maximum lift coefficient about 0.4 and the angle of attack at which the maximum lift occurs by at least 4°.

The section characteristics of the NASA GA(W)-1 airfoil (which has a thickness-to-chord ratio of 17 percent) and the three configurations of the NASA GA(PC)-1 airfoil (which has a thickness-to-chord ratio of 16 percent) are compared in figure 24 for the Reynolds numbers 2.0×10^6, 4.0×10^6, and 6.0×10^6. These Reynolds numbers are approximately those encountered by a light general-aviation airplane during landing, climb, and cruise, respectively. These data were obtained with roughness strips applied at $x/c = 0.08$ for the NASA GA(W)-1 airfoil and at $x/c = 0.05$ for the NASA GA(PC)-1 airfoil. The lift-curve slope for the NASA GA(W)-1 airfoil is slightly greater than those for the NASA GA(PC)-1 configurations. The differences between the lift coefficients for the climb and cruise configurations at the same angle of attack are between 0.4 and 0.5 when the flow is attached. Note that the angles of attack at which the climb and cruise design lift coefficients occur for the NASA GA(PC)-1 airfoil are about the same as intended ($\alpha = 6.1^\circ$). The stall behavior of each of the NASA GA(PC)-1 configurations is much more abrupt than that of the NASA GA(W)-1 airfoil. (See fig. 24.)

The effects of Reynolds number on the maximum section lift coefficients measured for the NASA GA(W)-1 and NASA GA(W)-2 airfoils and for the three configurations of the NASA GA(PC)-1 airfoil are shown in figure 25. At a Mach number of 0.15, the maximum lift coefficients for all three configurations of the NASA GA(PC)-1 airfoil increase substantially in the range of Reynolds numbers from 2.0×10^6 to 9.0×10^6 and reach values of 2.1, 1.8, and 1.5, respectively, for the landing, climb, and cruise configurations. The corresponding values for the NASA GA(W)-1 and NASA GA(W)-2 airfoils are both 2.1. At a Mach number of 0.15 and a Reynolds number of 2.0×10^6, the landing configuration of the NASA GA(PC)-1 airfoil and the fixed-geometry NASA GA(W)-1 and NASA GA(W)-2 airfoils have maximum lift coefficients of 1.7, 1.6, and 1.7, respectively.

Addition of roughness strips decreased $c_{l,max}$ performance for the NASA GA(W)-1 airfoil, the cruise configuration of the NASA GA(PC)-1 airfoil, and the climb configuration of the NASA GA(PC)-1 airfoil at a Reynolds number of 2.0×10^6. The effect of adding roughness strips is negligible for the NASA GA(W)-2 airfoil, the landing configuration of the NASA GA(PC)-1 airfoil at a Reynolds number of 4.0×10^6, and the climb configuration at Reynolds numbers of 4.0×10^6 and 6.0×10^6.

Pitching moment.- The data for the climb configuration (figs. 10 to 14) show that the section pitching-moment coefficient for this configuration is not affected appreciably by angle of attack and has a value in the range from -0.045 to -0.030 for angles of attack less than 8°. As the angle of attack is increased above 8° toward the stall angle, the value of the section pitching-moment coefficient increases but remains negative. Increasing the Reynolds

11

number to a value of 9.0×10^6 has the effect of decreasing the pitching-moment coefficient of the climb configuration slightly. The section pitching-moment coefficient is essentially independent of Reynolds numbers with values greater than 9.0×10^6. The pitching-moment coefficient of the climb configuration is insensitive to Mach number, except for the two largest values (M = 0.28 and 0.35) and angles of attack near stall. Under these conditions, the effect of the Mach number is to increase the value of the section pitching-moment coefficient toward zero. Roughness strips increase the value of the section pitching-moment coefficient slightly.

The data for the cruise configuration (figs. 15 to 19) show that the section pitching-moment coefficient for this configuration has no appreciable dependence on angle of attack in the range from $\alpha = 0^\circ$ to the stall angle and has a value between 0.035 and 0.055 in this angle-of-attack range. The Reynolds number effects and Mach number effects are the same as those of the climb configuration. The addition of roughness strips decreases the value of the section pitching-moment coefficient of the cruise configuration. This effect is opposite to that found for the climb configuration.

The data for the landing configuration (figs. 20 to 23) show that the section pitching-moment coefficient increases from a value between -0.130 and -0.120 to a value between -0.080 and -0.065 as the angle of attack is increased from -8° to the stall angle. In general, the section pitching-moment coefficient of the landing configuration decreases with increasing Reynolds number as it did for the climb and cruise configurations, but the amount of decrease is larger. Mach number has no effect in the range tested. The standard strip roughness and the standard NACA roughness increase the value of the section pitching-moment coefficient of the landing configuration toward zero as they did for the climb configuration.

The attached-flow section pitching-moment coefficients for the NASA GA(W)-1 airfoil and the landing, climb, and cruise configurations of the NASA GA(PC)-1 airfoil have values of the order of -0.1, -0.1, -0.03, and 0.05, respectively. (See fig. 24.)

Drag.- The effects of Reynolds number on the drag polars for the smooth (natural transition) climb, cruise, and landing configurations are shown in figures 10, 15, and 20, respectively, at several Mach numbers. The Reynolds number range extends from 2.0×10^6 to 20.0×10^6. The effects of Reynolds number on the climb and cruise configurations with transition fixed at x/c = 0.05 are shown in figures 12 and 17 for the Reynolds number range from 2.0×10^6 to 6.0×10^6. In general, drag decreases as Reynolds number increases for a given lift coefficient. For Reynolds numbers greater than about 9.0×10^6, the decrease in drag with increasing Reynolds number is small.

In figures 11, 16, and 21, the effects of Mach number on the drag polars for the smooth climb, cruise, and landing configurations are shown for Reynolds numbers of 4.0×10^6, 6.0×10^6, and 4.0×10^6, respectively. The effects of Mach number on these three configurations are shown in figures 13, 18, and 22 at the same respective Reynolds numbers with roughness strips applied at x/c = 0.05. There are very slight increases in the drag coefficients of the roughened configurations as the Mach number increases. The results for the

12

smooth configurations show the same trend. However, for lift coefficients near the design values, the variation of the drag coefficient with Mach number for the smooth climb and cruise configurations is larger than that for the roughened configurations. Apparently the drag reduction due to the presence of regions of laminar flow on the smooth model decreases with increasing Mach number. This is probably a wind-tunnel effect due to increases in the turbulence level of the tunnel with increasing dynamic pressure (ref. 15).

The effects of adding roughness strips to the climb, cruise, and landing configurations are shown in figures 14, 19, and 23, respectively, for Reynolds numbers from 2.0×10^6 to 6.0×10^6. The greatest differences in the drag coefficients of the smooth and rough versions of the climb configuration occur for a broad band of lift coefficients approximately centered about the climb design value of 0.9. The greater differences for the cruise configuration occur near 0.4, the design value of the lift coefficient for cruise. Adding a roughness strip increases the drag coefficient of the landing configuration for all lift coefficients. The increase in drag coefficient caused by this roughness strip is comparable to that caused by the standard NACA roughness.

The drag coefficients for the three configurations of the NASA GA(PC)-1 airfoil with roughness strips added at $x/c = 0.05$ and for the NASA GA(W)-1 airfoil with roughness strips added at $x/c = 0.08$ are compared in figure 24 for Reynolds numbers from 2.0×10^6 to 6.0×10^6. In general, the drag coefficient of the climb configuration is slightly lower than that of the cruise configuration. As expected, the drag of the landing configuration is larger than that of the other configurations.

The variations with Reynolds number of the section drag coefficients of the climb and cruise configurations, at the respective design lift coefficients, are compared in figure 27 with those of the NASA GA(W)-1 and NASA GA(W)-2 airfoils. Similar comparisons of the variations with Reynolds number of the section lift-drag ratio are presented in figure 28. The variations of the lift-drag ratio with lift coefficient for these airfoils with fixed transition are compared in figure 29 for Reynolds numbers from 2.0×10^6 to 6.0×10^6. For the same design climb conditions as the NASA GA(PC)-1 airfoil ($c_l = 0.9$, $R = 4.0 \times 10^6$), the lift-drag ratios of the climb configuration of the 16-percent-thick NASA GA(PC)-1 airfoil and of the 17-percent-thick NASA GA(W)-1 airfoil are about 78 and 76. The value for the 13-percent-thick NASA GA(W)-2 airfoil is about 88. At the design cruise conditions ($c_l = 0.4$, $R = 6.0 \times 10^6$), the lift-drag ratios of the climb and cruise configurations of the NASA GA(PC)-1 airfoil are about 43 and 40, respectively. The ratios for the NASA GA(W)-1 and NASA GA(W)-2 airfoils are about 38 and 47, respectively. The climb configuration of the NASA GA(PC)-1 airfoil obtains the maximum lift-drag ratio at larger values of the lift coefficient than the NASA GA(W)-1 and NASA GA(W)-2 airfoils at Reynolds numbers of 4.0×10^6 and 6.0×10^6. (See fig. 29.) At a Reynolds number of 2.0×10^6, the climb configuration of the NASA GA(PC)-1 airfoil and the NASA GA(W)-2 airfoil obtain the maximum lift-drag ratio at about the same lift coefficient.

Comparison of Experimental and Theoretical Results

Experimental pressure distributions obtained with fixed transition are compared in figure 30 with theoretical pressure distributions calculated with the method of reference 16 for viscous attached flow. This viscous-flow method is composed of a potential-flow treatment and an integral boundary-layer treatment. A surface vortex singularity method is used in the potential-flow treatment.

In figures 30(a) and (b), the experimental results for the climb and cruise configurations are compared with the results of the viscous-flow method for $M = 0.15$ and $\alpha = 6^{\circ}$. At this angle of attack, the section lift coefficients for these configurations are near the design values of 0.9 and 0.4, respectively. The Reynolds number is about 4.0×10^6 for the climb configuration and 6.0×10^6 for the cruise configuration. The agreement between experimental and theoretical pressure distributions is good. Comparisons between experiment and theory are not made for the landing configuration because the flow on the upper surface of the flap is separated for all angles of attack of interest.

The experimental aerodynamic characteristics for the climb configuration with transition fixed, at the conditions $M = 0.15$ and $R = 4.0 \times 10^6$, are compared in figure 31 with the theoretical results of the viscous, attached-flow method of reference 16. The theoretical predictions for the section lift coefficient agree well with experimental data for angles of attack where there is no flow separation (up to about 10°). In general, the levels for the section pitching-moment coefficient obtained from theory and experiment are in fair agreement for lift coefficients less than about 1.0. However, the theoretical method predicts a slight decrease in the pitching-moment coefficient with increasing lift coefficient, whereas the experimental results show a slight increase. In the lift-coefficient range where there is attached flow ($c_l < 1.1$), the theory generally predicts the shape of the drag polar. However, the values for the section drag coefficient are overpredicted.

CONCLUDING REMARKS

Tests have been conducted in the Langley low-turbulence pressure tunnel to determine the aerodynamic characteristics of the climb, cruise, and landing configurations of a 16-percent-thick variable-geometry airfoil designed for general-aviation applications (NASA GA(PC)-1). These tests were conducted over a Mach number range from 0.10 to 0.35, a chord Reynolds number range from 2.0×10^6 to 20.0×10^6, and an angle-of-attack range from -8° to 20°. The test data were compared with the test data for the fixed-geometry NASA GA(W)-1 and NASA GA(W)-2 airfoils and with the predictions of a theoretical method. The following results were determined from this investigation:

1. Maximum section lift coefficients increased substantially at a Mach number of 0.15 in the Reynolds number range from 2.0×10^6 to 9.0×10^6 for all three configurations and reached values of approximately 2.1, 1.8, and 1.5 for the landing, climb, and cruise configurations, respectively. These values compare to a value of approximately 2.1 for the fixed-geometry NASA GA(W)-1 and

14

NASA GA(W)-2 airfoils. At a Mach number of 0.15 and a Reynolds number of 2.0×10^6, the NASA GA(PC)-1 airfoil landing configuration has a maximum lift coefficient of 1.7 compared to 1.6 and 1.7, respectively, for the NASA GA(W)-1 and NASA GA(W)-2 airfoils. Stall characteristics were of the trailing-edge type but were abrupt for all three configurations of the NASA GA(PC)-1 airfoil.

2. The design section lift coefficients of 0.9 and 0.4 for the climb and cruise configurations, respectively, were obtained at the same angle of attack, about 6°, as intended.

3. At a Mach number of 0.15, the pitching-moment coefficients of the landing, climb, and cruise configurations of the NASA GA(PC)-1 airfoil are of the order of -0.1, -0.03, and 0.05, respectively.

4. The section lift-drag ratio is about 78 for the climb configuration of the NASA GA(PC)-1 airfoil with transition fixed near the leading edge at the design climb condition (section lift coefficient = 0.9, Reynolds number = 4.0×10^6). The section lift-drag ratio is about 42 for the cruise configuration with transition fixed near the leading edge at the design cruise condition (section lift coefficient = 0.4, Reynolds number = 6.0×10^6).

5. Predictions obtained with a viscous, attached-flow theoretical method showed generally good agreement with experimental results.

Langley Research Center
National Aeronautics and Space Administration
Hampton, VA 23665
October 25, 1978

REFERENCES

1. McGhee, Robert J.; and Beasley, William D.: Low-Speed Aerodynamic Characteristics of a 17-Percent-Thick Airfoil Section Designed for General Aviation Applications. NASA TN D-7428, 1973.

2. Wentz, W. H., Jr.; and Seetharam, H. C.: Development of a Fowler Flap System for a High Performance General Aviation Airfoil. NASA CR-2443, 1974.

3. Wentz, W. H., Jr.: Effectiveness of Spoilers on the GA(W)-1 Airfoil With a High Performance Fowler Flap. NASA CR-2538, 1975.

4. McGhee, Robert J.; and Beasley, William D.: Effects of Thickness on the Aerodynamic Characteristics of an Initial Low-Speed Family of Airfoils for General Aviation Applications. NASA TM X-72843, 1976.

5. Wentz, W. H., Jr.: Wind Tunnel Tests of the GA(W)-2 Airfoil With 20% Aileron, 25% Slotted Flap, 30% Fowler Flap, and 10% Slot-Lip Spoiler. NASA CR-145139, 1977.

6. Morgan, Harry L., Jr.; and Paulson, John W., Jr.: Aerodynamic Characteristics of Wing-Body Configuration With Two Advanced General Aviation Airfoil Sections and Simple Flap Systems. NASA TN D-8524, 1977.

7. Chen, Allen W.: Advanced Technology Airfoils for General Aviation Aircraft. Experimental Aircraft Symposium: Homebuilt Experimental Aircraft - Theory and Practice, Western Periodicals Co., c1975, pp. 1-12.

8. Peterson, John B., Jr.; and Chen, Allen W.: Design Procedure for Low-Drag Subsonic Airfoils. NASA Tech Brief B75-10256, 1975.

9. Schlichting, Herman (J. Kestin, transl.): Boundary Layer Theory. McGraw-Hill Book Co., Inc., c1955.

10. Ormsbee, Allen I.; and Chen, Allen W.: Multiple Element Airfoils Optimized for Maximum Lift Coefficient. AIAA J., vol. 10, no. 12, Dec. 1972, pp. 1620-1624.

11. Von Doenhoff, Albert E.; and Abbott, Frank T., Jr.: The Langley Two-Dimensional Low-Turbulence Pressure Tunnel. NACA TN 1283, 1947.

12. Braslow, Albert L.; and Knox, Eugene C.: Simplified Method for Determination of Critical Height of Distributed Roughness Particles for Boundary-Layer Transition at Mach Numbers From 0 to 5. NACA TN 4363, 1958.

13. Pankhurst, R. C.; and Holder, D. W.: Wind-Tunnel Technique. Sir Isaac Pitman & Sons, Ltd. (London), 1965.

14. Smith, A. M. O.: High-Lift Aerodynamics. J. Aircr., vol. 12, no. 6, June 1975, pp. 501-530.

15. Dryden, Hugh L.; and Abbott, Ira H.: The Design of Low-Turbulence Wind Tunnels. NACA Rep. 940, 1948.

16. Smetana, Frederick O.; Summey, Delbert C.; Smith, Neill S.; and Carden, Ronald K.: Light Aircraft Lift, Drag, and Moment Prediction - A Review and Analysis. NASA CR-2523, 1975.

TABLE I.- MEASURED COORDINATES FOR NASA GA(PC)-1 AIRFOIL

(a) Main section

Upper surface		Lower surface	
x/c	z/c	x/c	z/c
0.0002	0.0001	------	-------
.0051	.0159	0.0048	-0.0203
.0096	.0238	.0099	-.0276
.0147	.0306	.0147	-.0322
.0248	.0407	.0253	-.0391
.0350	.0488	.0352	-.0433
.0502	.0584	.0503	-.0475
.0600	.0637	.0597	-.0493
.0750	.0705	.0751	-.0514
.0998	.0794	.0999	-.0534
.1496	.0910	.1500	-.0556
.1997	.0969	.2000	-.0571
.2497	.0990	.2498	-.0584
.2998	.0994	.3000	-.0598
.3498	.0980	.3498	-.0611
.3998	.0949	.4001	-.0623
.4498	.0910	.4501	-.0632
.4999	.0858	.5002	-.0631
.5496	.0793	.5501	-.0618
.5998	.0718	.6007	-.0597
.6500	.0640	.6503	-.0558
.6998	.0556	.7004	-.0488
.7499	.0463	.7505	-.0382
.7995	.0364	.8006	-.0258

TABLE I.- Concluded

(b) Flap

Upper surface		Lower surface	
x/c	z/c	x/c	z/c
Climb configuration			
0.8498	0.0261	0.8507	−0.0206
.9003	.0153	.9008	−.0167
.9503	.0044	.9509	−.0128
.9910	−.0043	.9909	−.0098
1.0000	−.0067	1.0000	−.0091
Cruise configuration			
0.8396	0.0326	0.8485	−0.0132
.8912	.0309	.8970	−.0006
.9422	.0290	.9456	.0121
.9830	.0275	.9845	.0221
.9930	.0268	.9933	.0244
Landing configuration			
0.8581	0.0180	0.8506	−0.0280
.9060	−.0014	.9005	−.0328
.9528	−.0205	.9504	−.0377
.9908	−.0361	.9907	−.0417
1.0000	−.0401	1.0000	−.0425
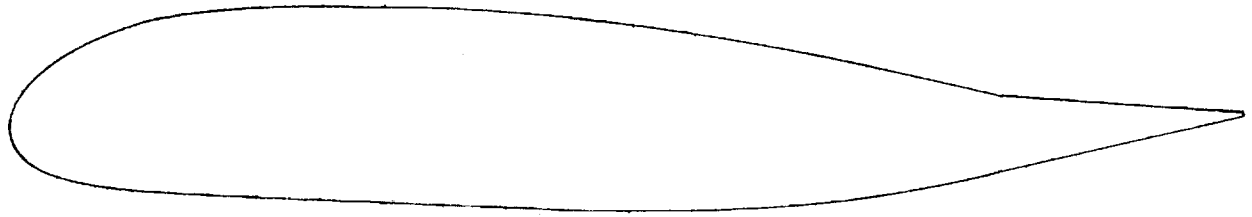
Cruise
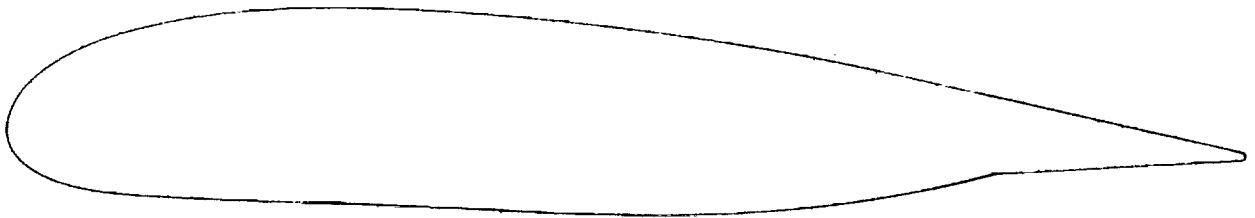
Climb
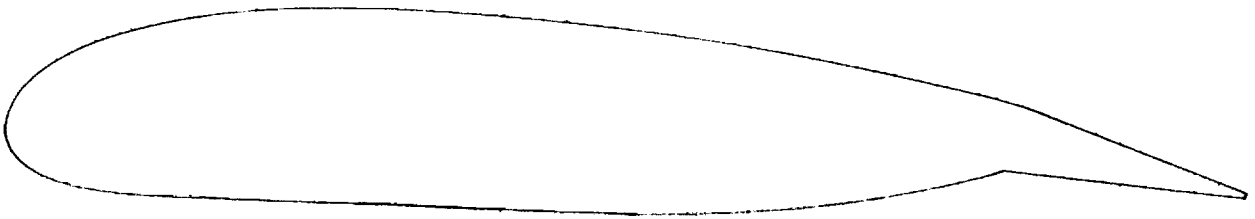
Landing

Figure 1.- Profiles of cruise, climb, and landing configurations of
NASA GA(PC)-1 airfoil.
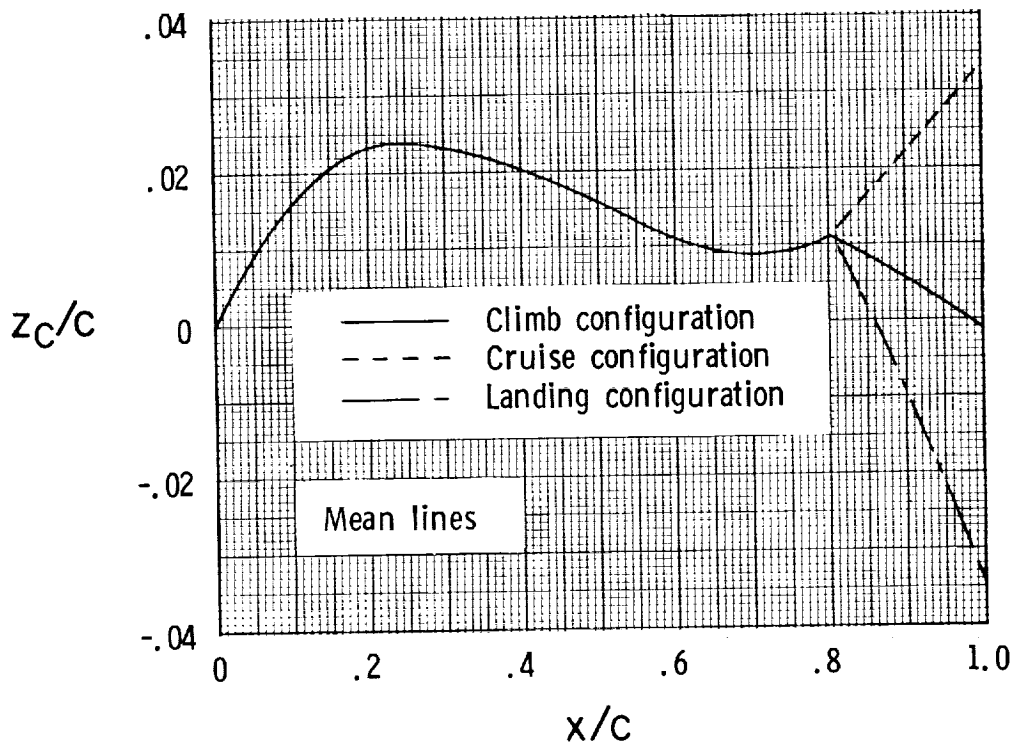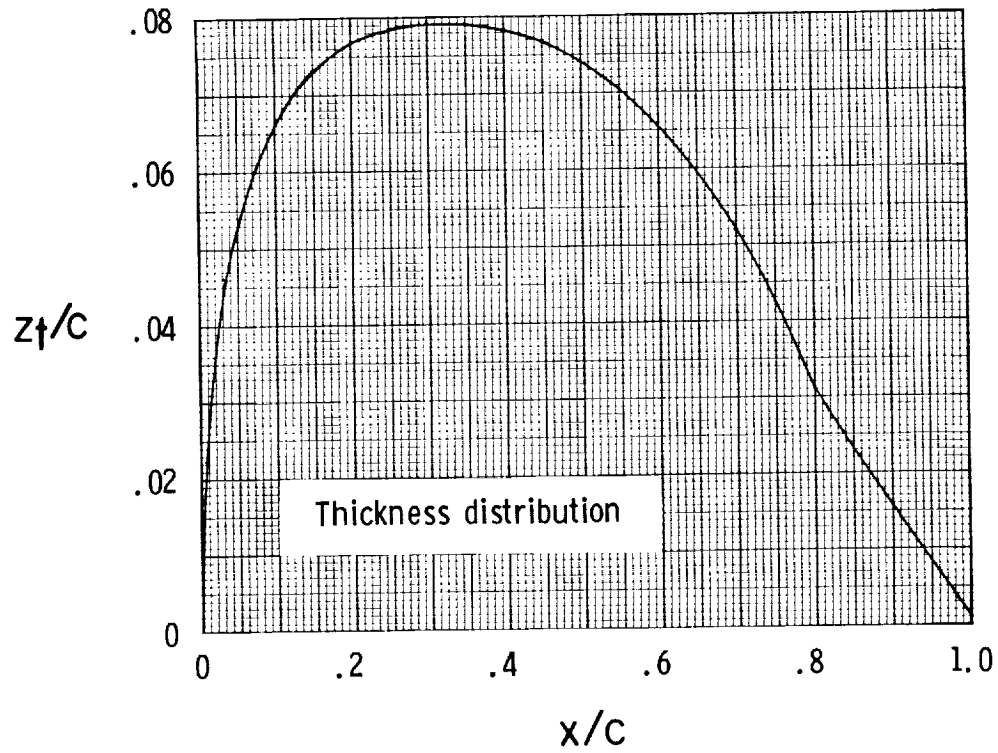
Figure 2.- Thickness distribution and mean lines for NASA GA(PC)-1 airfoil.

L-75-5718

Figure 3.- NASA GA(PC)-1 airfoil climb configuration.

22

Tunnel side walls

Diam = 1.67c

Airflow

1.50c

A — — — — — — — — A

Circular plate

"z"

Metal seals

Airfoil positioning attachment

Top view

Seal detail "z"

Model-attachment plate

Zero incidence reference

Tunnel center line

c/4

c

End view ,section A—A
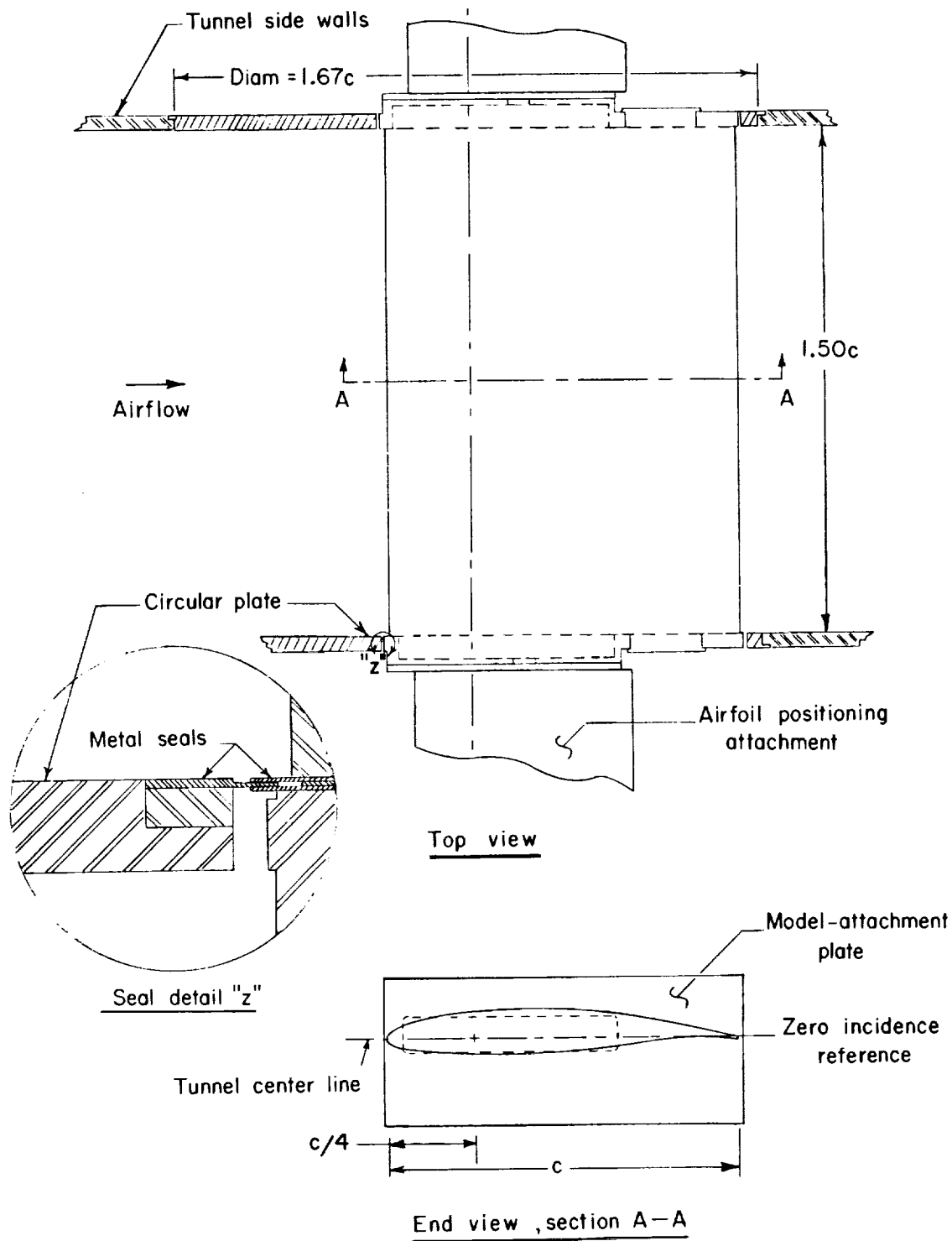
Figure 4.- Typical airfoil mounted in wind tunnel. All dimensions in terms of airfoil chord. c = 61 cm (24 in.).
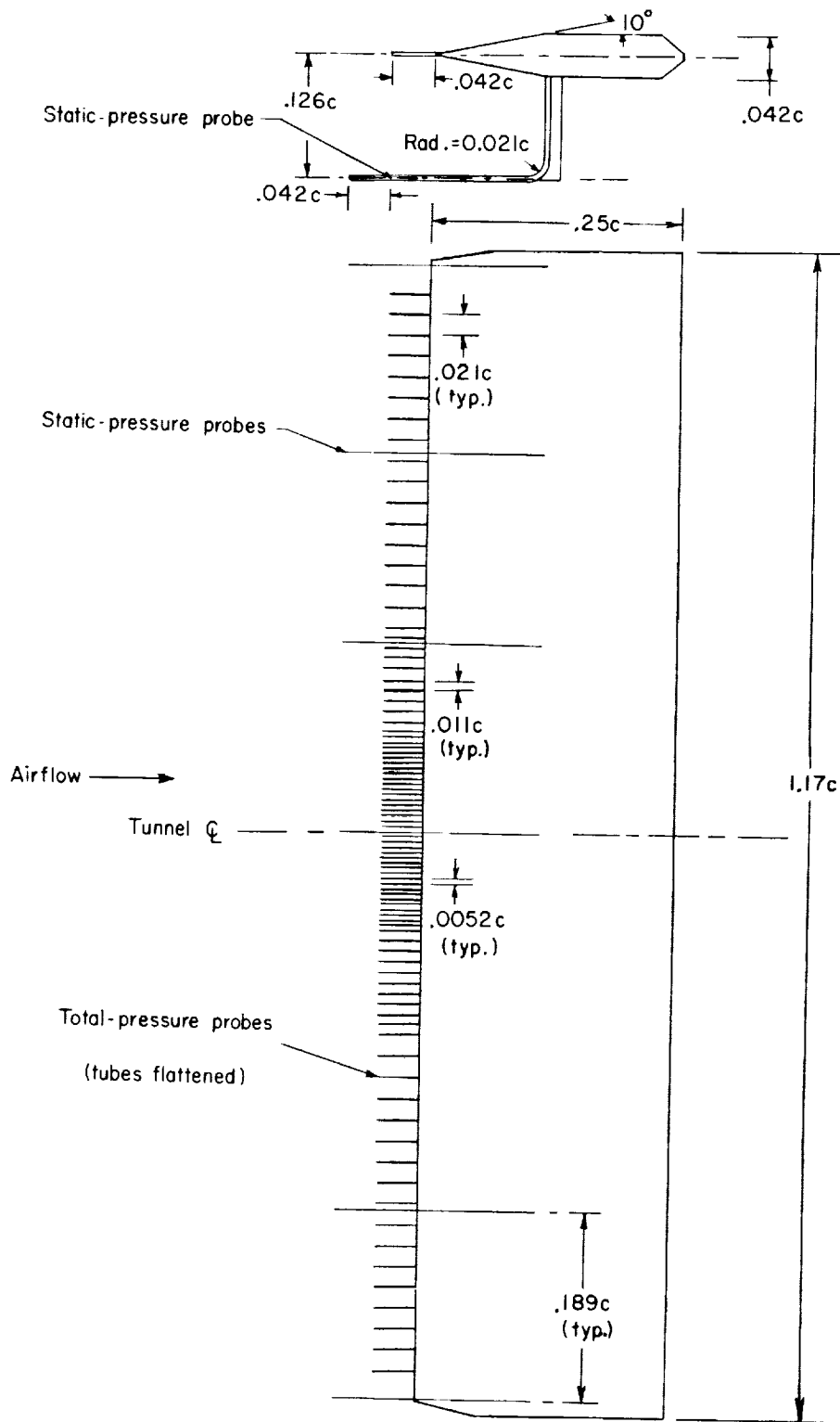
Figure 5.- Wake survey rake. All dimensions in terms of airfoil chord.
c = 61 cm (24 in.).

	α	c_l	c_d	c_m
○	-4.0	-.210	.0097	-.0348
□	0.0	.240	.0101	-.0349
◇	4.1	.690	.0103	-.0340
△	5.9	.880	.0114	-.0330
◹	8.4	1.150	.0140	-.0310

○ □ ◇ △ ◹ Upper surface

⊙ ⊞ ◈ ▲ ◮ Lower surface
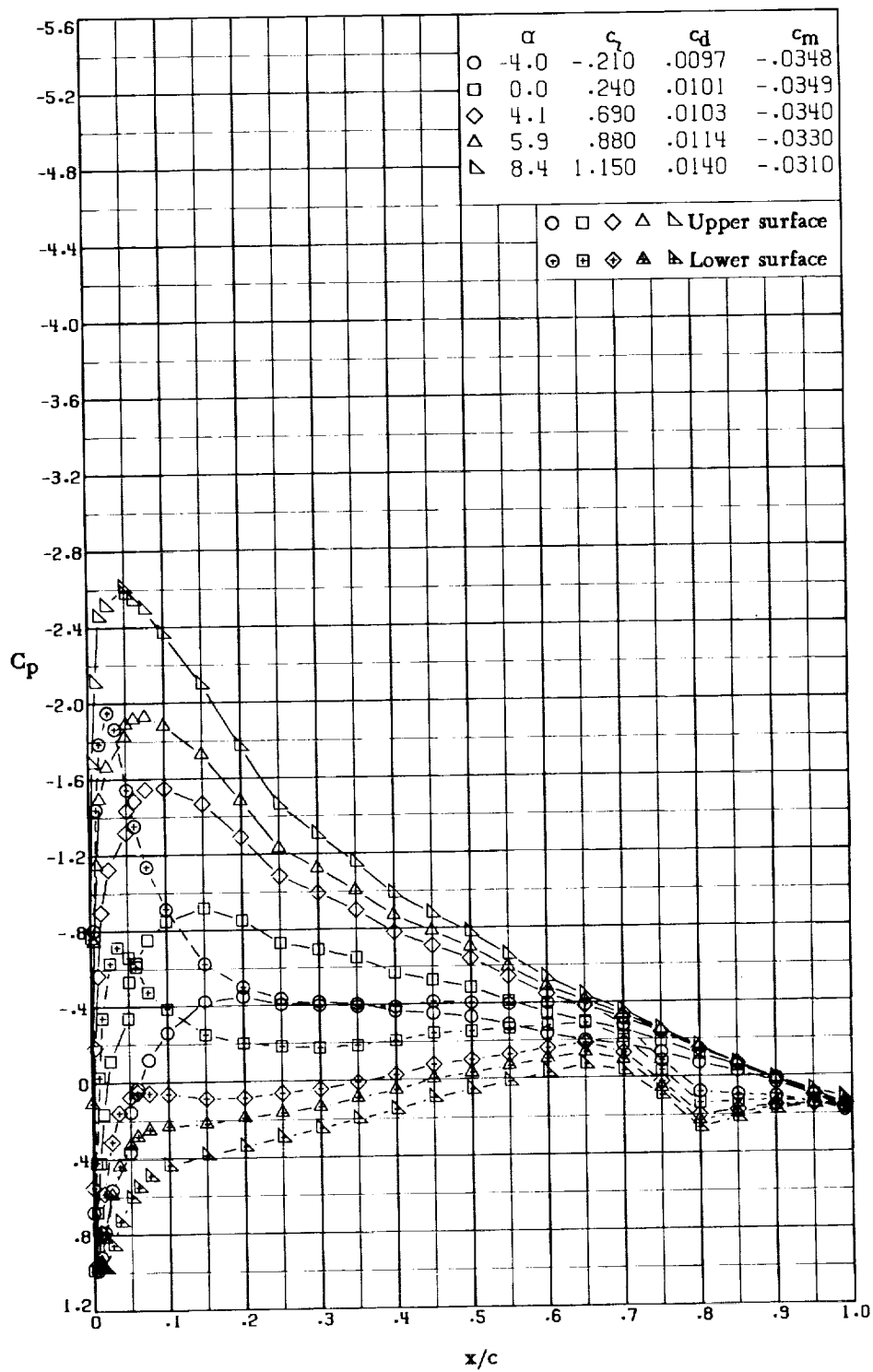
(a) α = -4.0°, 0.0°, 4.1°, 5.9°, and 8.4°.

Figure 6.- Effect of angle of attack on chordwise pressure distributions for climb configuration. Transition fixed at x/c = 0.05; M = 0.15; R ≈ 4.0 × 10^6.

25

	α	c_l	c_d	c_m
◁	8.4	1.150	.0140	-.0310
◻	12.0	1.490	.0172	-.0244
◯	15.1	1.680	.0304	-.0142
◇	16.1	1.220		-.0452

◁ ◻ ◯ ◇			Upper surface	
◣ ◪ ⊕ ⊕			Lower surface	

(b) $\alpha = 8.4^o$, 12.0^o, 15.1^o, and 16.1^o.
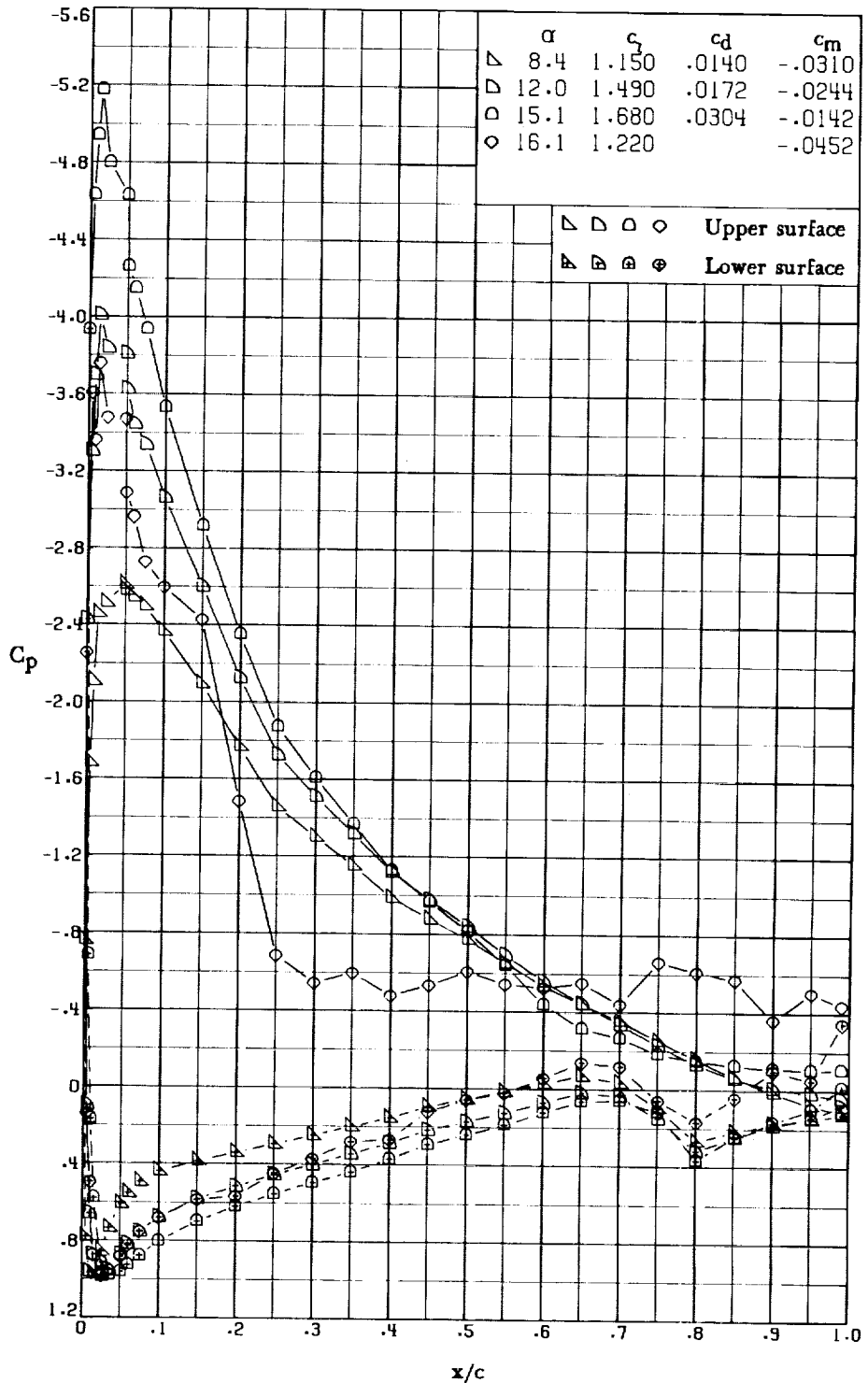
Figure 6.- Concluded.

26
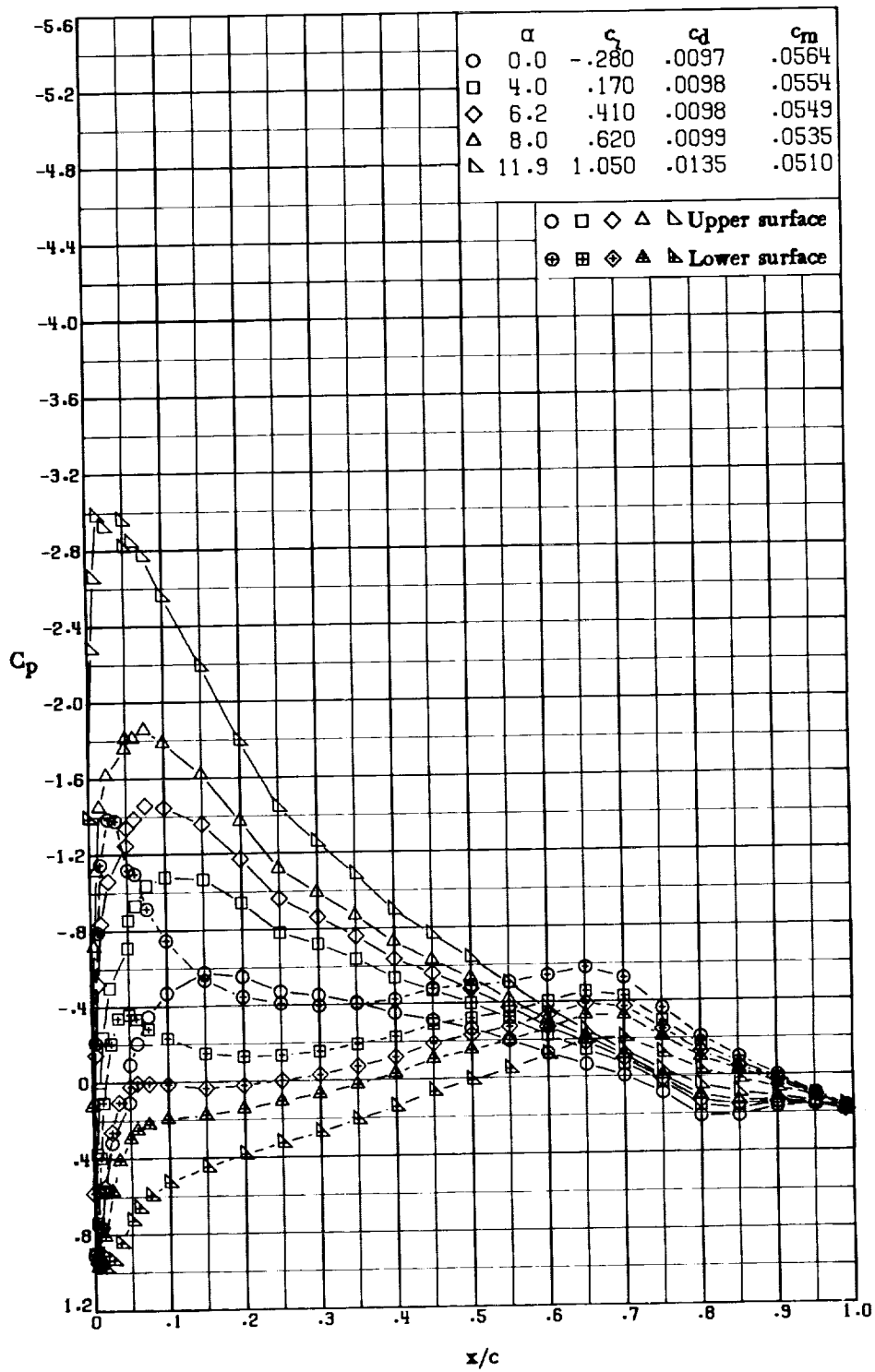
(a) α = 0.0°, 4.0°, 6.2°, 8.0°, and 11.9°.

Figure 7.- Effect of angle of attack on chordwise pressure distributions
for cruise configuration. Transition fixed at x/c = 0.05; M = 0.15;
R ≈ 6.0 × 10⁶.

27

	α	c_l	c_d	c_m
◁	11.9	1.050	.0135	.0510
◻	14.0	1.260	.0179	.0501
◯	16.3	1.420	.0389	.0461
◇	17.0	1.070		.0062

◁ ◻ ◯ ◇	Upper surface
◭ ◪ ⊕ ⊕	Lower surface
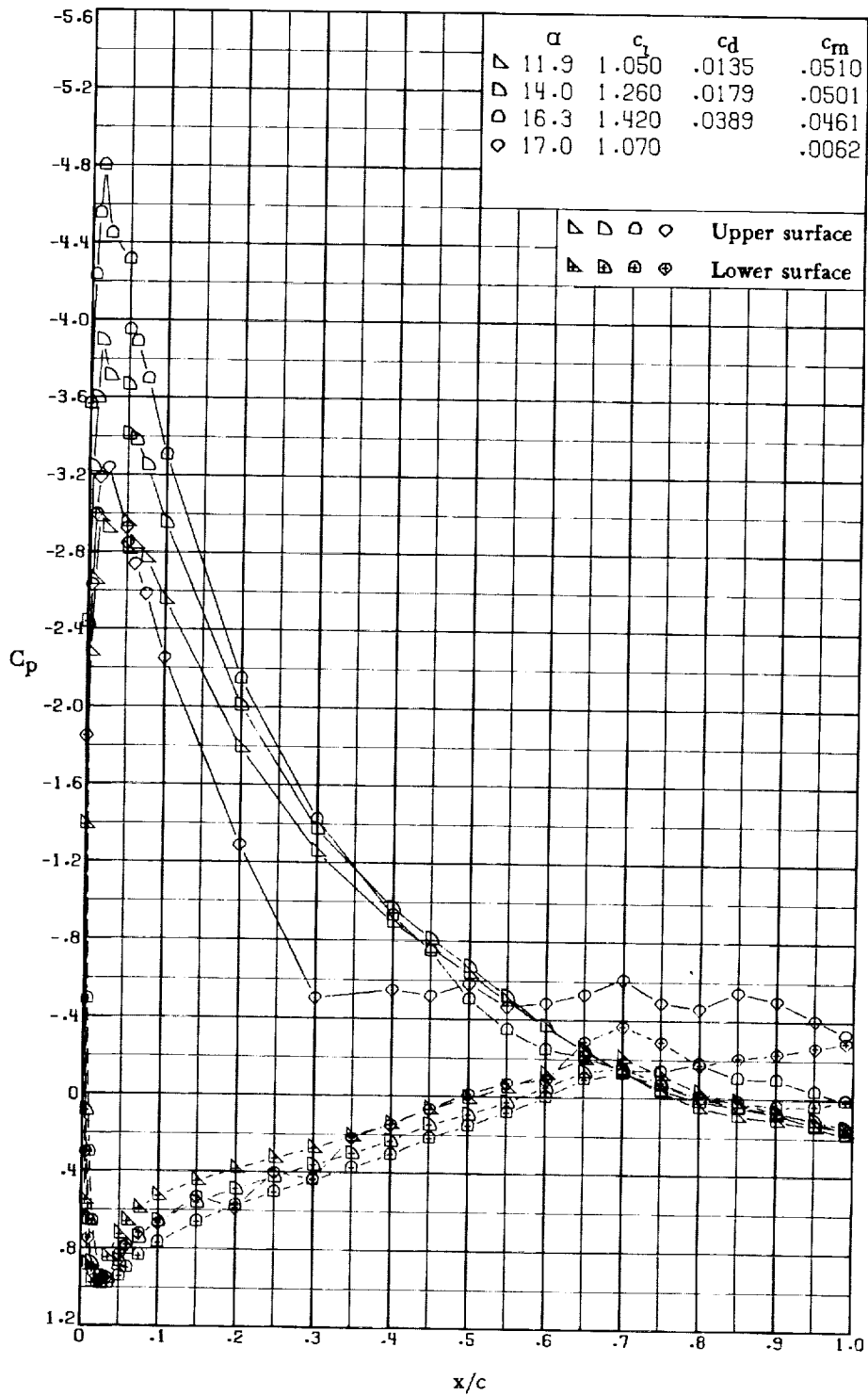
(b)   α = 11.9°, 14.0°, 16.3°, and 17.0°.

Figure 7.- Concluded.
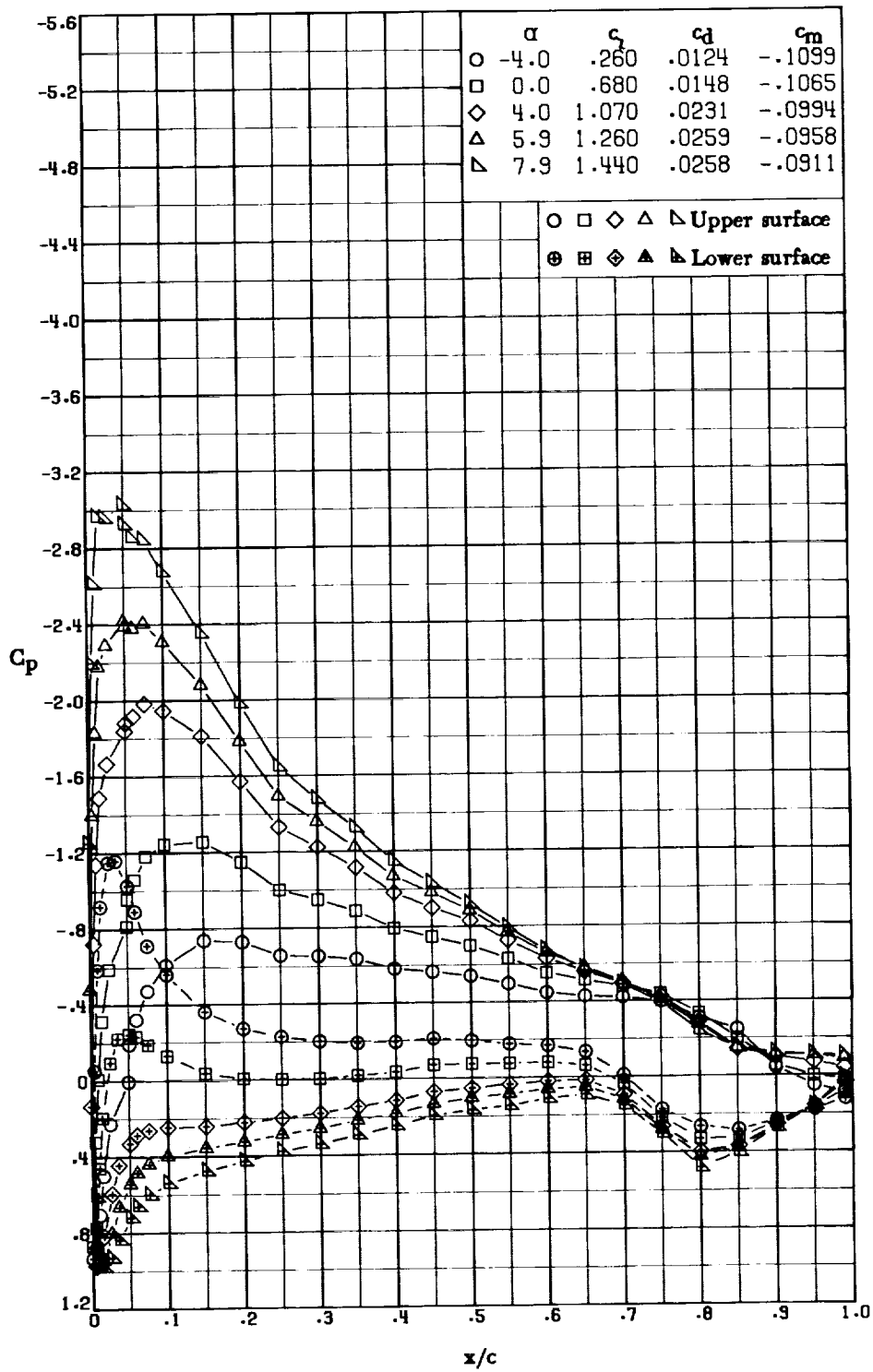
(a) α = -4.0°, 0.0°, 4.0°, 5.9°, and 7.9°.

Figure 8.- Effect of angle of attack on chordwise pressure distributions for landing configuration. Transition fixed at x/c = 0.05; M = 0.15; R $\approx$ 4.0 × 10⁶.
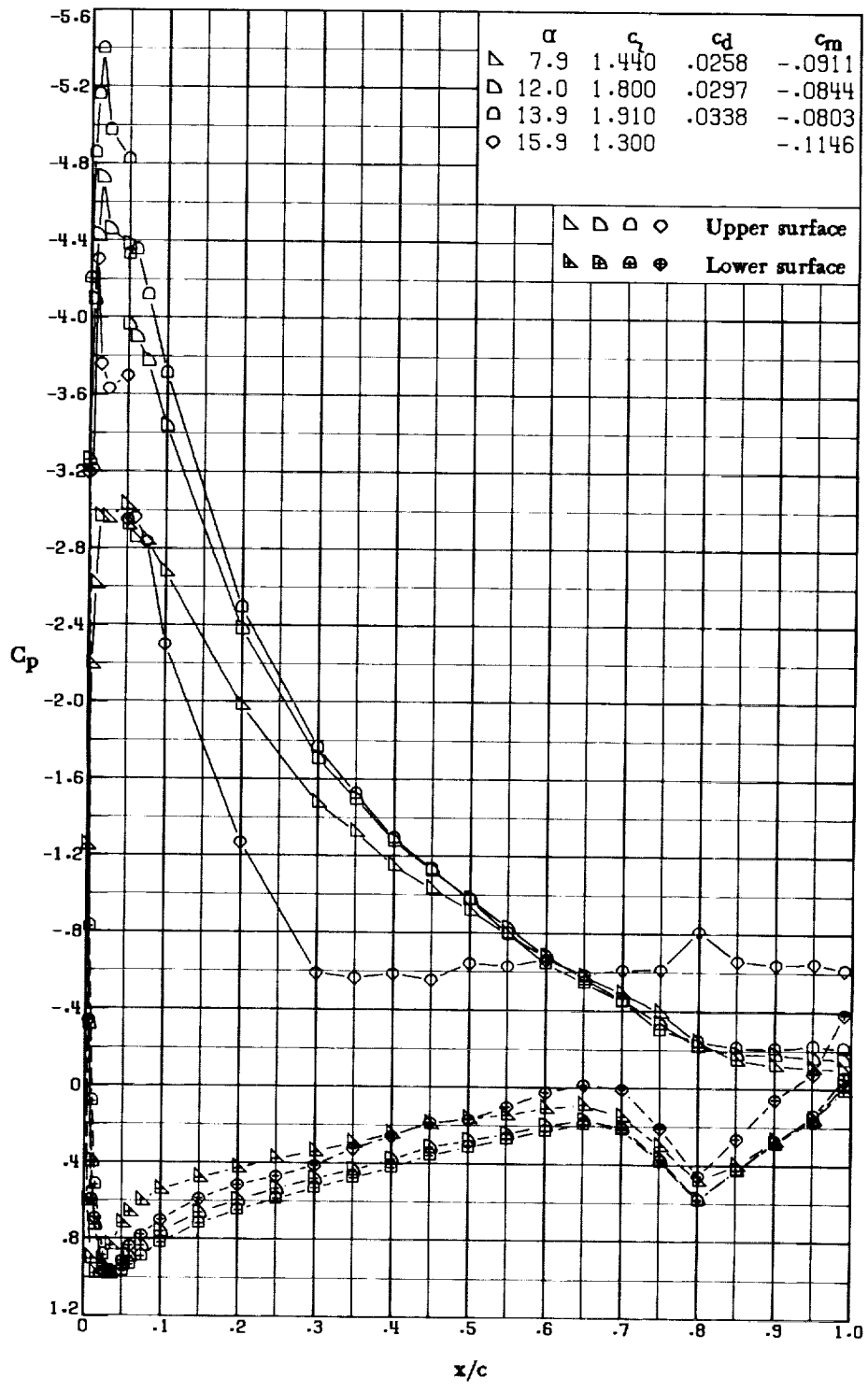
(b) $\alpha = 7.9^{\circ}$, 12.0°, 13.9°, and 15.9°.

Figure 8.- Concluded.

30
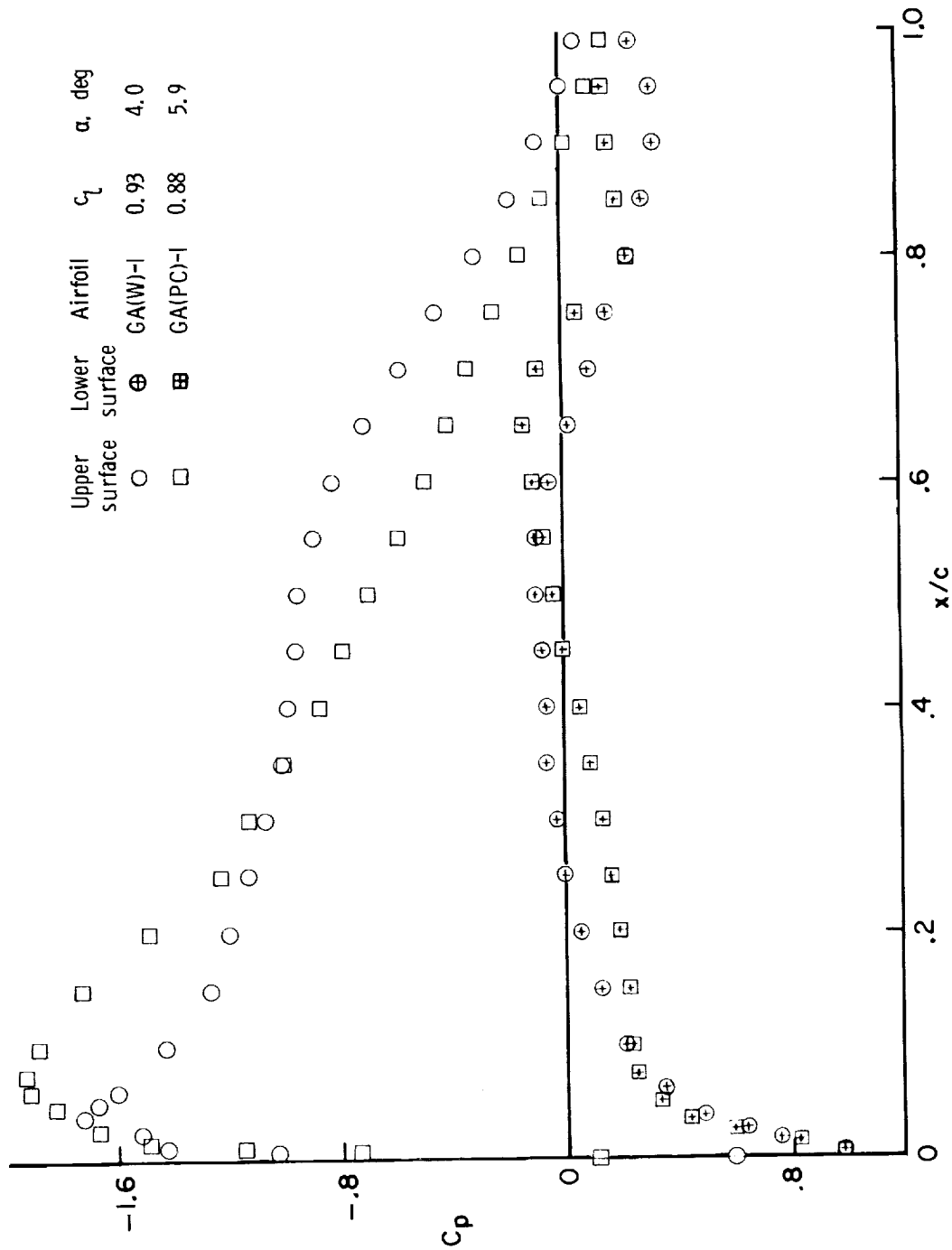
Figure 9.- Comparison of pressure distributions for climb configuration of NASA GA(PC)-1 airfoil and for NASA GA(W)-1 airfoil. Transition fixed; M = 0.15; R ≈ 4.0 × 10⁶.

31
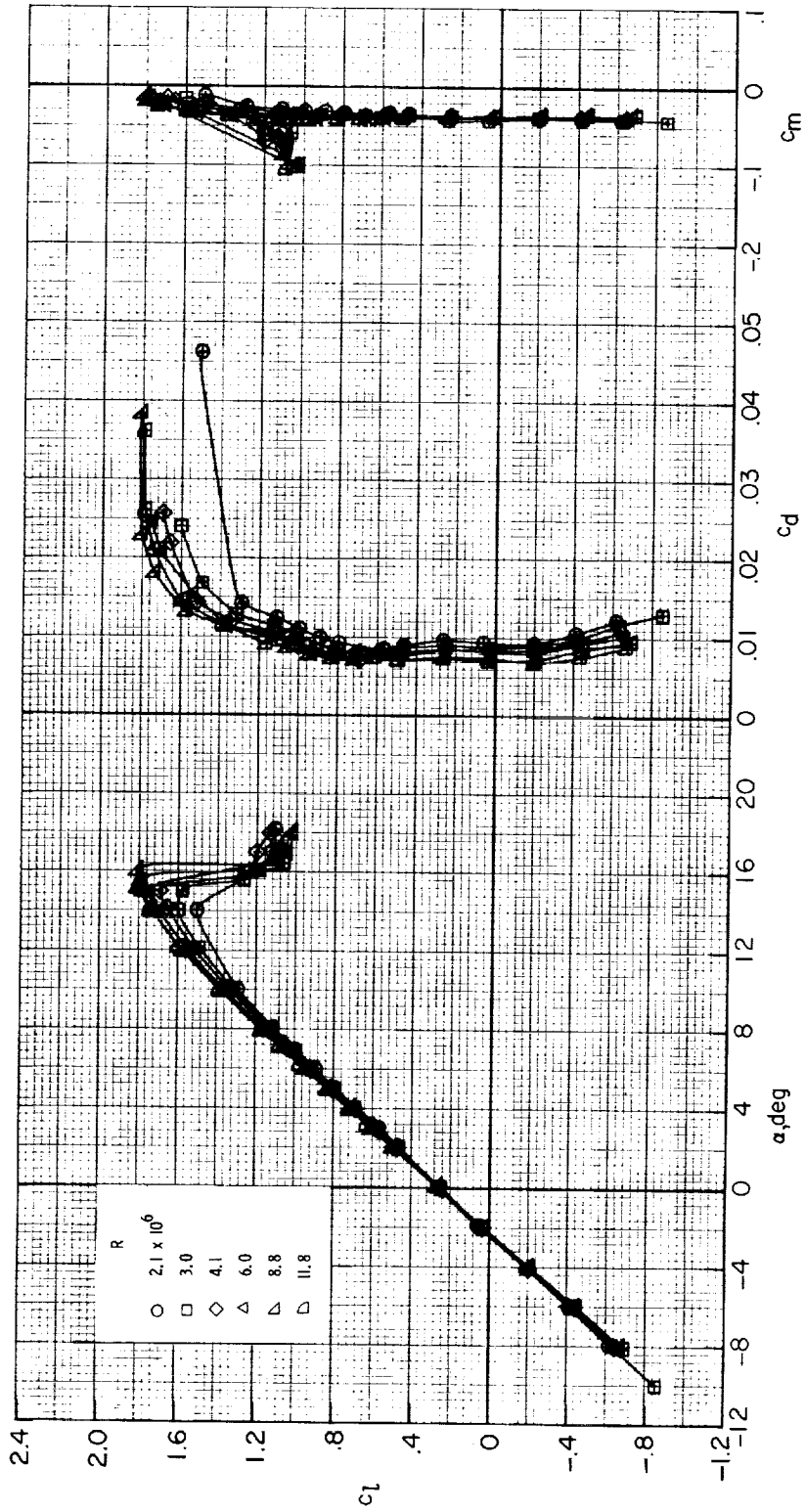
(a) M = 0.15.

Figure 10.- Effect of Reynolds number on section characteristics of climb configuration. Model smooth.
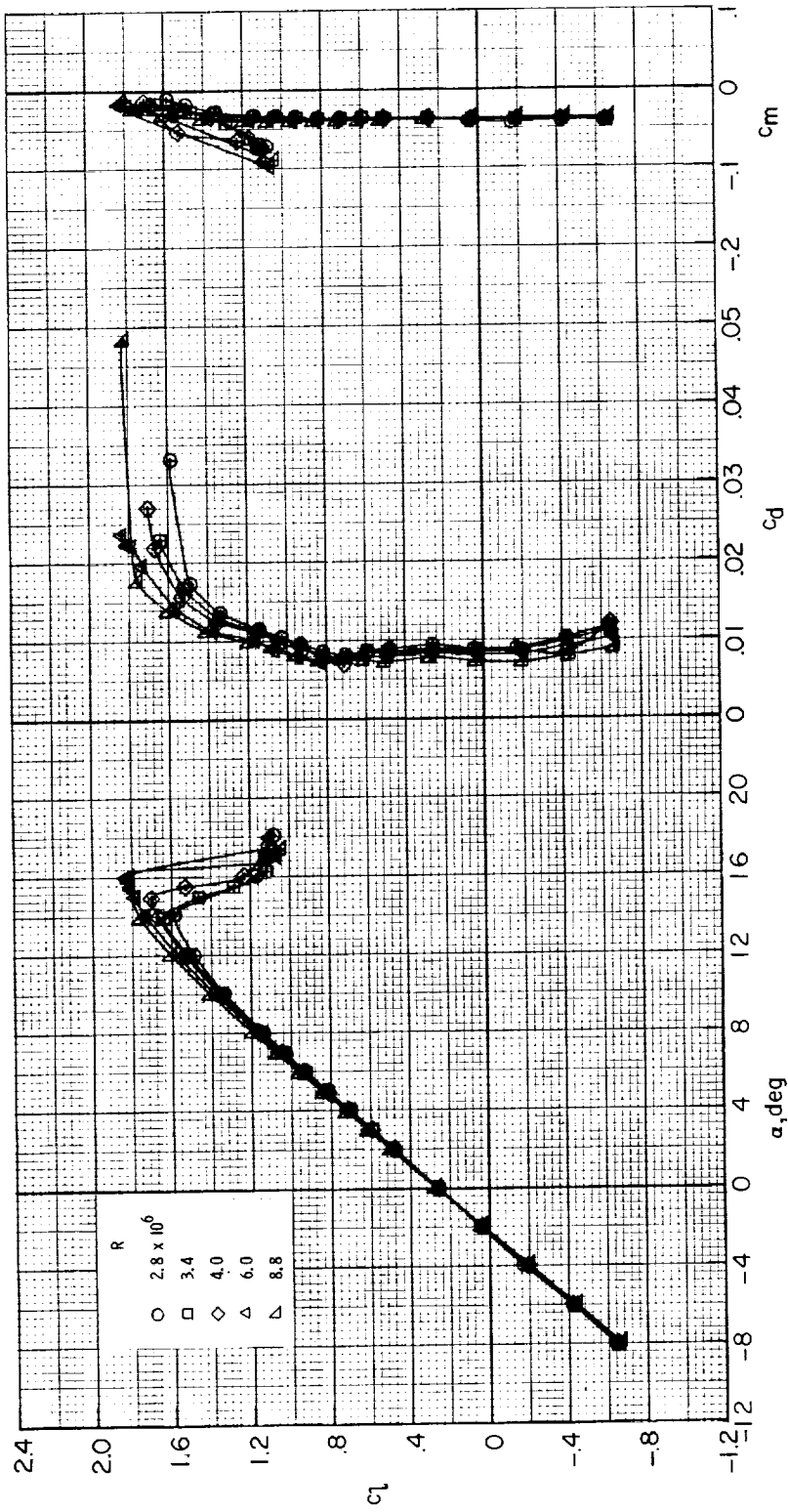
(b) M = 0.20.

Figure 10.— Continued.
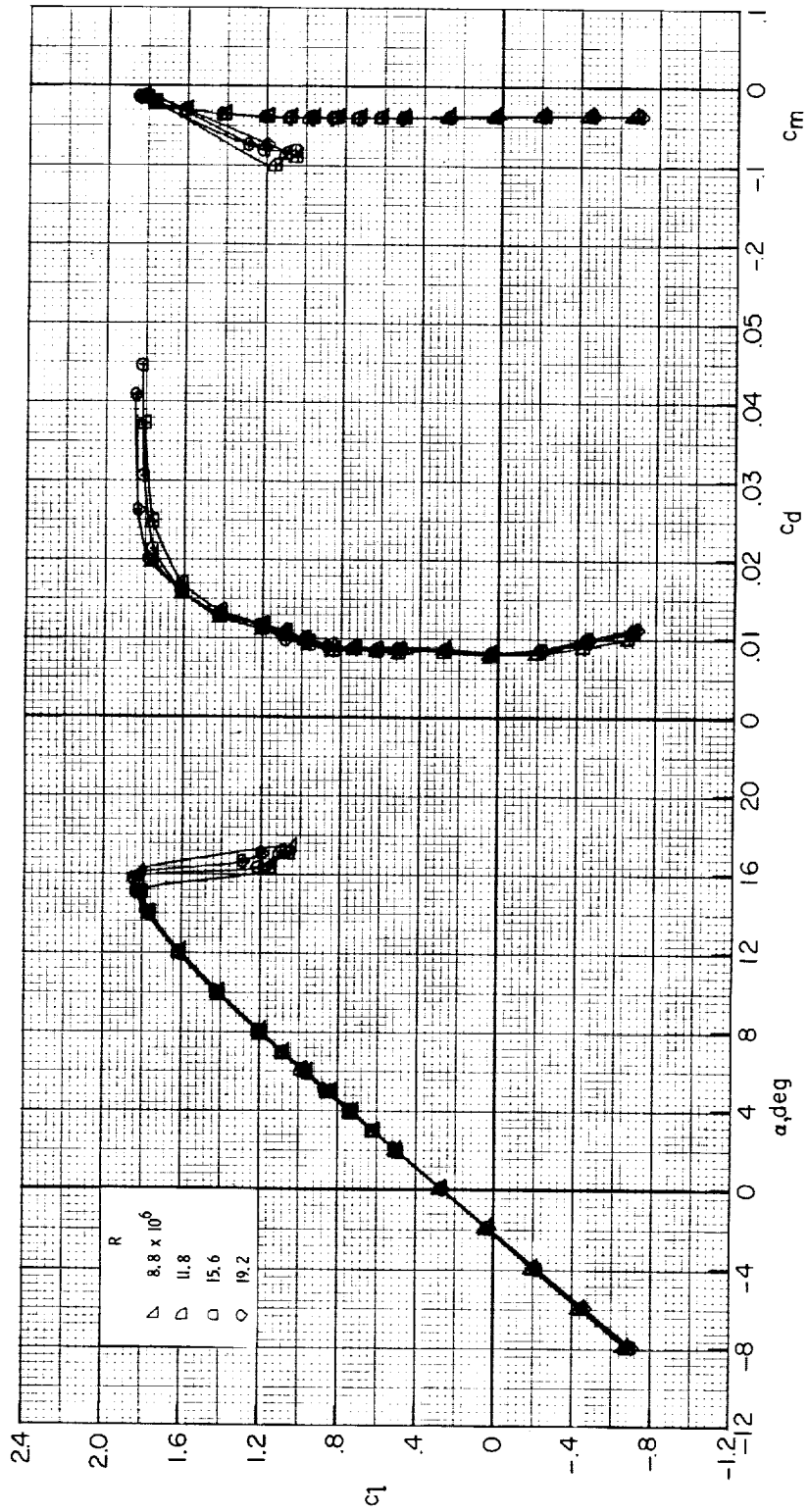
(b) Concluded.

Figure 10.- Continued.
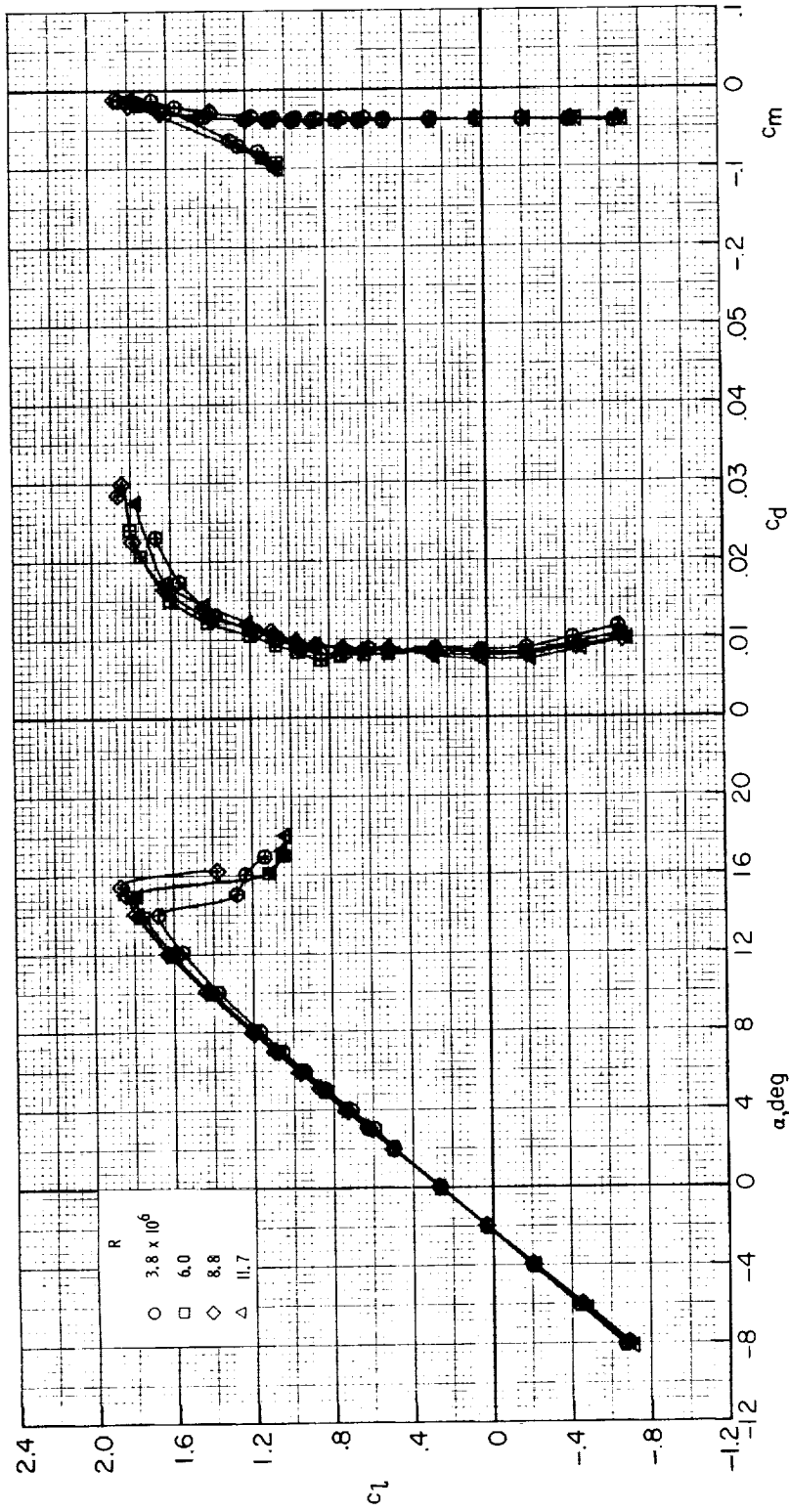
(c)   M = 0.28.

Figure 10.- Concluded.

35
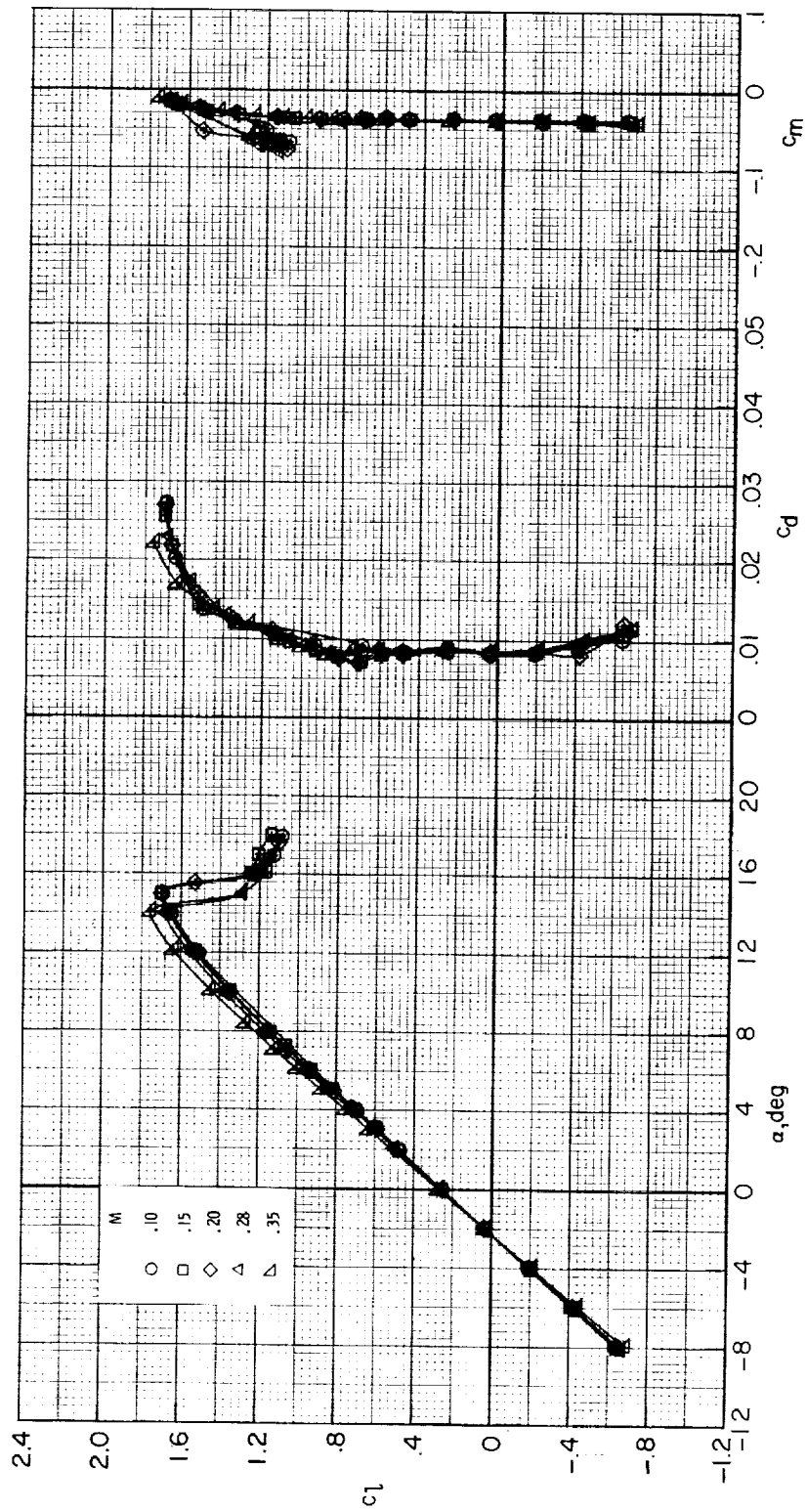
Figure 11.- Effect of Mach number on section characteristics of climb configuration. Model smooth; $R \approx 4.0 \times 10^6$.
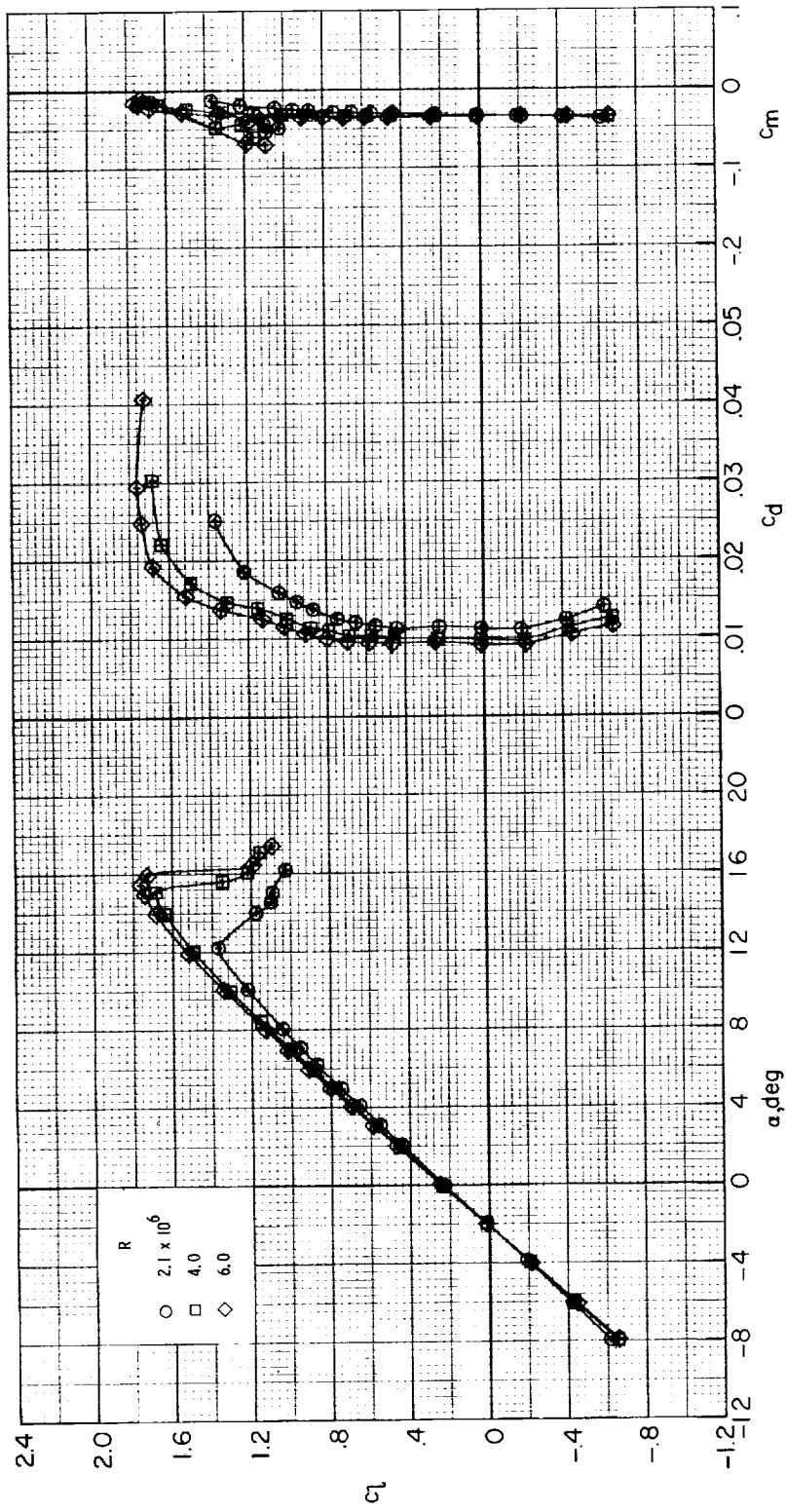
Figure 12.- Effect of Reynolds number on section characteristics of climb configuration.
Transition fixed at x/c = 0.05; M = 0.15.

37
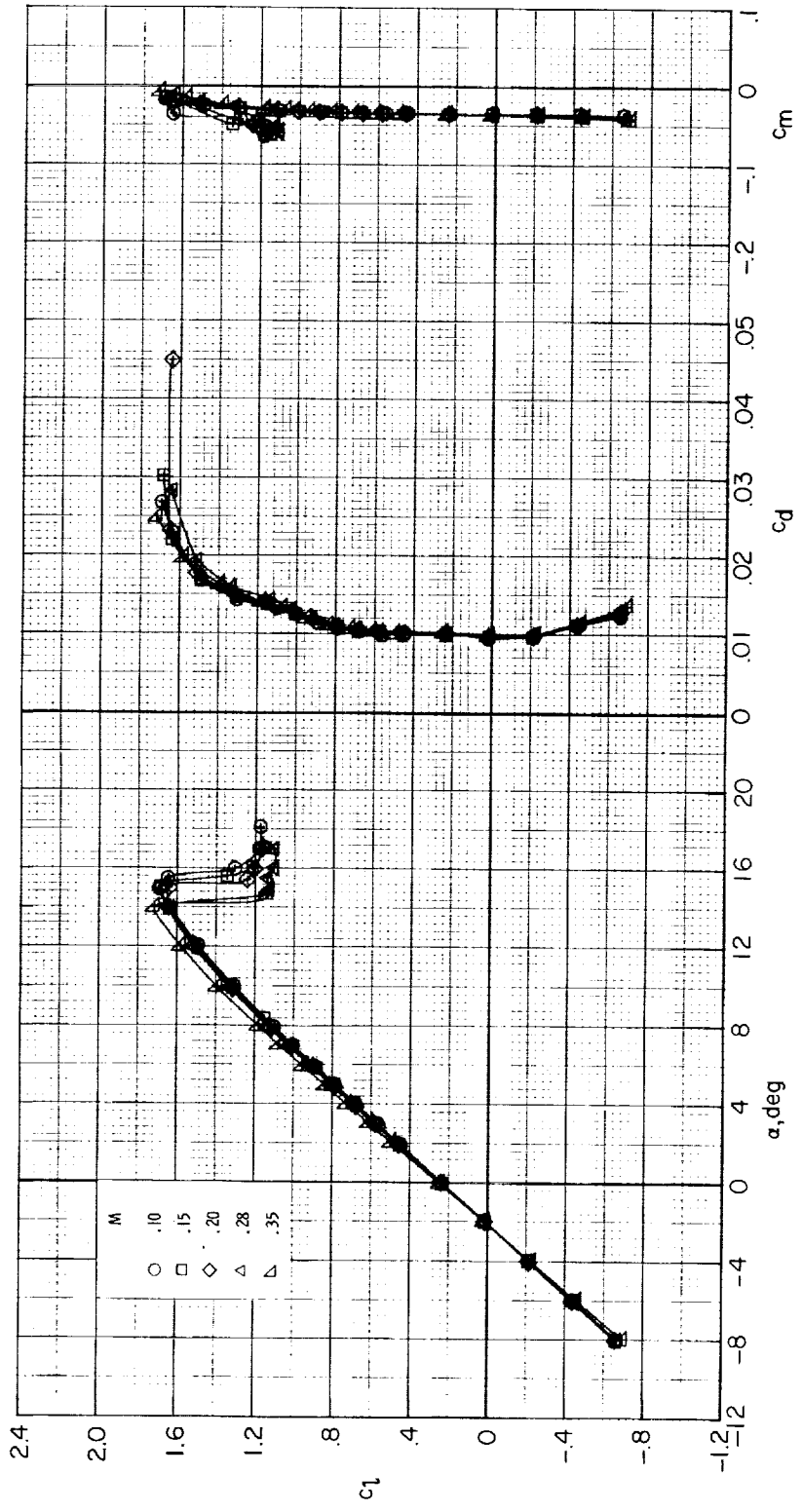
Figure 13.- Effect of Mach number on section characteristics of climb configuration. Transition fixed at $x/c = 0.05$; $R \approx 4.0 \times 10^6$.
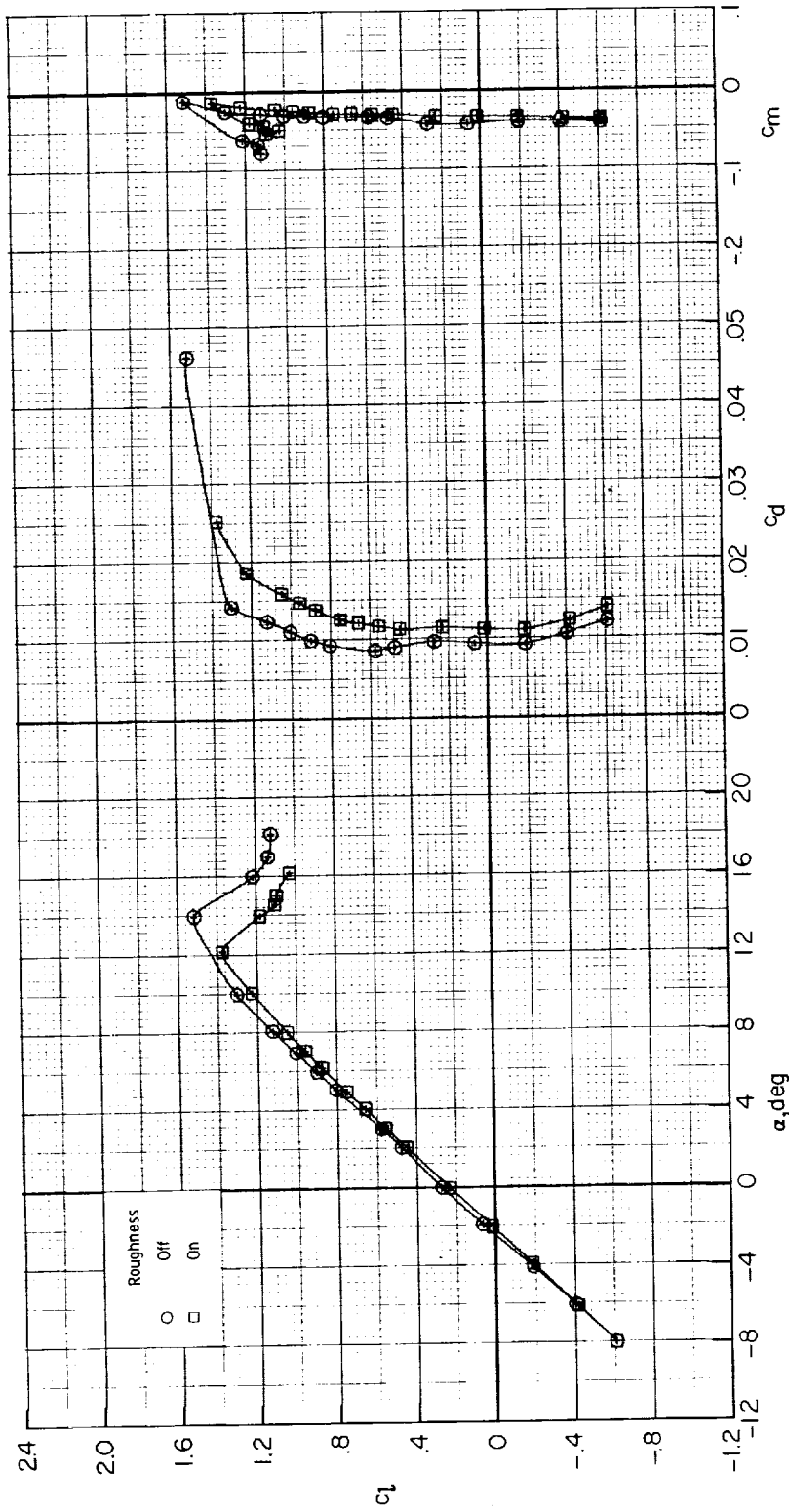
(a) R ≈ 2.1 × 10⁶.

Figure 14.- Effect of roughness on section characteristics of climb configuration.   M = 0.15.

39
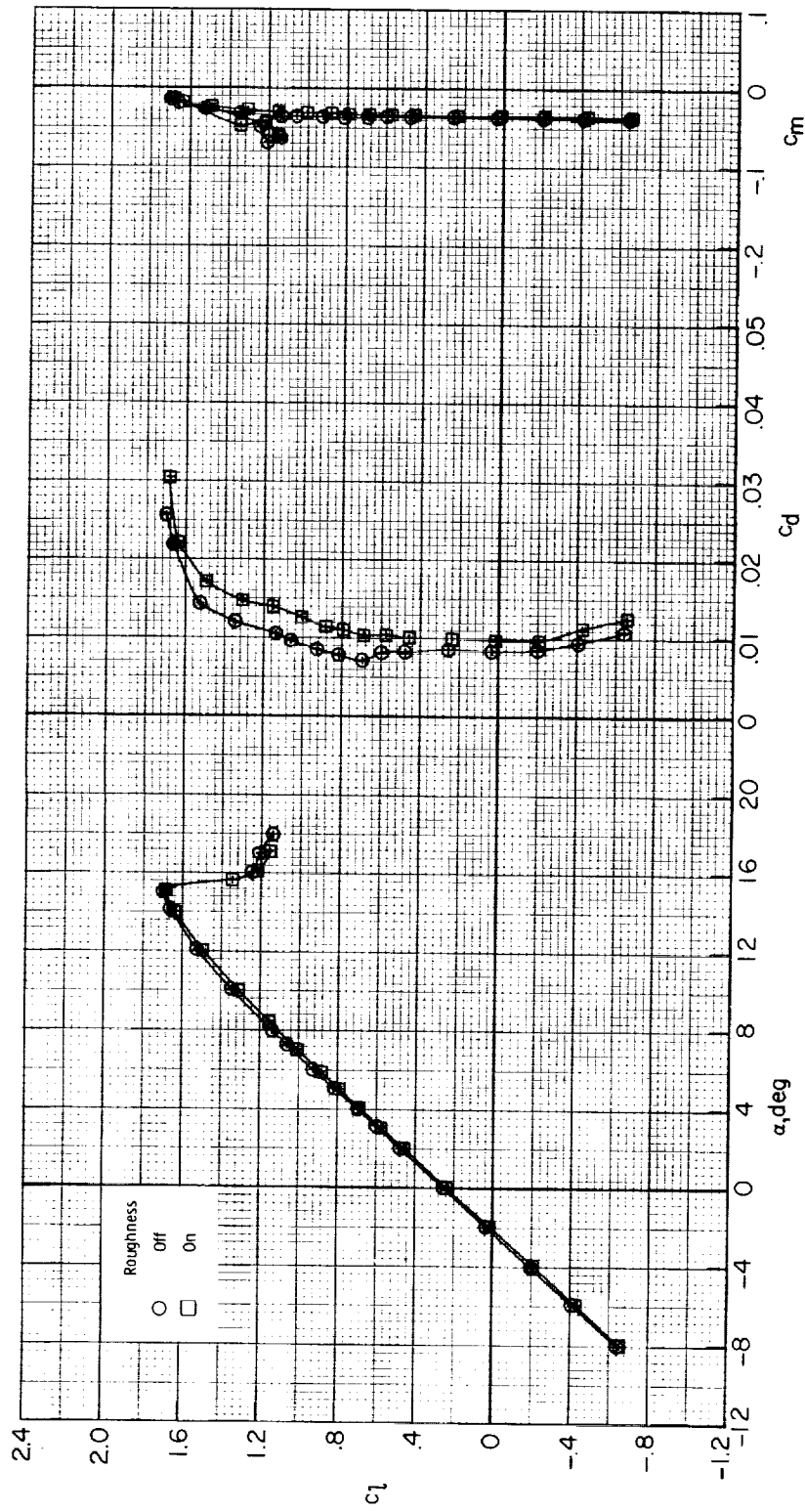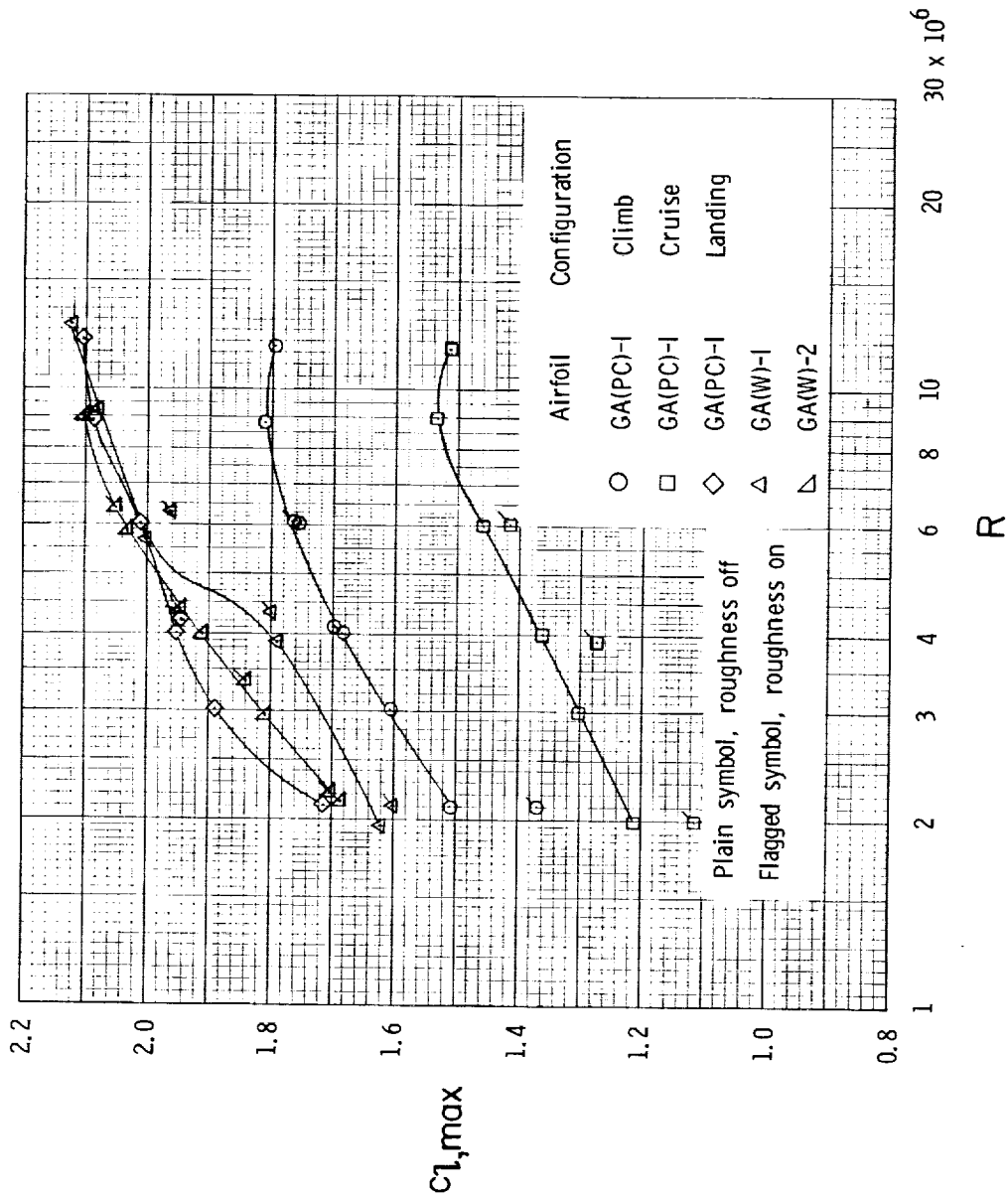
(b) $R \approx 4.0 \times 10^6$.

Figure 14.— Continued.

40
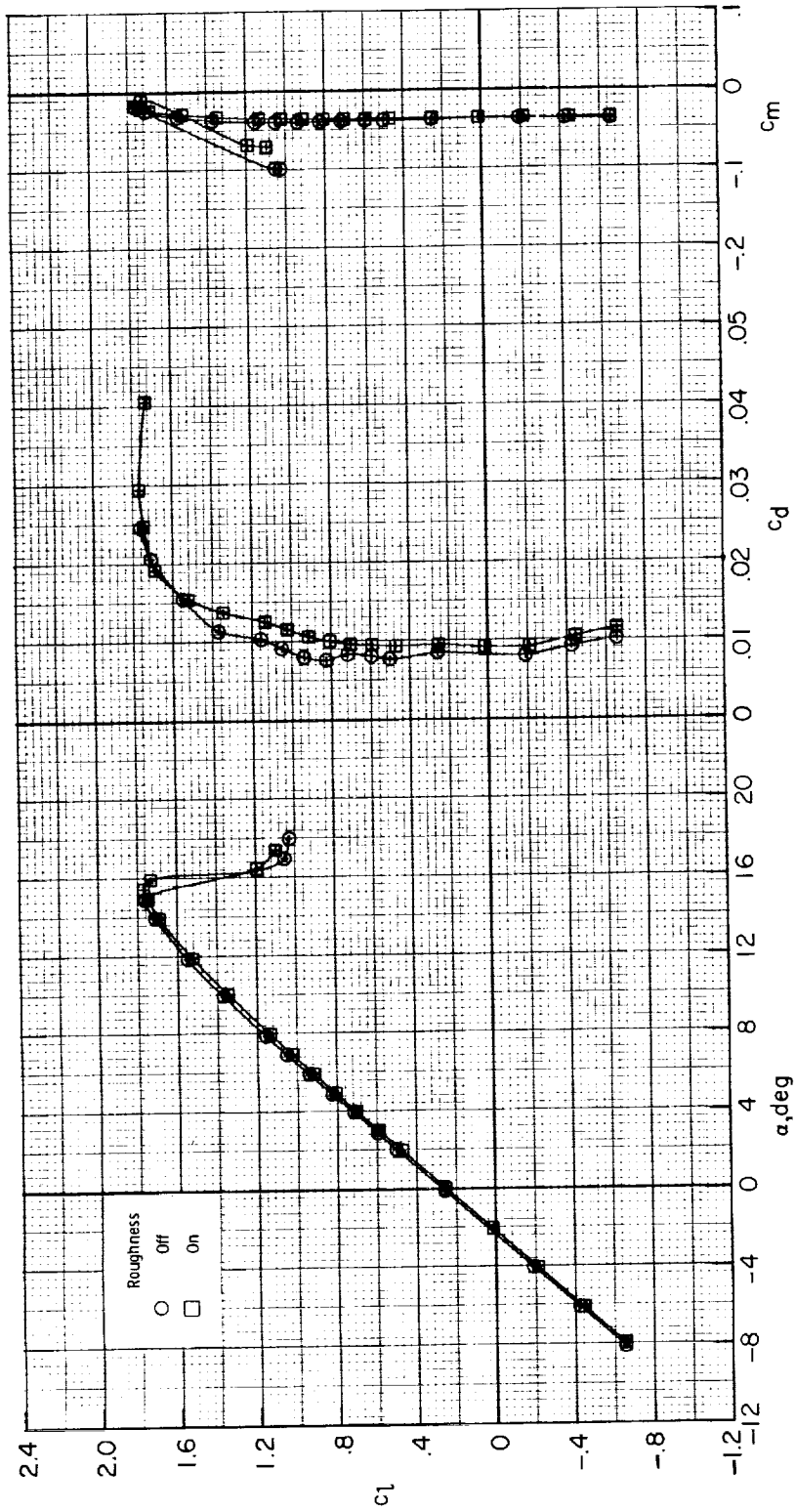
(c) $R \approx 6.0 \times 10^6$.

Figure 14.- Concluded.
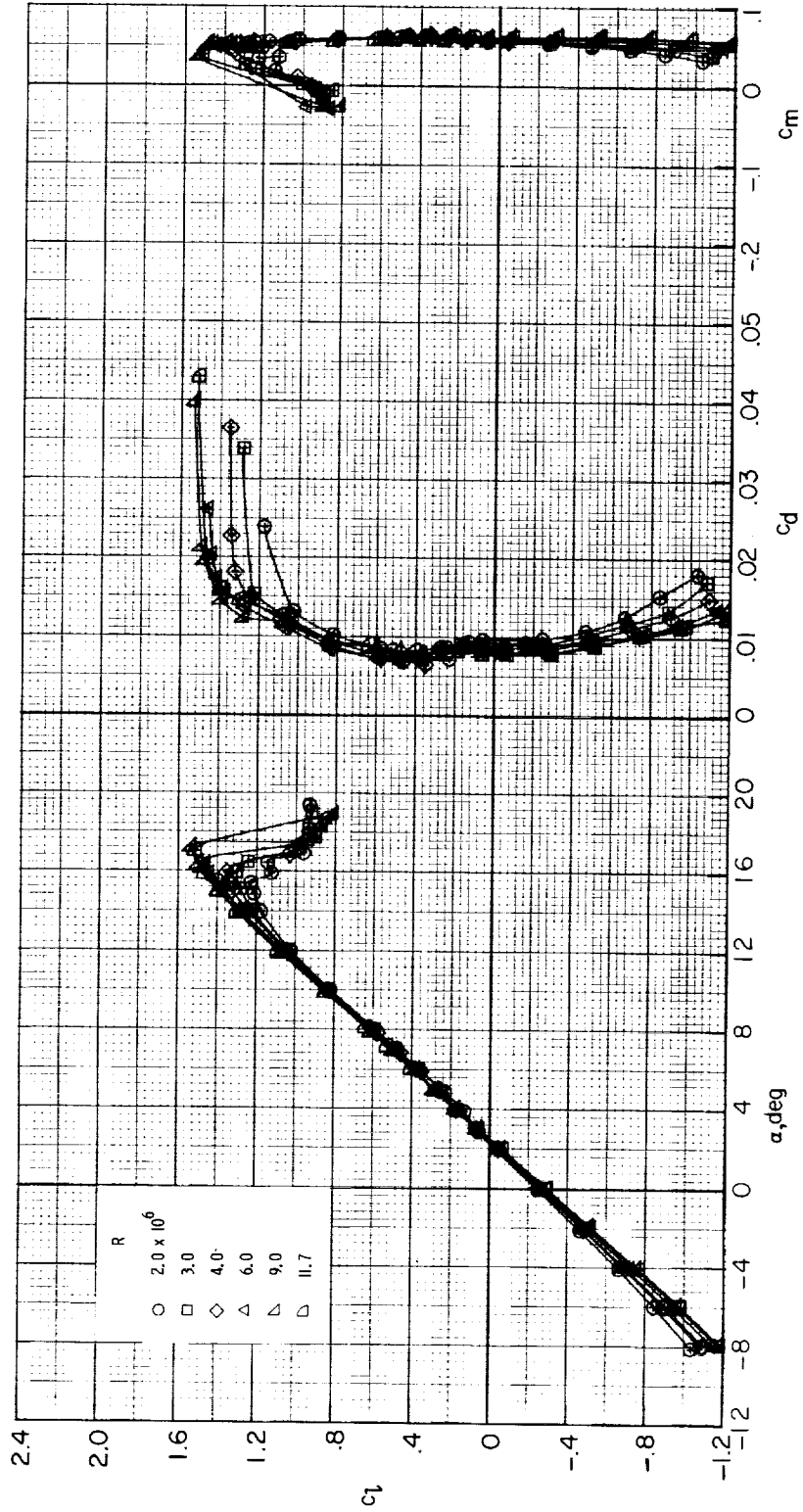
(a) M = 0.15.

Figure 15.- Effect of Reynolds number on section characteristics of cruise configuration. Model smooth.

42
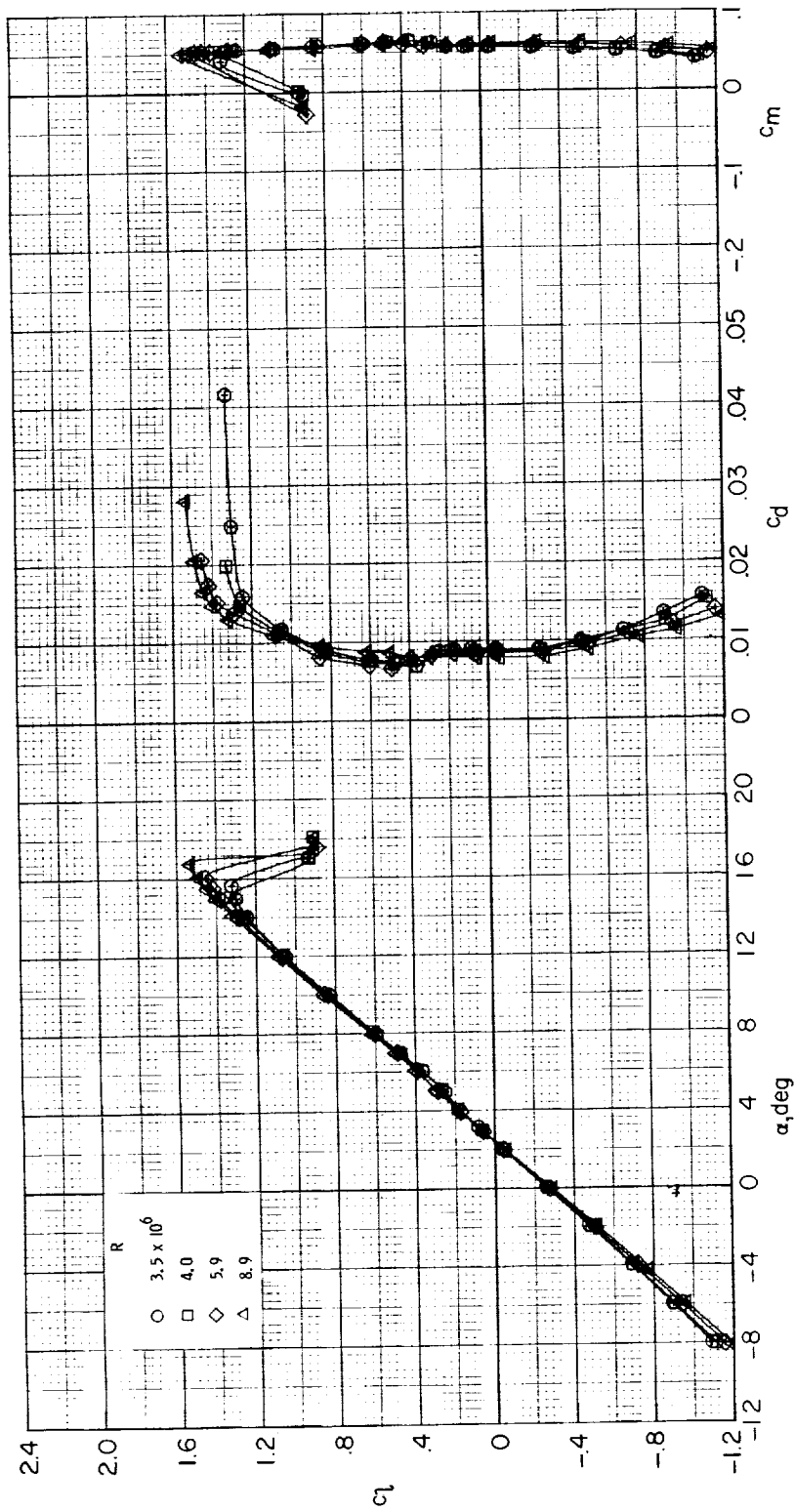
(b) M = 0.20.

Figure 15.- Continued.
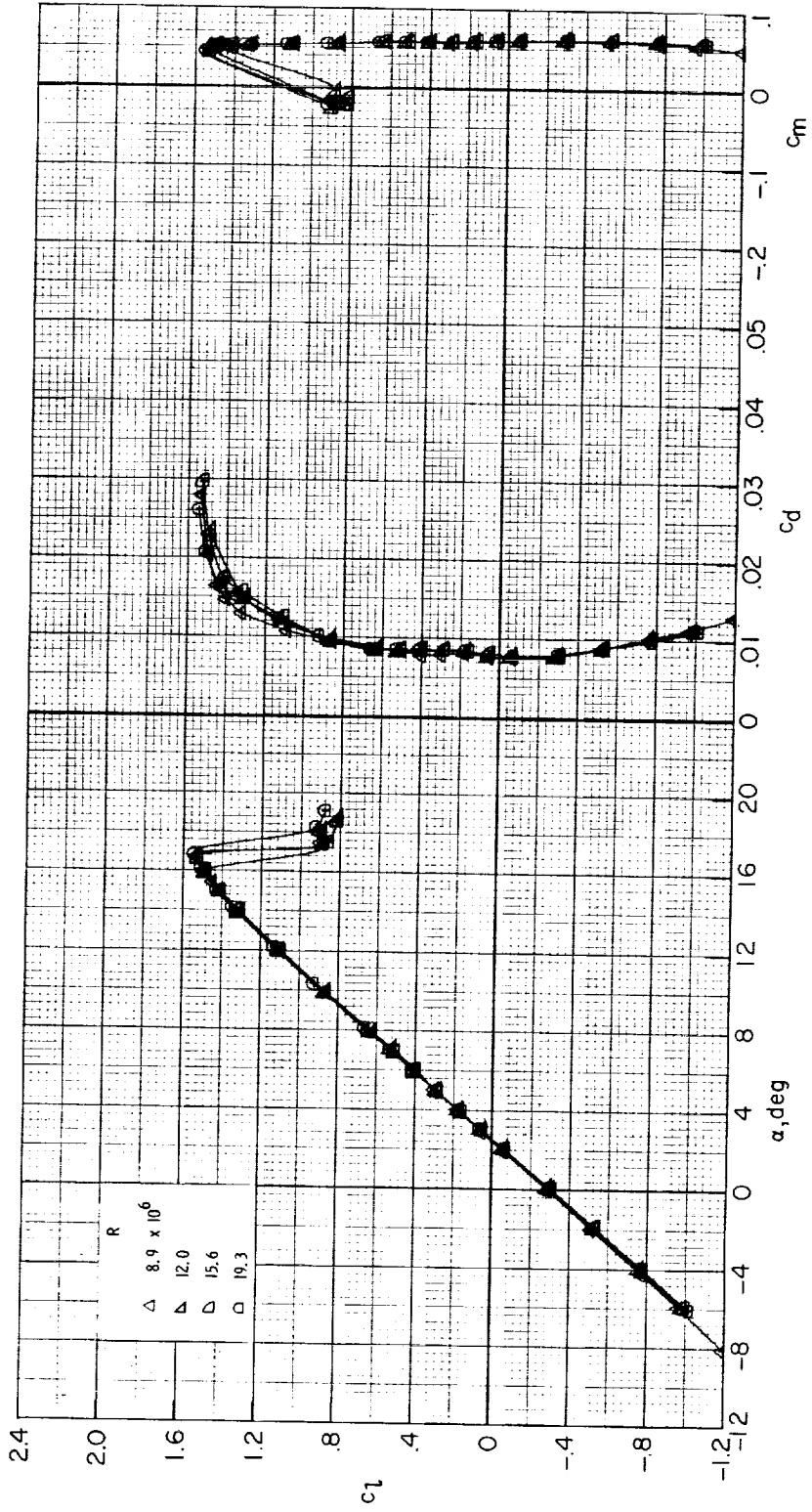
(b) Concluded.

Figure 15.- Continued.

44
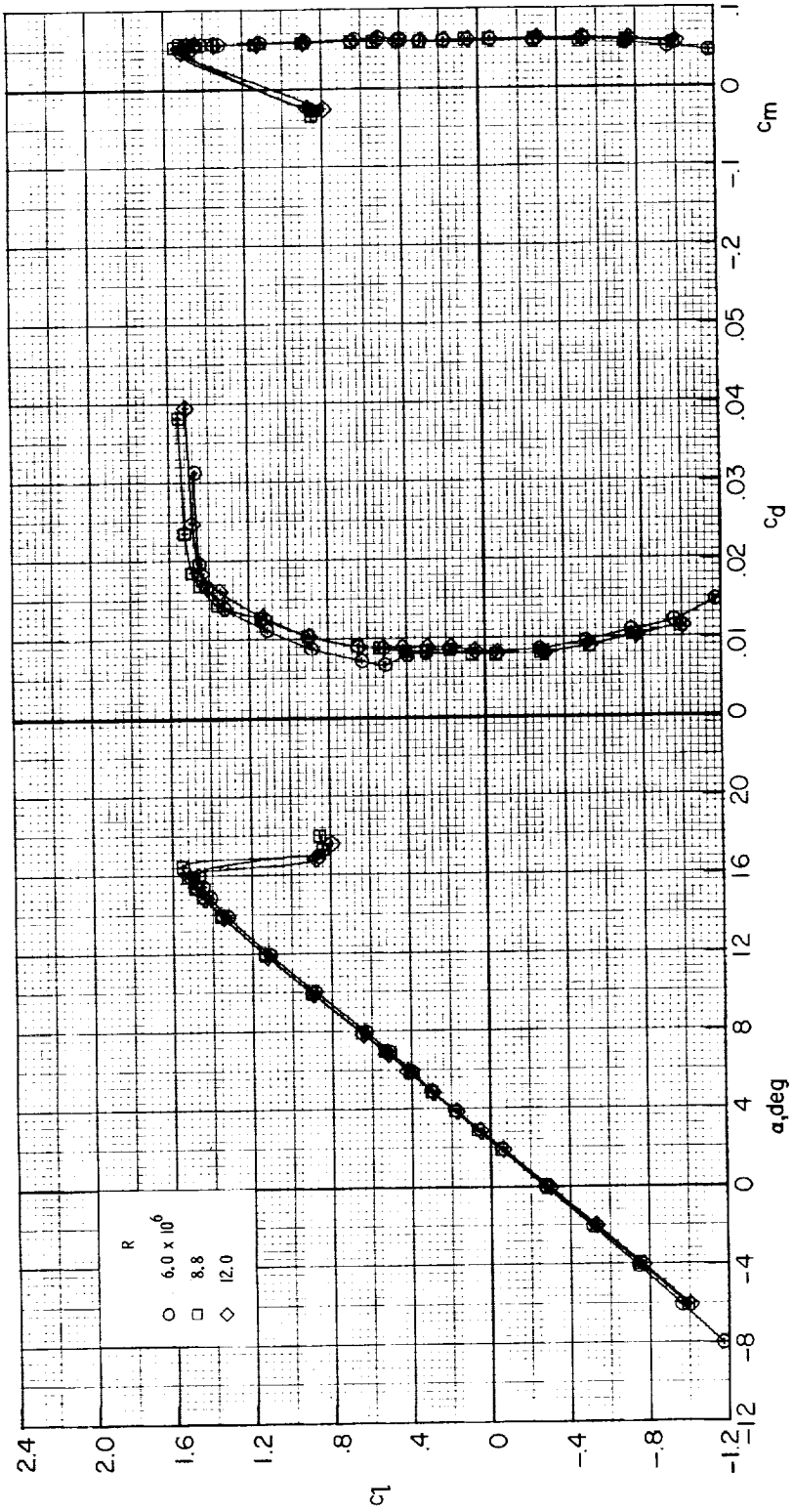
(c)   M = 0.28.

Figure 15.- Concluded.
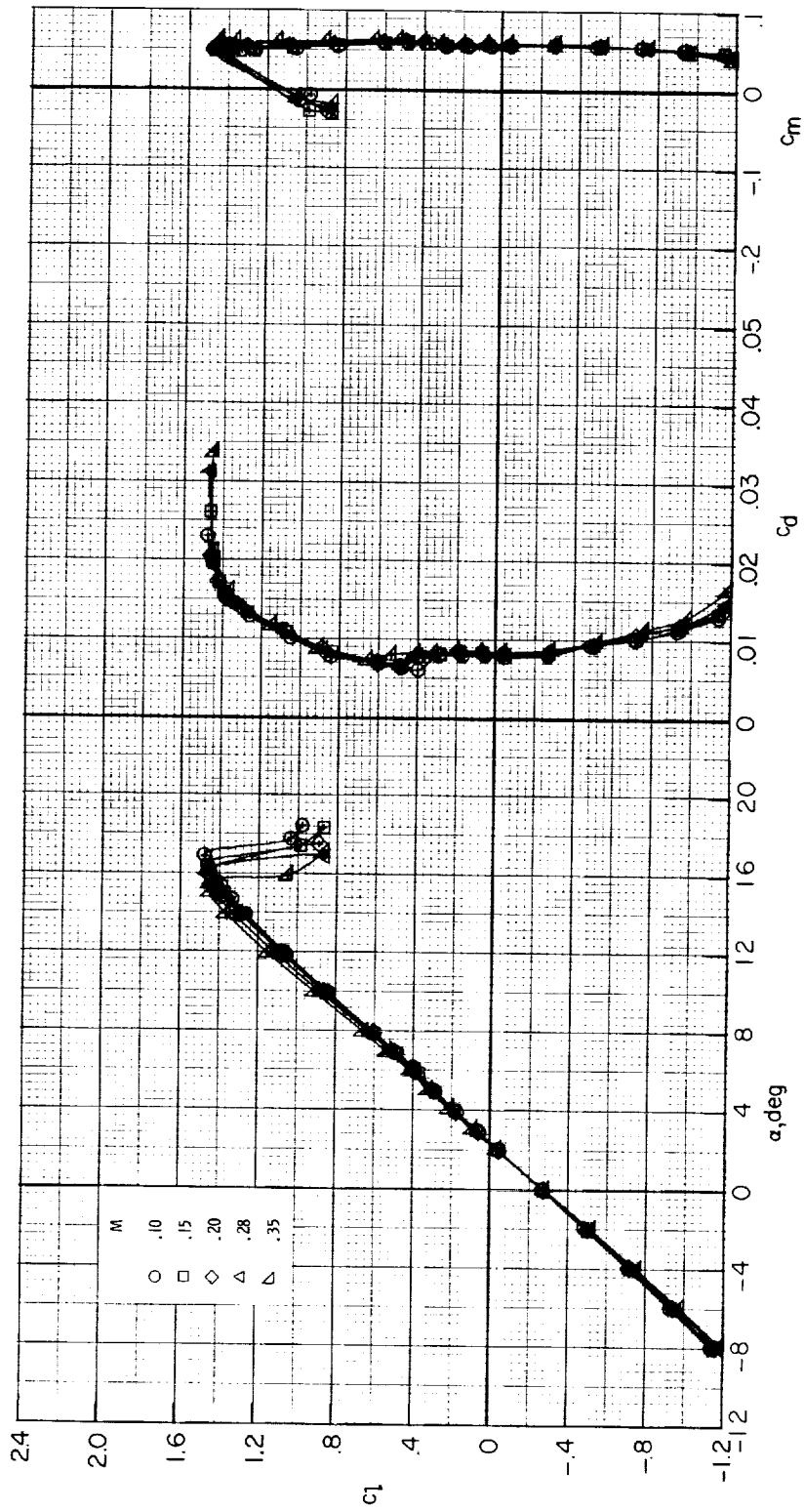
Figure 16.– Effect of Mach number on section characteristics of cruise configuration. Model smooth; $R \approx 6.0 \times 10^6$.
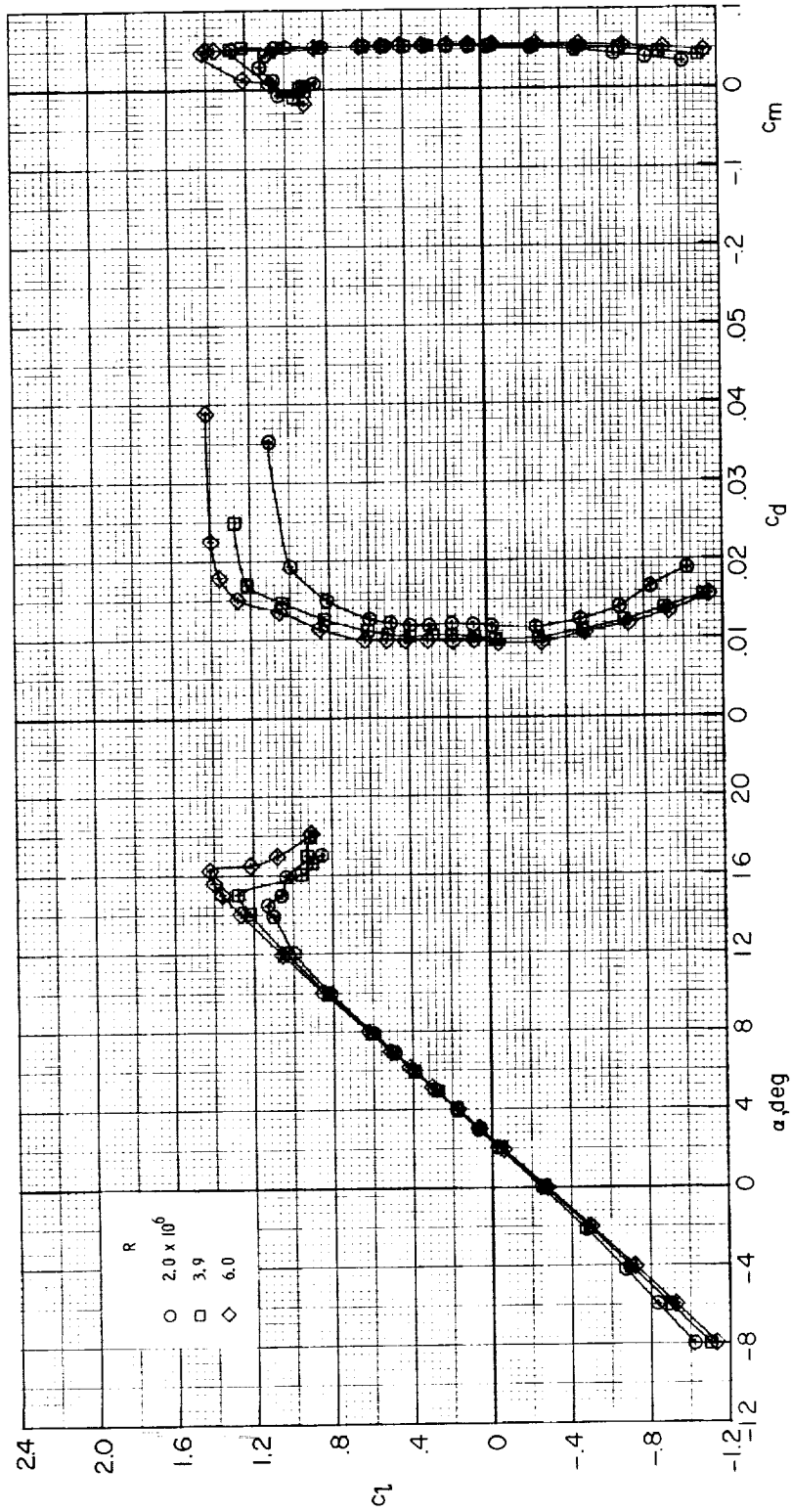
Figure 17.- Effect of Reynolds number on section characteristics of cruise configuration. Transition fixed at x/c = 0.05; M = 0.15.
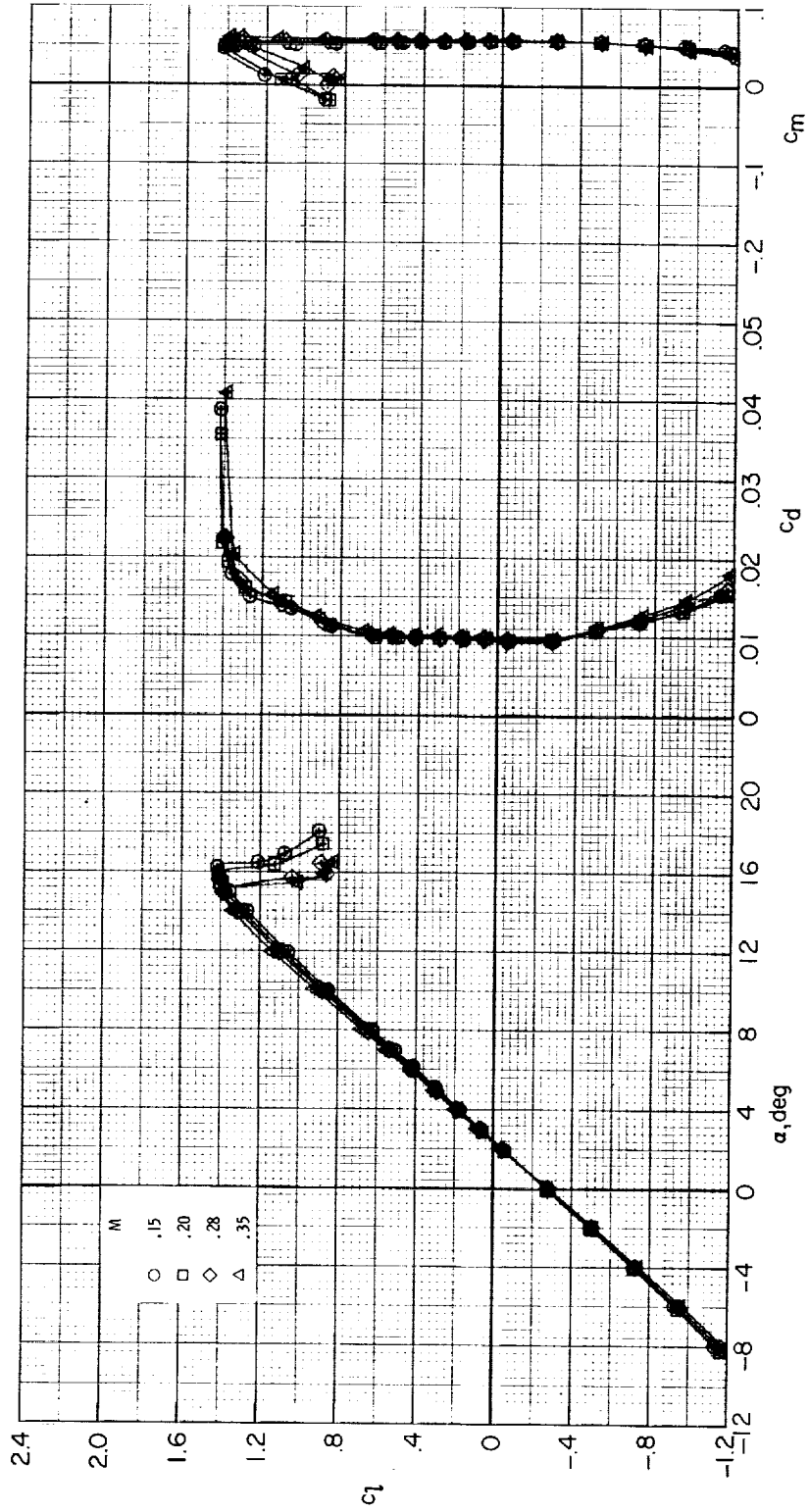
Figure 18.- Effect of Mach number on section characteristics of cruise configuration. Transition fixed at $x/c = 0.05$; $R \approx 6.0 \times 10^6$.

48
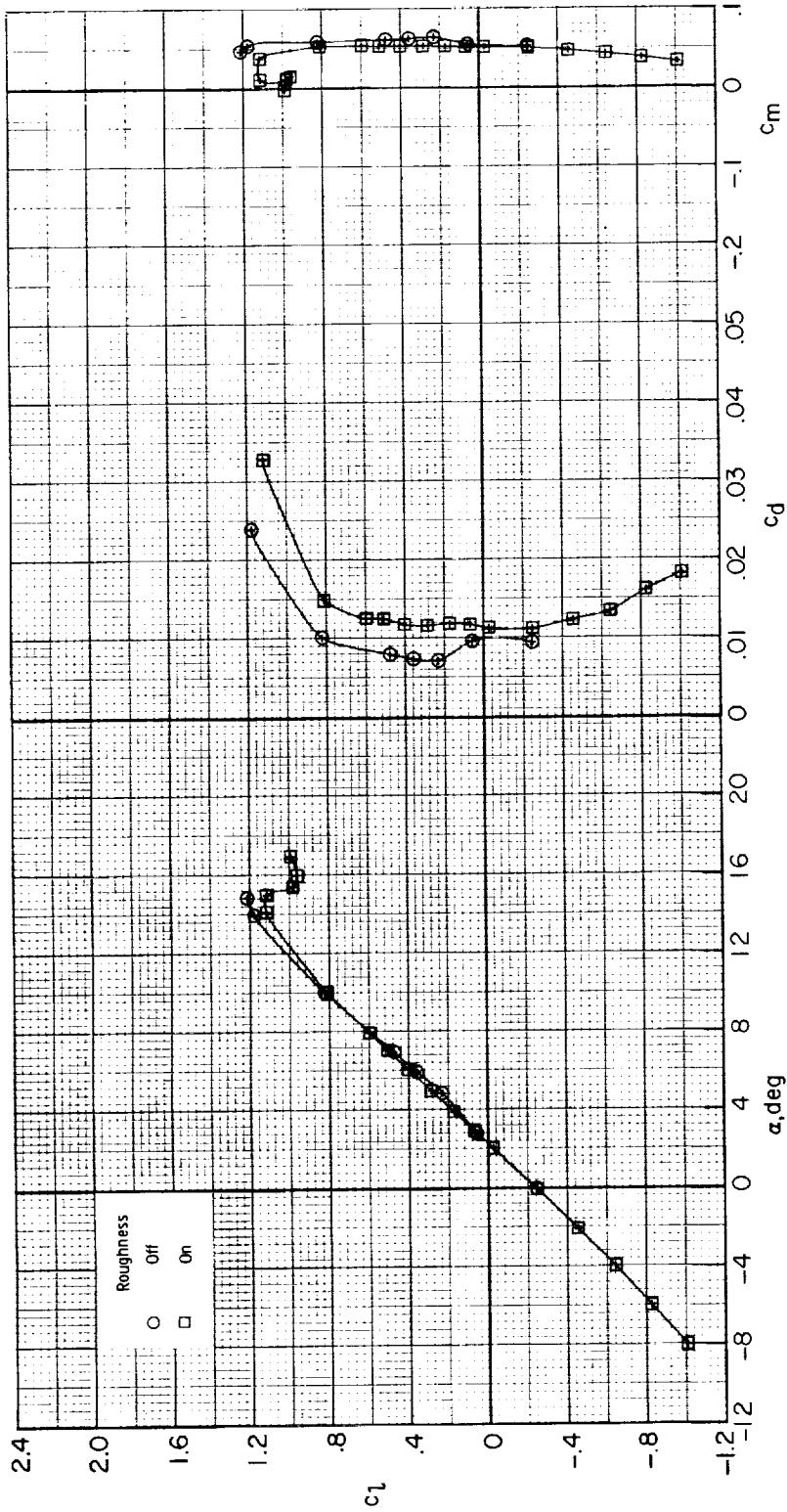
(a) $R \approx 2.0 \times 10^6$.

Figure 19.- Effect of roughness on section characteristics of cruise configuration. $M = 0.15$.
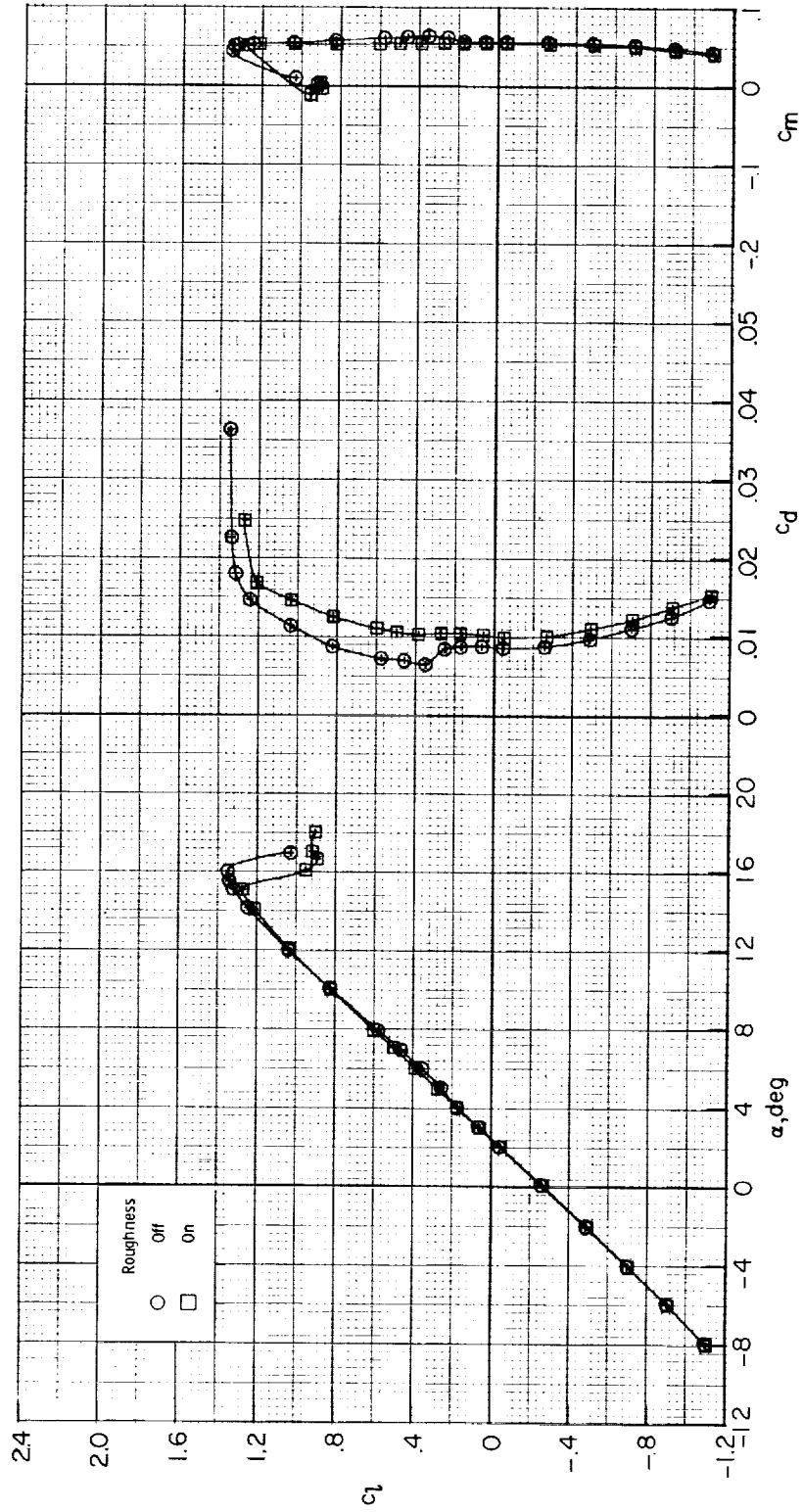
(b) $R \approx 4.0 \times 10^6$.

Figure 19.- Continued.
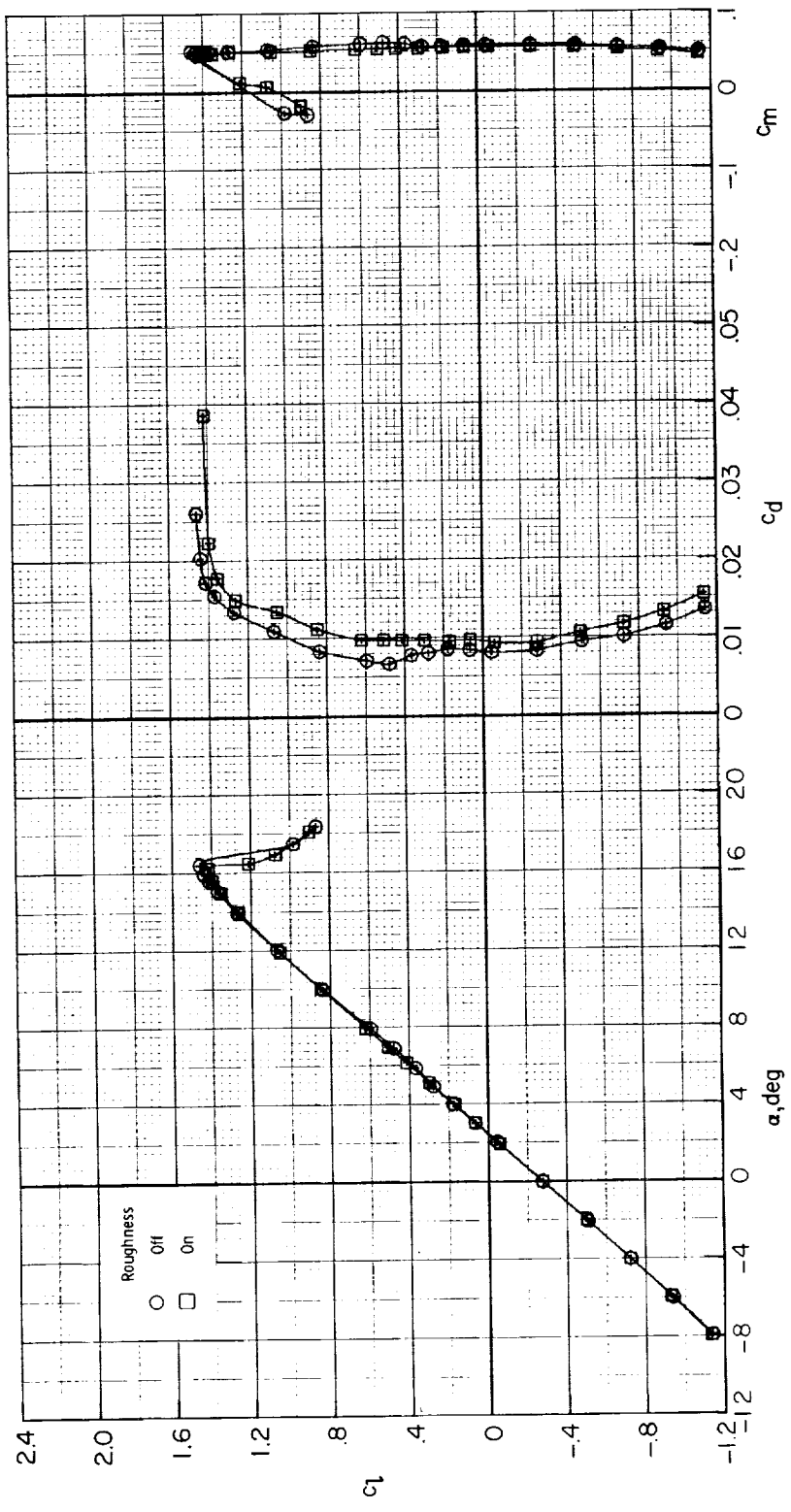
(c) R ≈ 6.0 × 10^6.

Figure 19.– Concluded.

51
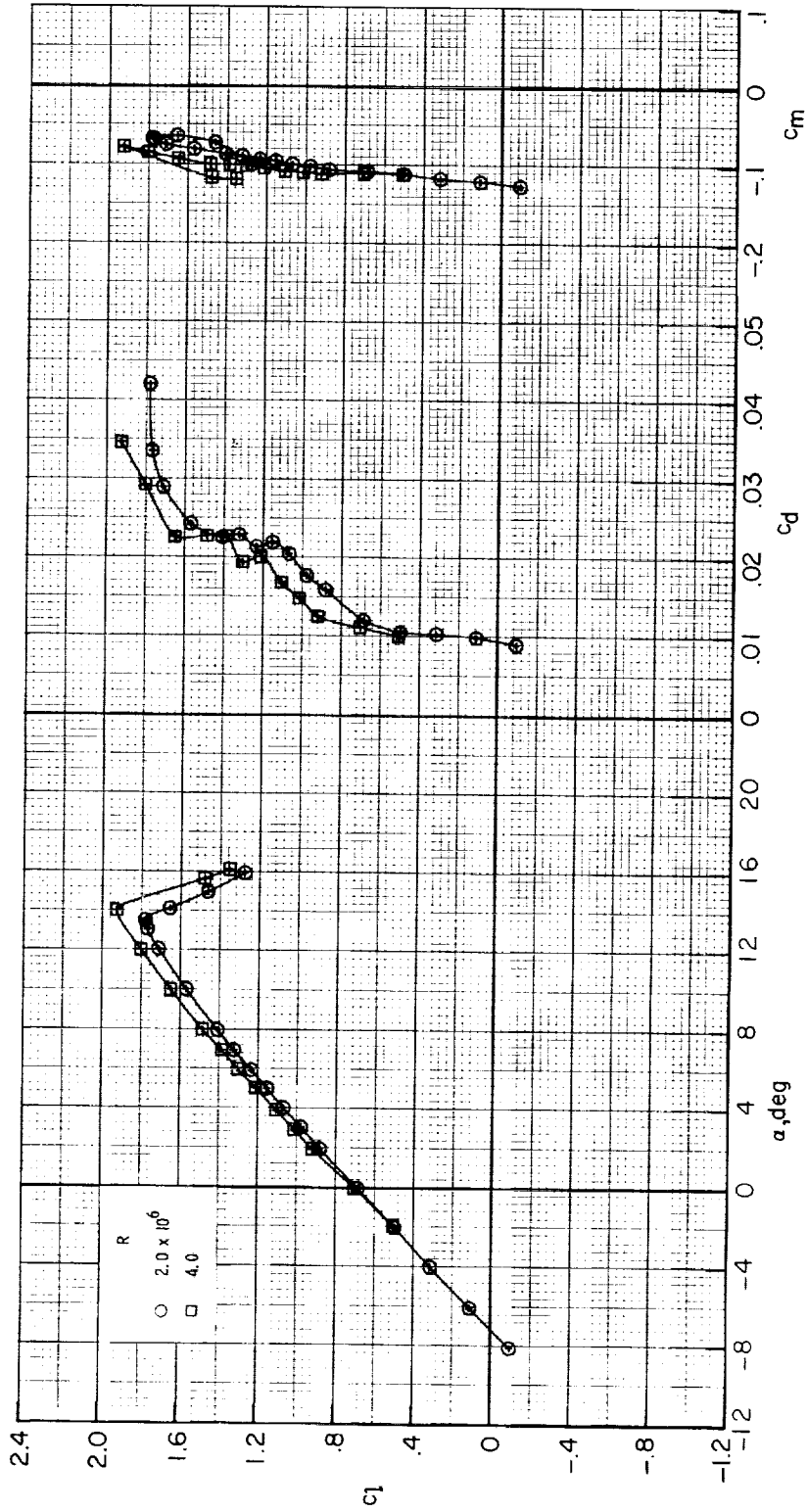
(a) M = 0.10.

Figure 20.- Effect of Reynolds number on section characteristics of landing configuration. Model smooth.
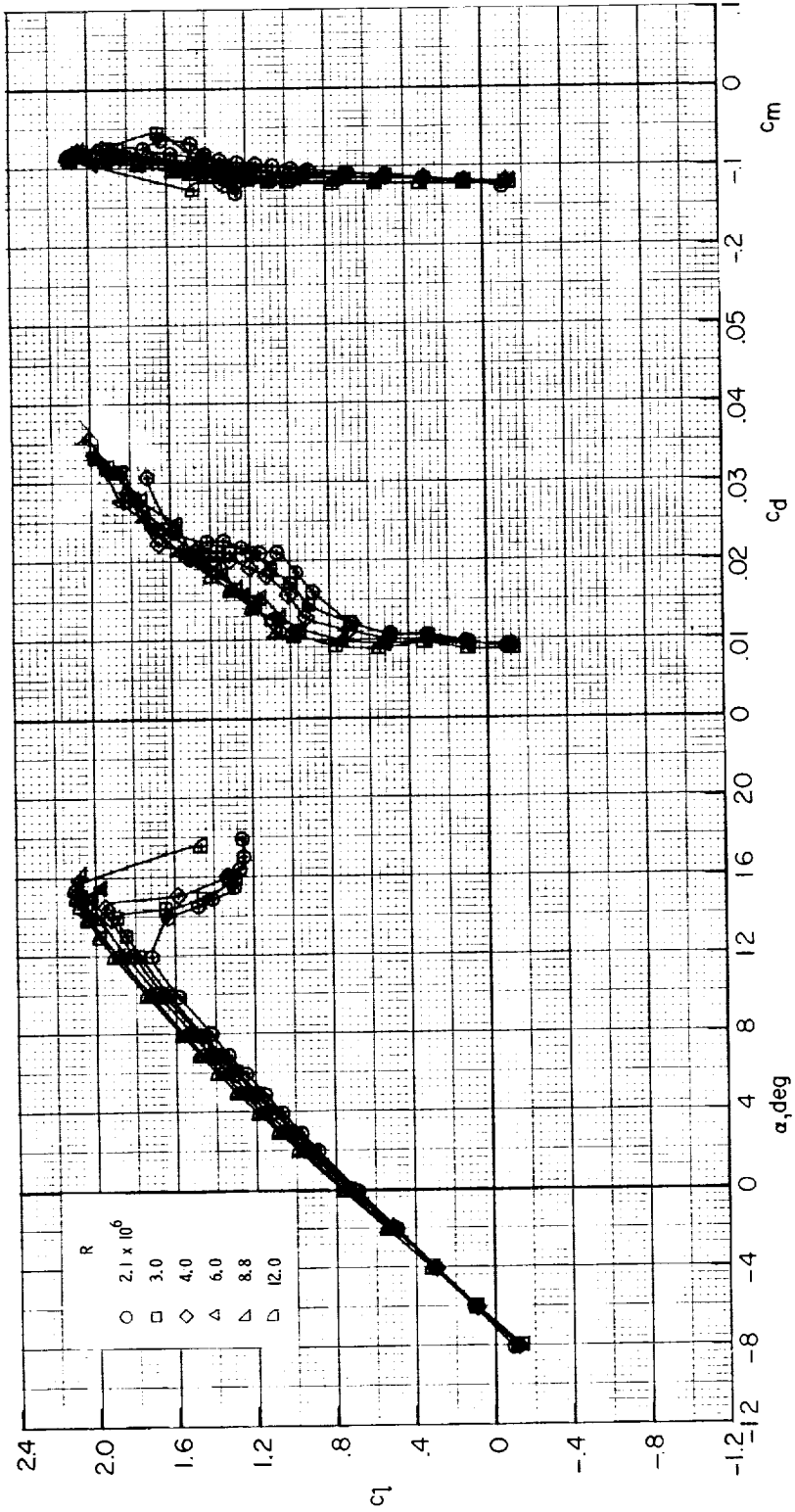
(b) M = 0.15.

Figure 20.- Concluded.
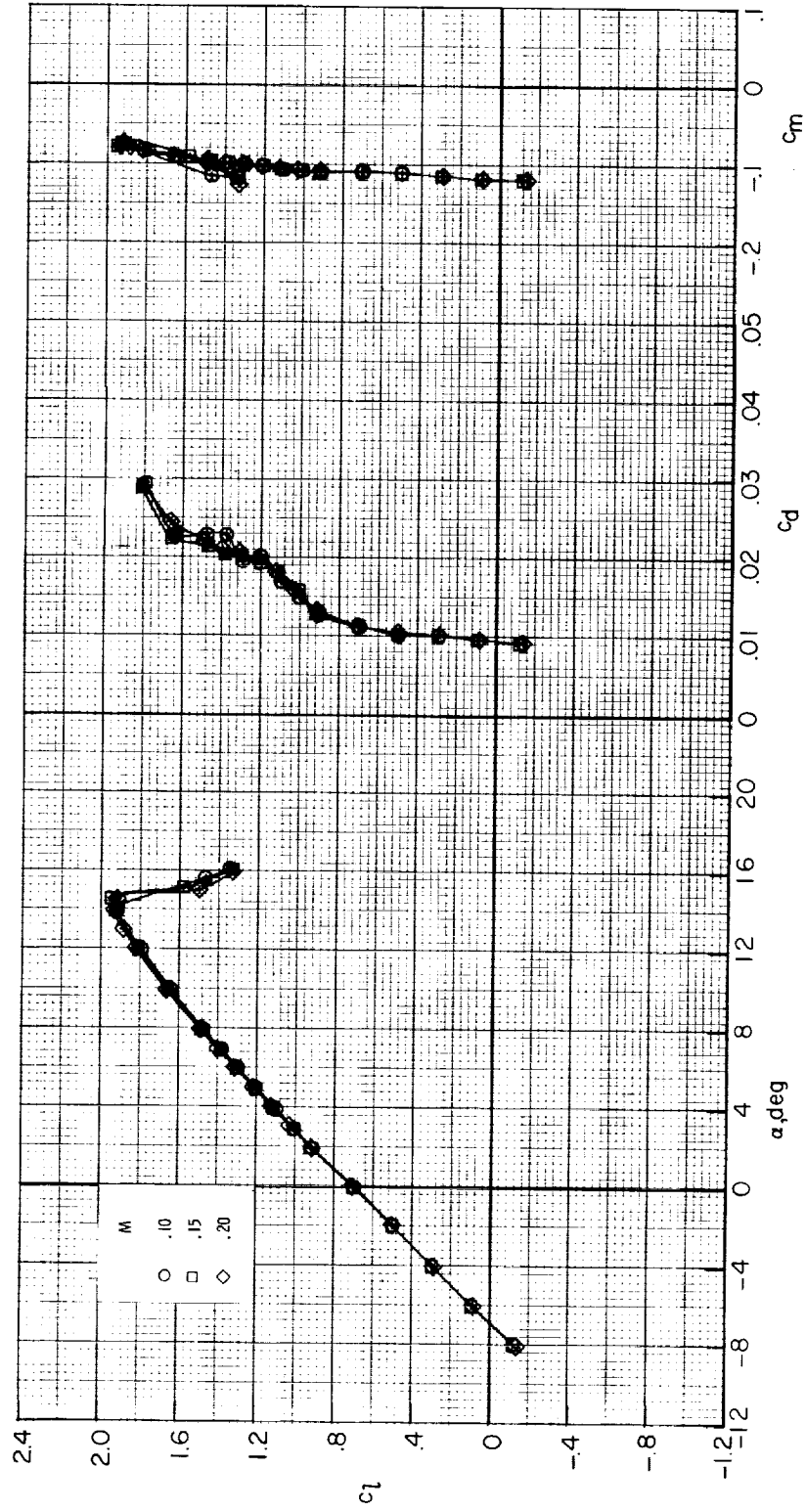
Figure 21.- Effect of Mach number on section characteristics of landing configuration. Model smooth; $R \approx 4.0 \times 10^6$.
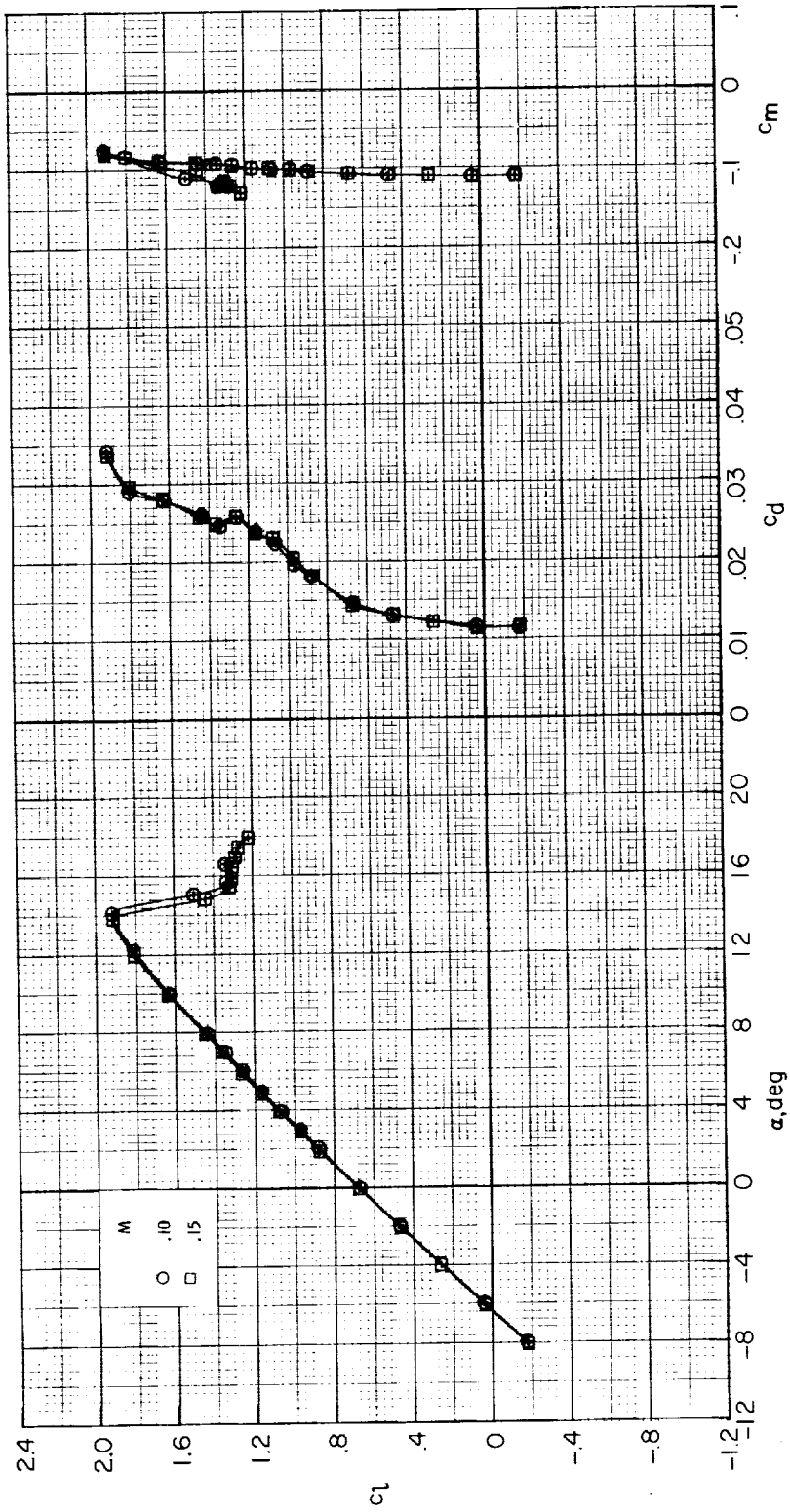
Figure 22.- Effect of Mach number on section characteristics of landing configuration. Transition fixed at $x/c = 0.05$; $R \approx 4.0 \times 10^6$.
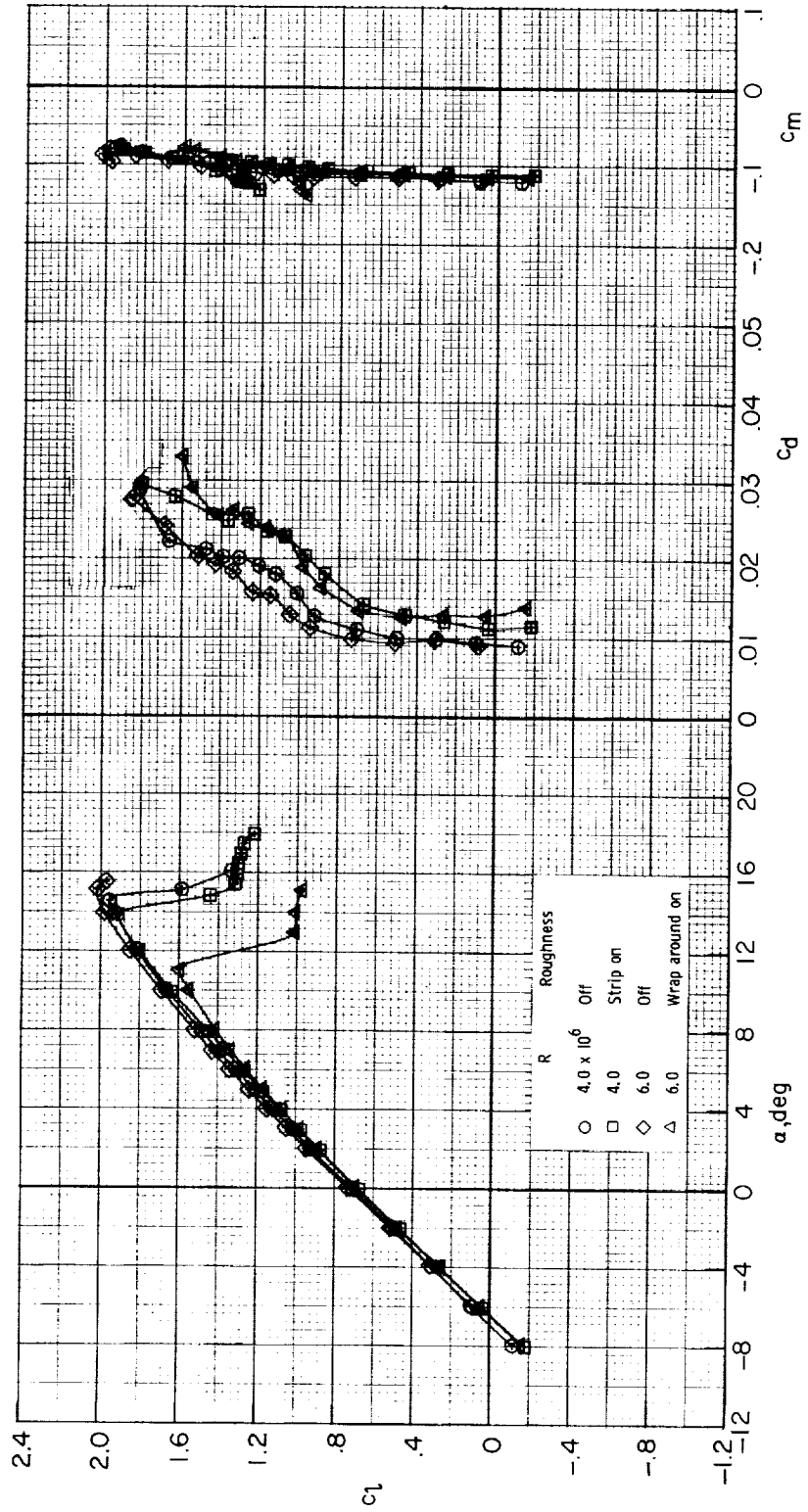
Figure 23.- Effect of roughness on section characteristics of landing configuration. M = 0.15.
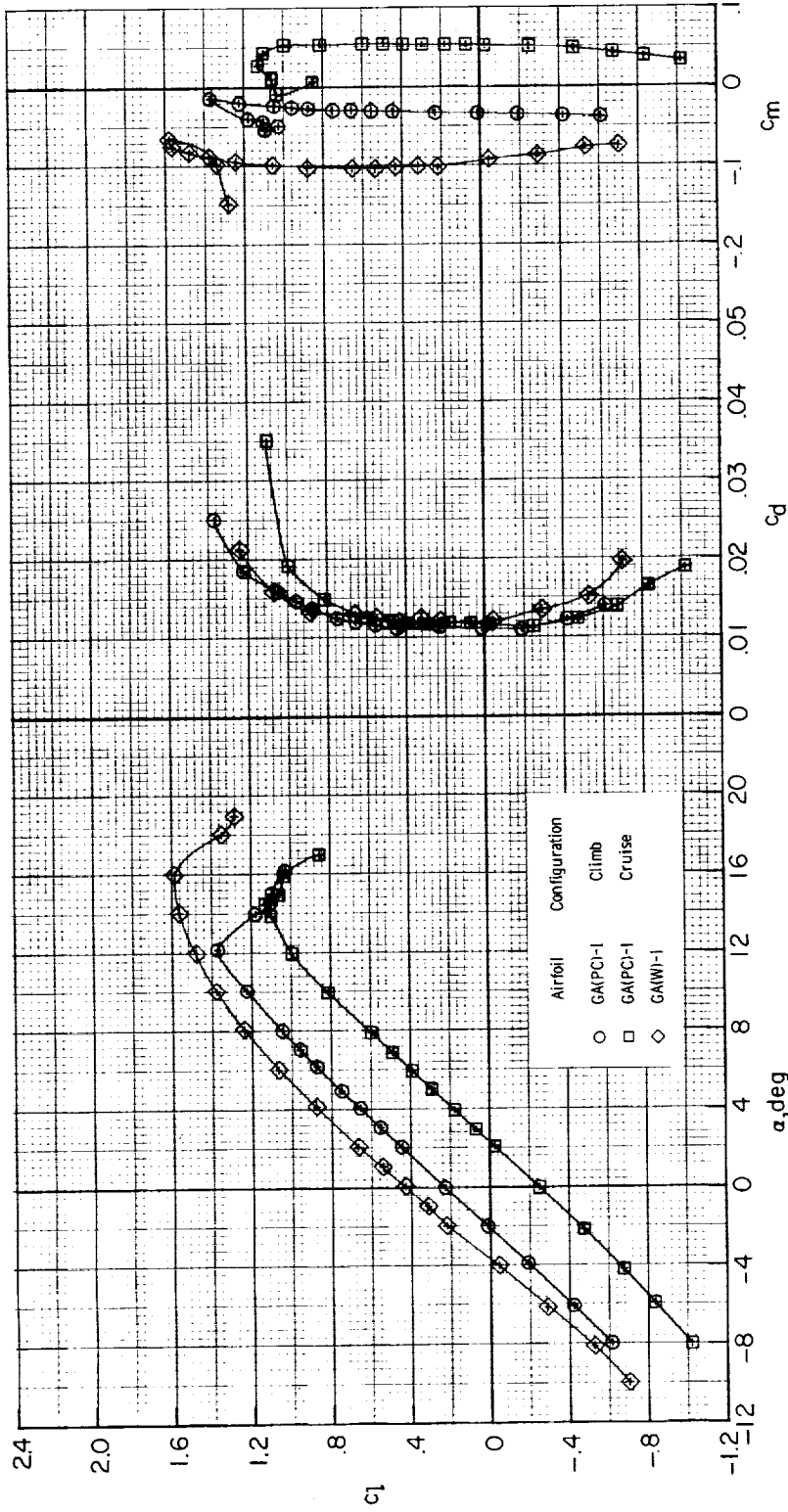
(a) R ≈ 2.0 × 10^6.

Figure 24.- Comparison of section characteristics for NASA GA(PC)-1 and NASA GA(W)-1 airfoils.
Transition fixed; M = 0.15.

57
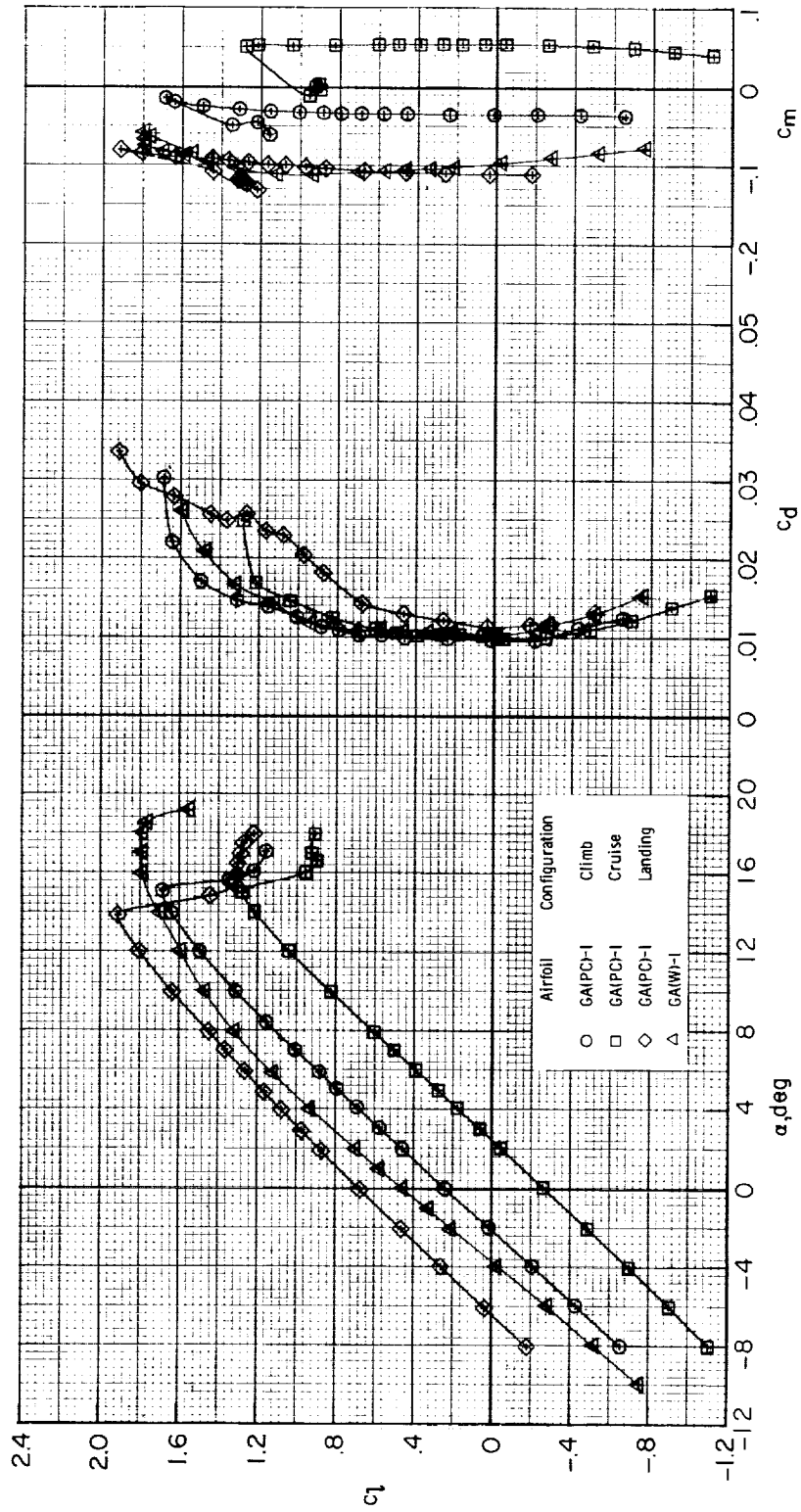
(b) R ≈ 4.0 × 10⁶.

Figure 24.- Continued.

58
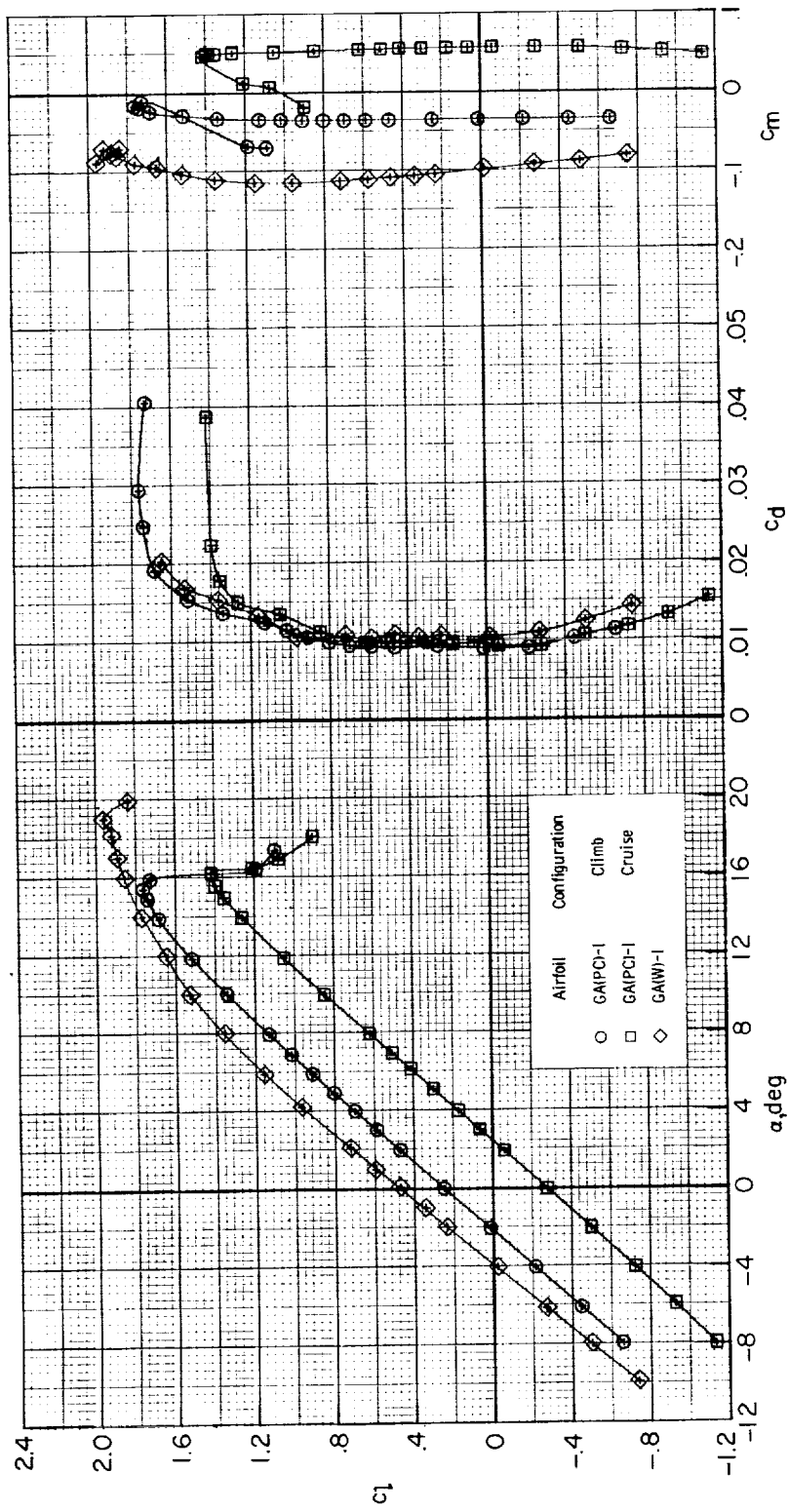
(c) $R \approx 6.0 \times 10^6$.

Figure 24.- Concluded.

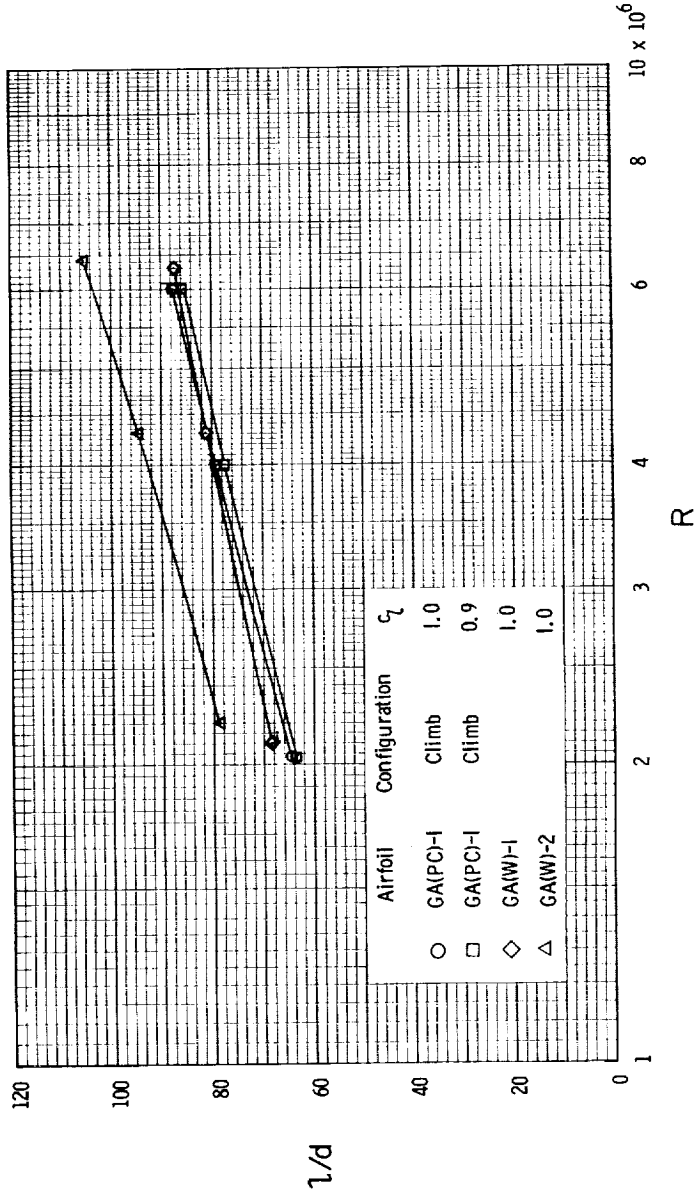(a) M = 0.15.

Figure 25.- Variation of maximum section lift coefficient with Reynolds number for NASA GA(PC)-1, NASA GA(W)-1, and NASA GA(W)-2 airfoils.

60
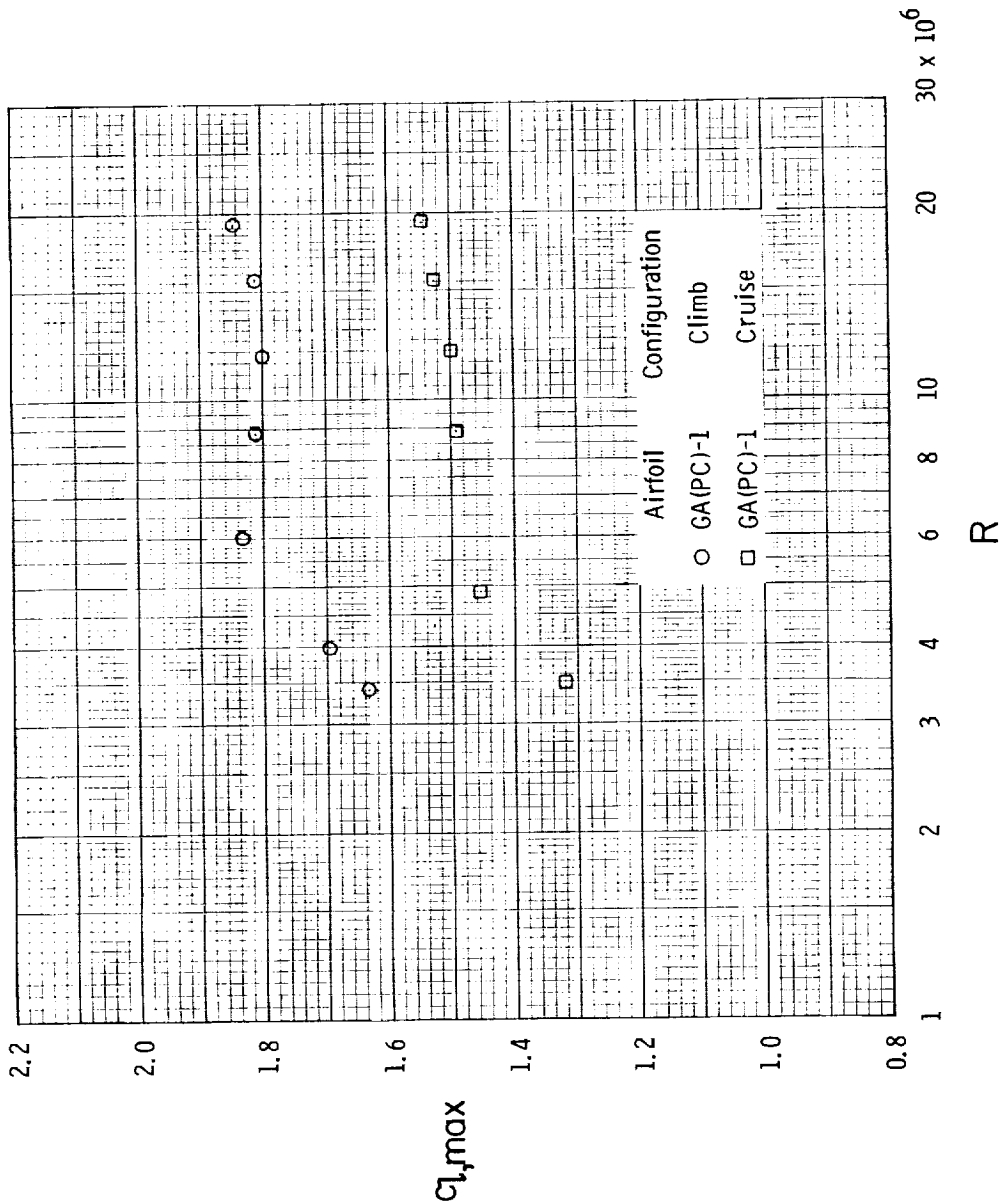
(b) M = 0.20.

Figure 25.- Continued.
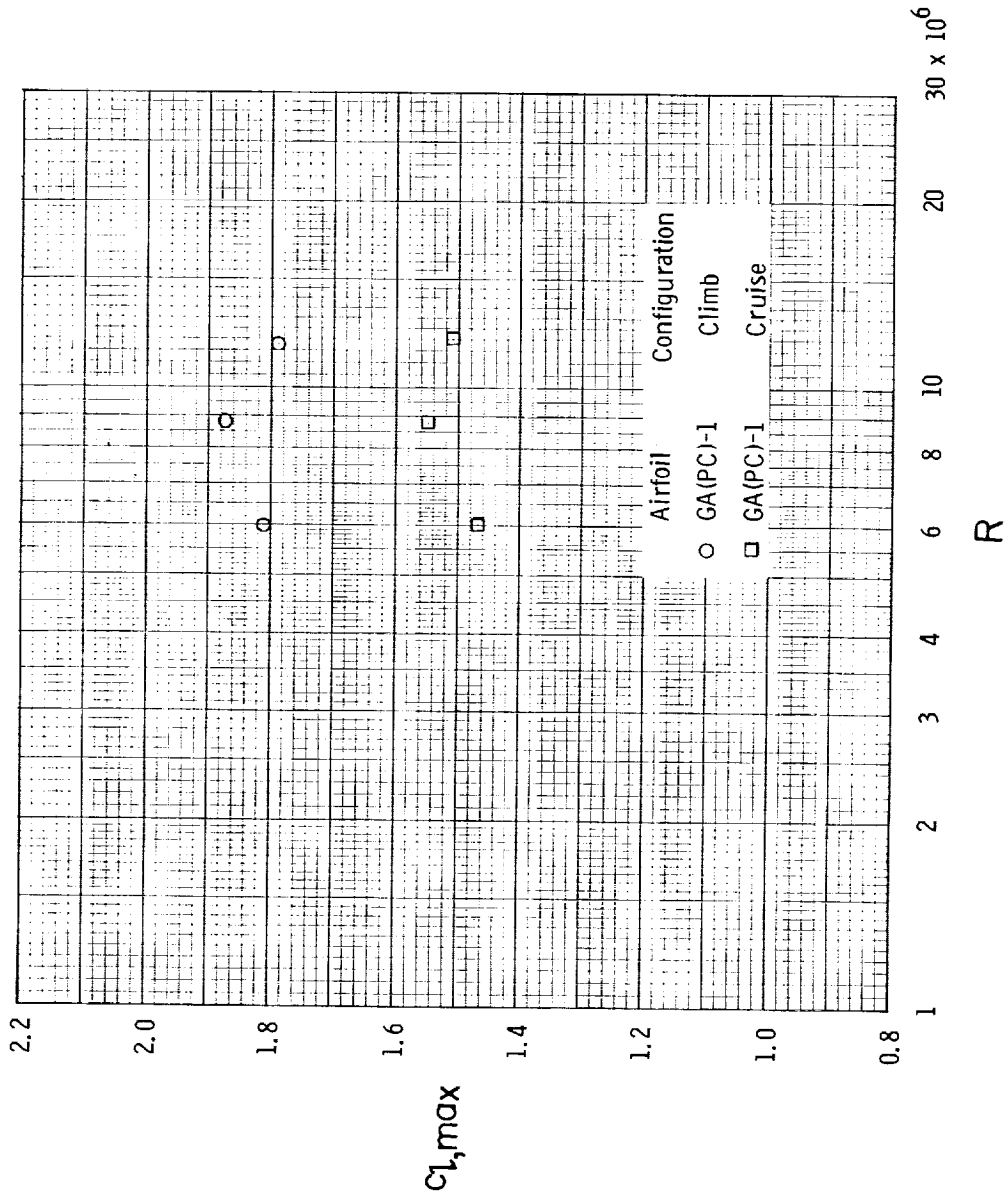
(c)   M = 0.28.

Figure 25.- Concluded.

62
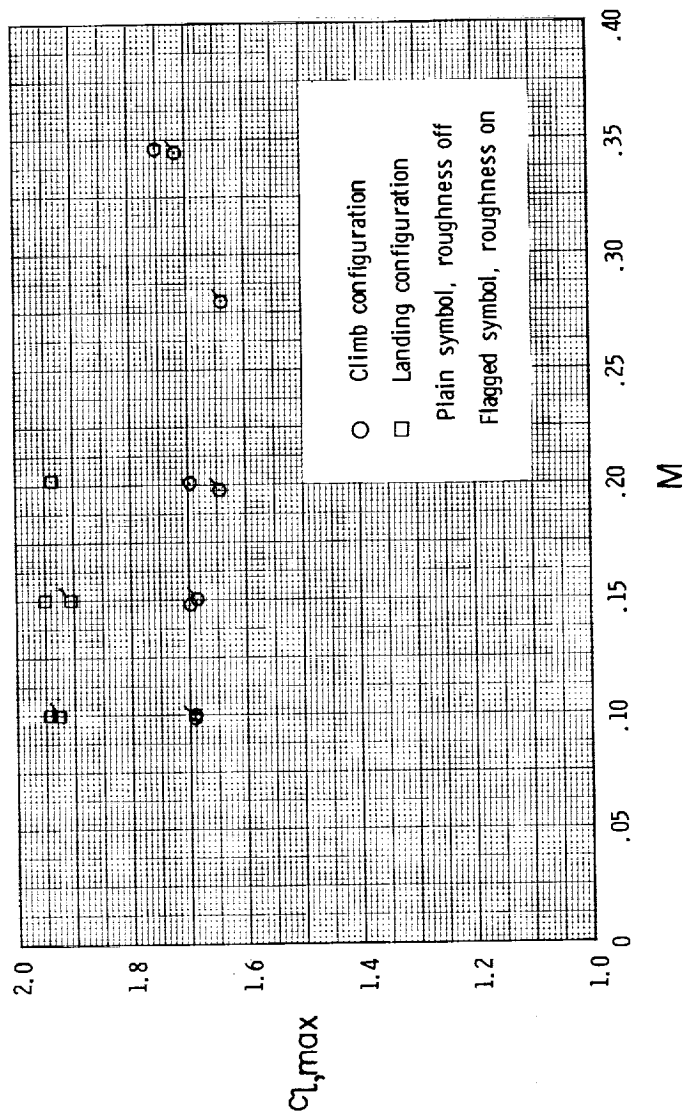
(a) Climb and landing configurations. $R \approx 4.0 \times 10^6$.

Figure 26.- Variation of maximum section lift coefficient with Mach number for NASA GA(PC)-1 airfoil.
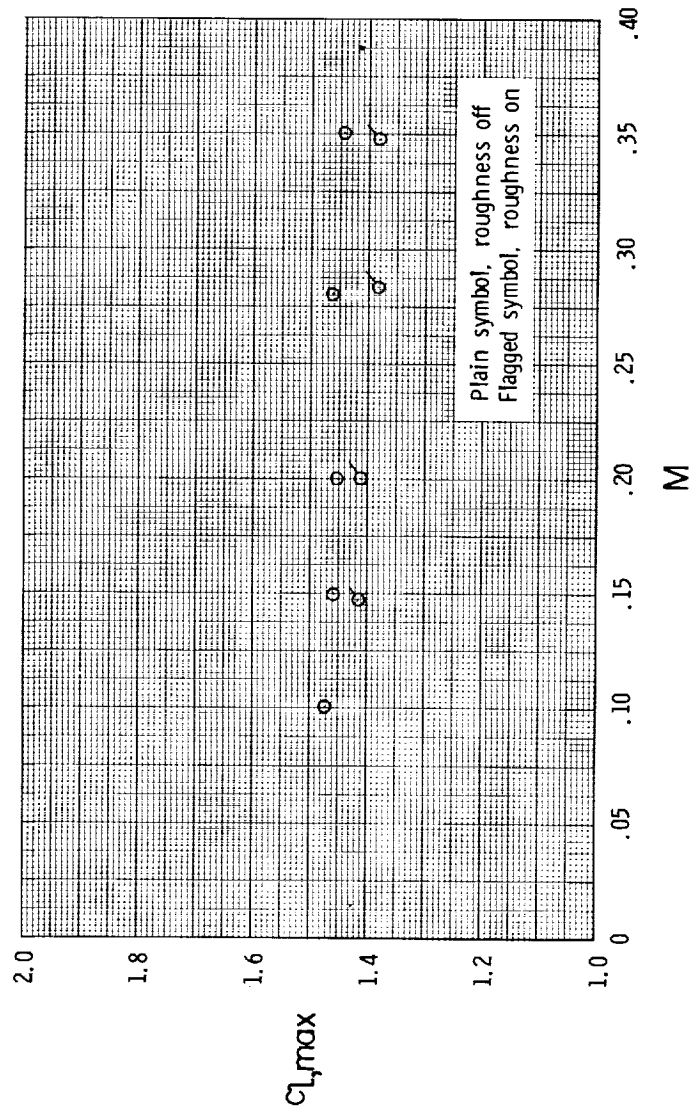
(b) Cruise configuration. $R \approx 6.0 \times 10^6$.

Figure 26.- Concluded.
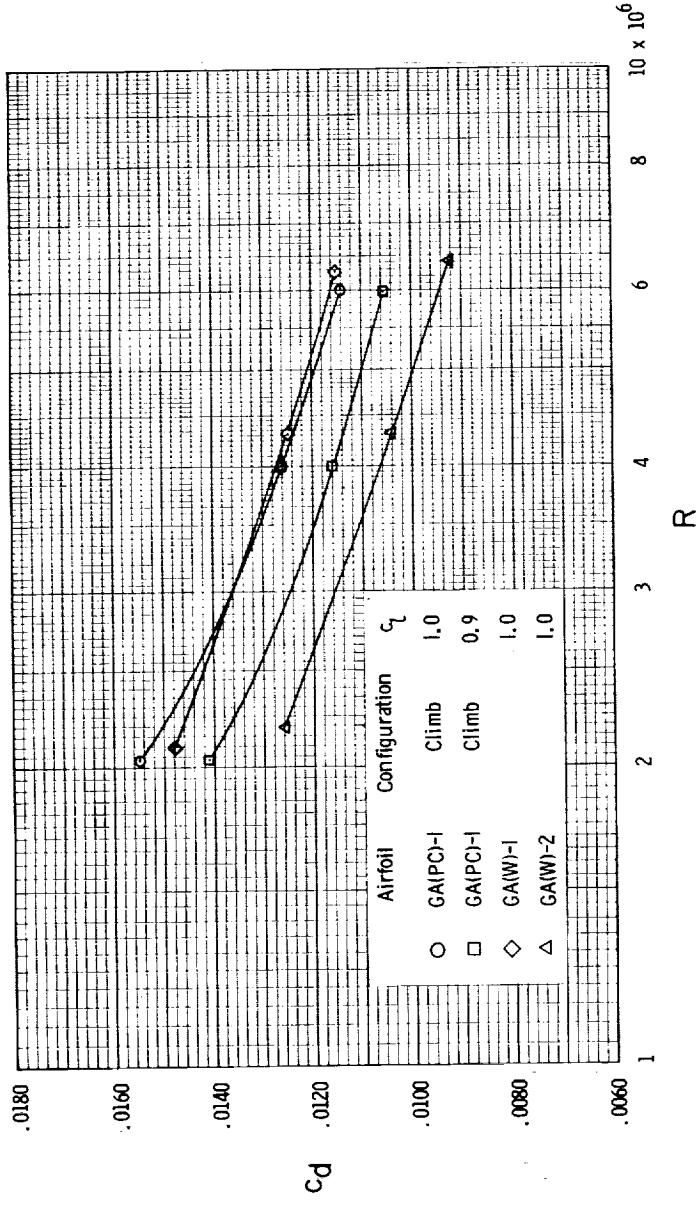
(a) Climb condition.

Figure 27.- Variation of section drag coefficient with Reynolds number for NASA GA(PC)-1, NASA GA(W)-1, and NASA GA(W)-2 airfoils. M = 0.15; transition fixed.
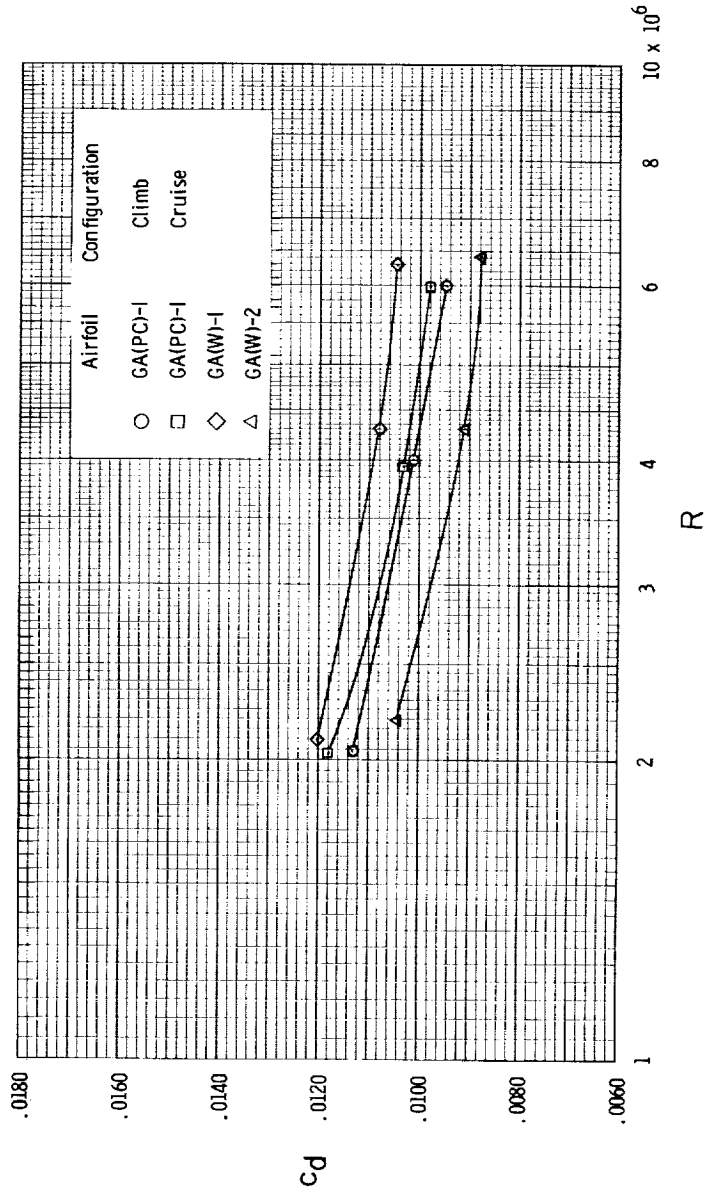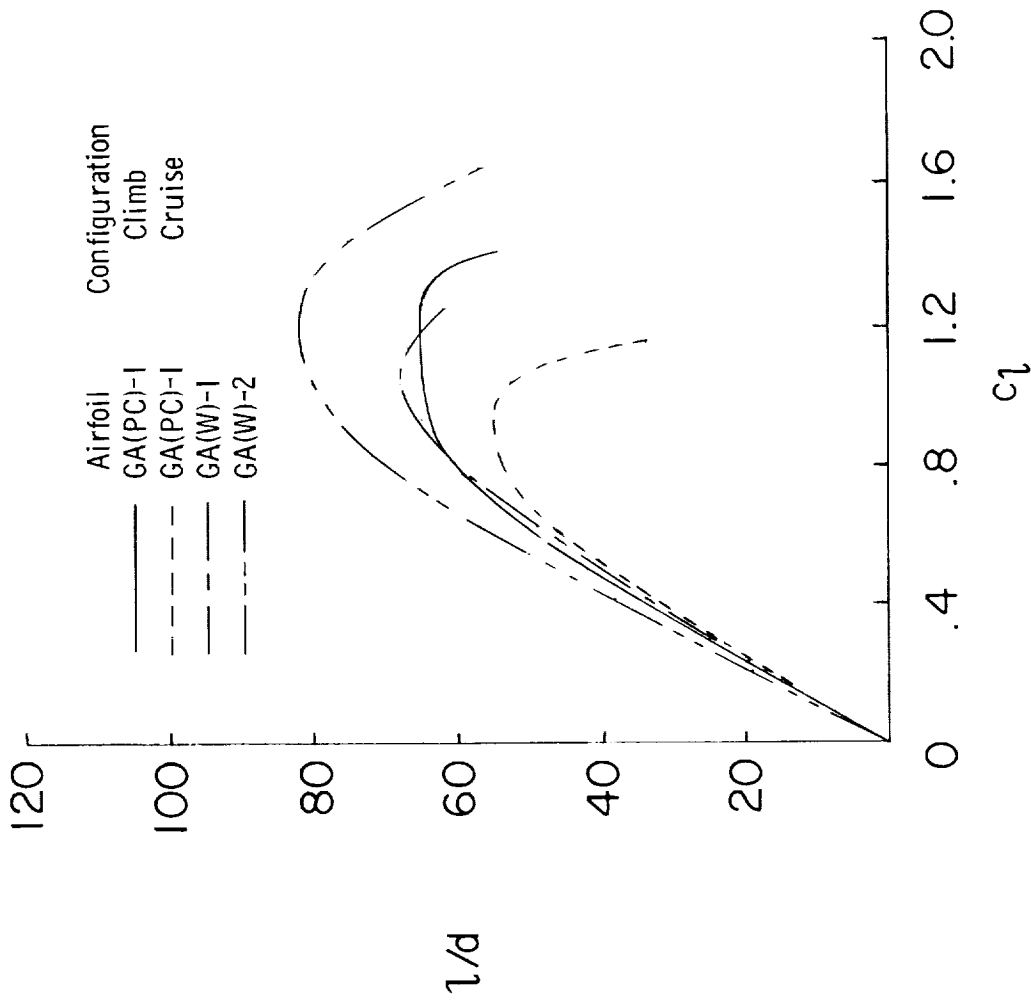
(b) Cruise condition. $c_l = 0.4$.

Figure 27.- Concluded.

(a) Climb condition.

Figure 28.— Variation of section lift-drag ratio with Reynolds number for NASA GA(PC)-1, NASA GA(W)-1, and NASA GA(W)-2 airfoils. M = 0.15; transition fixed.
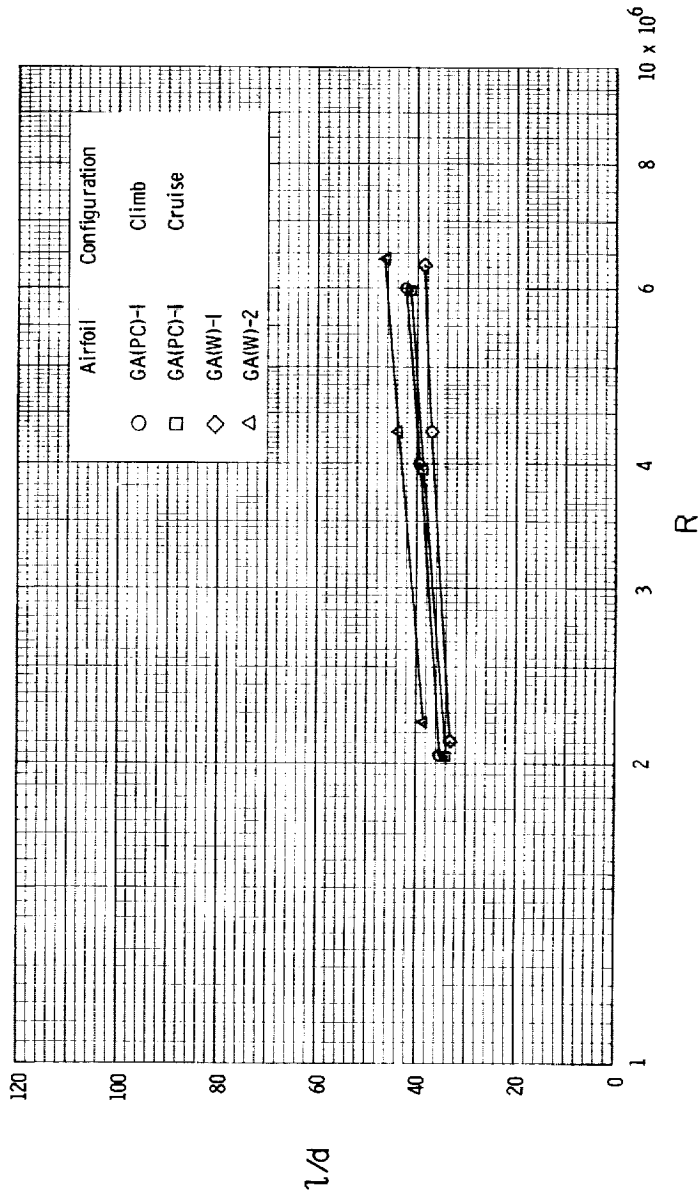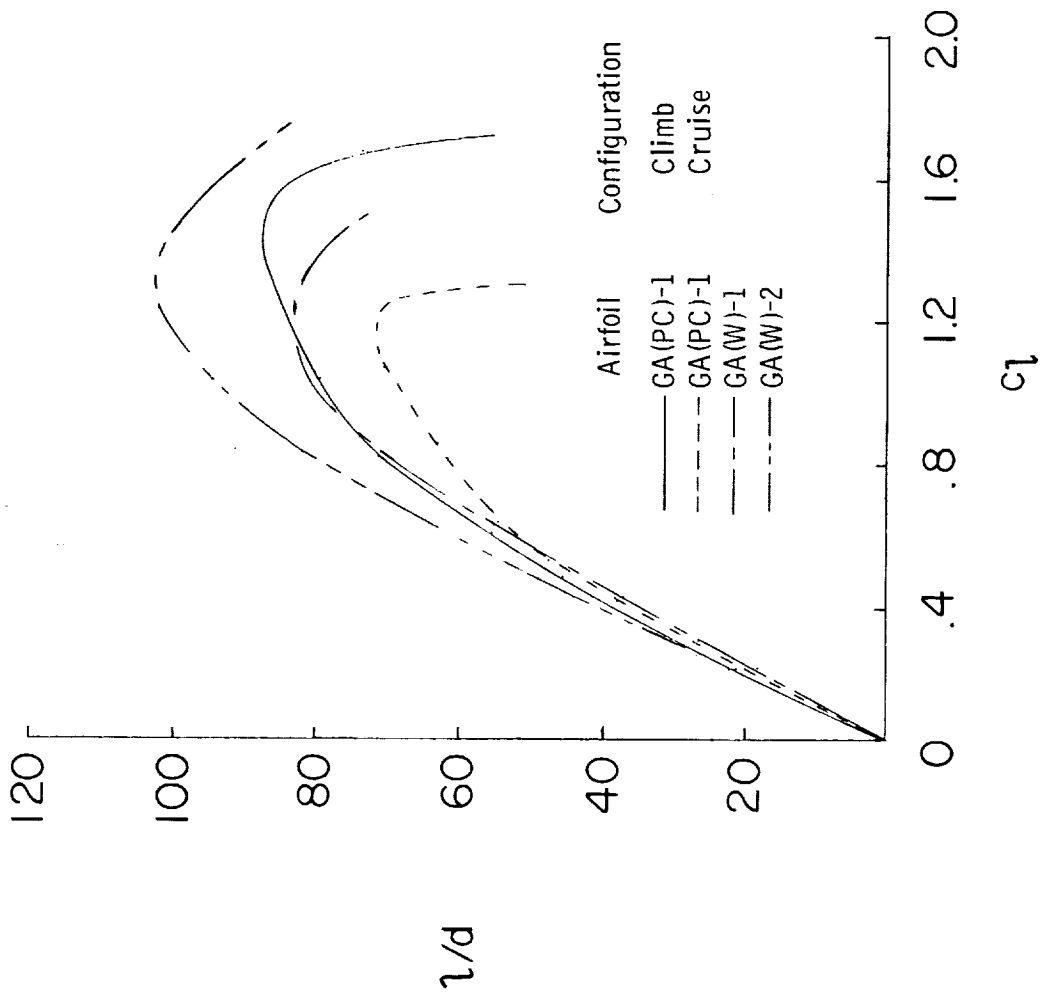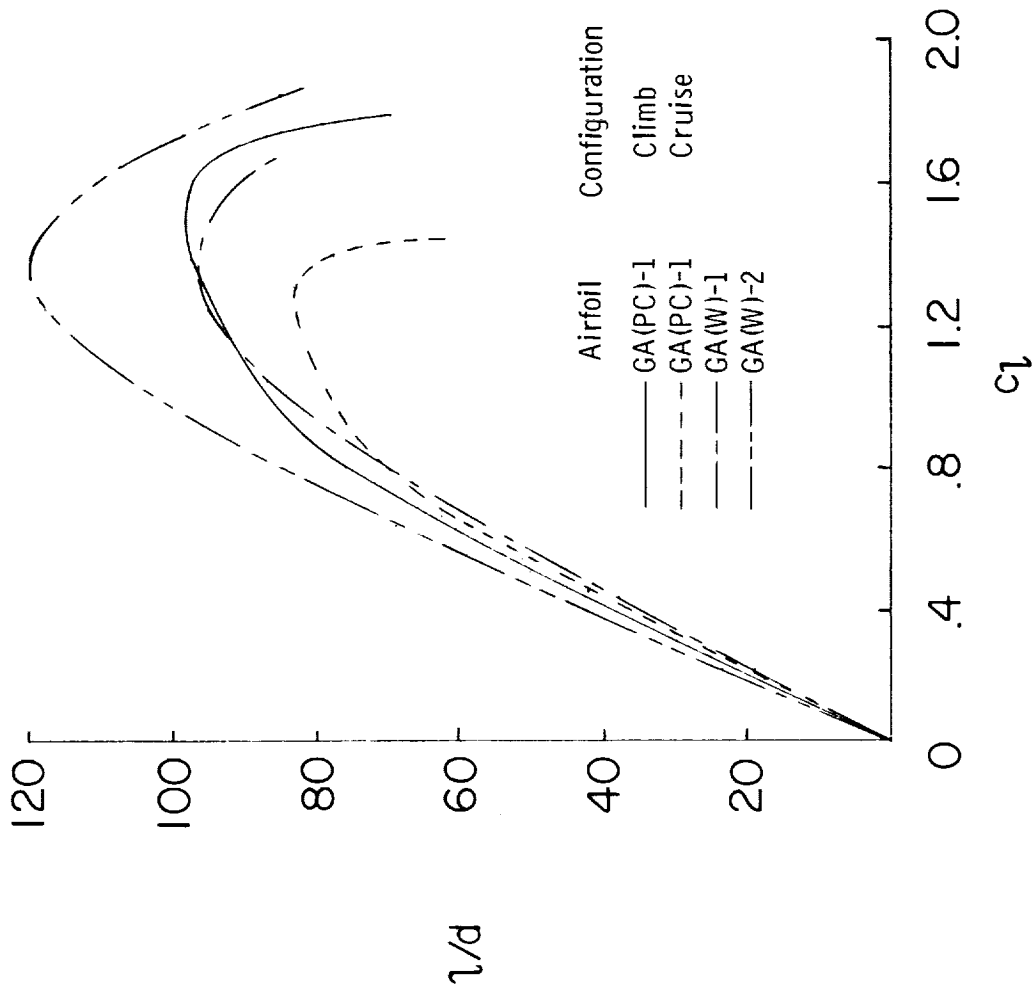
(b) Cruise condition. $c_l = 0.4$.

Figure 28.- Concluded.

Figure 29.- Variation of section lift-drag ratio with section lift coefficient for NASA GA(PC)-1, NASA GA(W)-1, and NASA GA(W)-2 airfoils. M = 0.15; transition fixed.
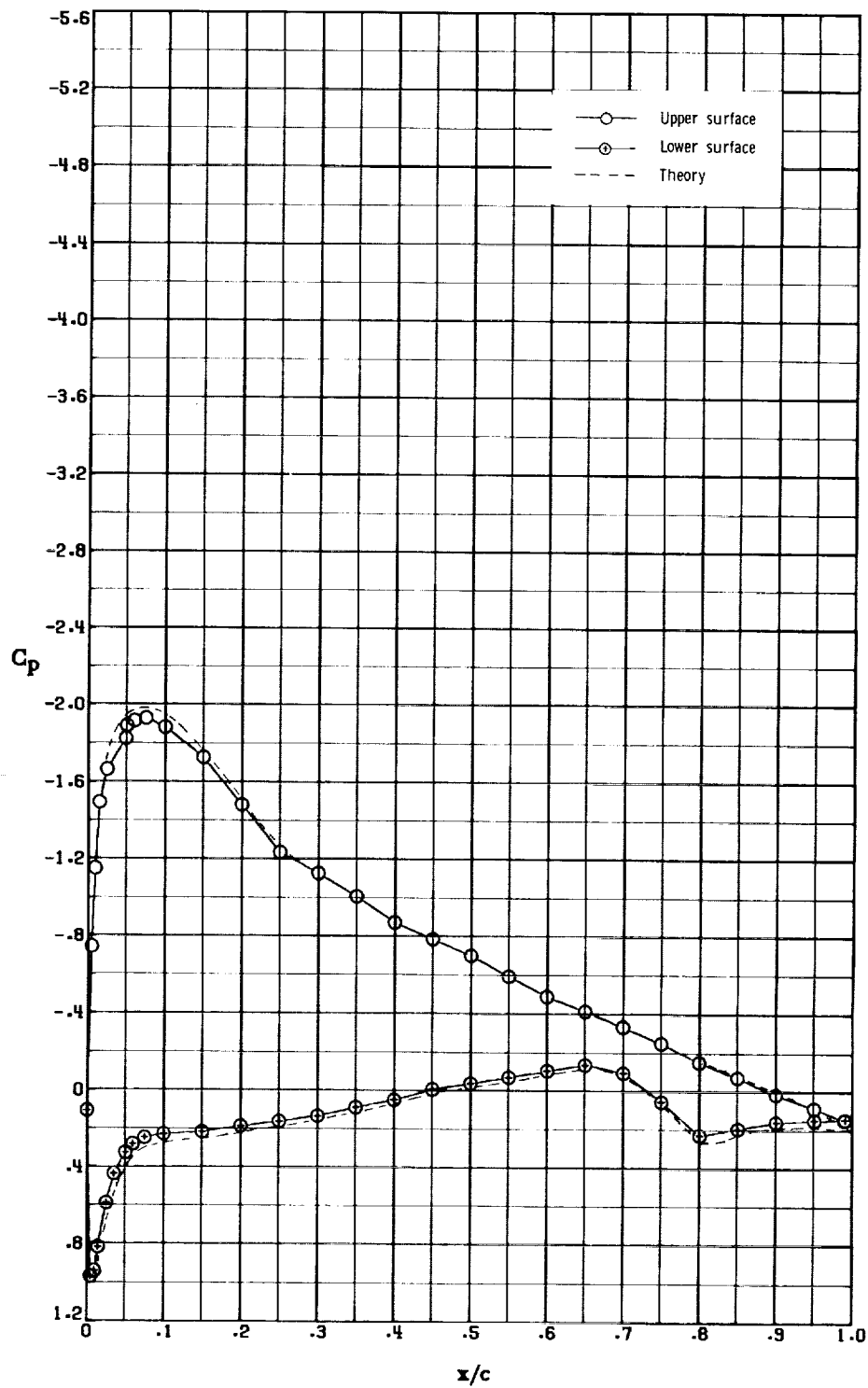
(a) $R \approx 2.0 \times 10^{6}$.

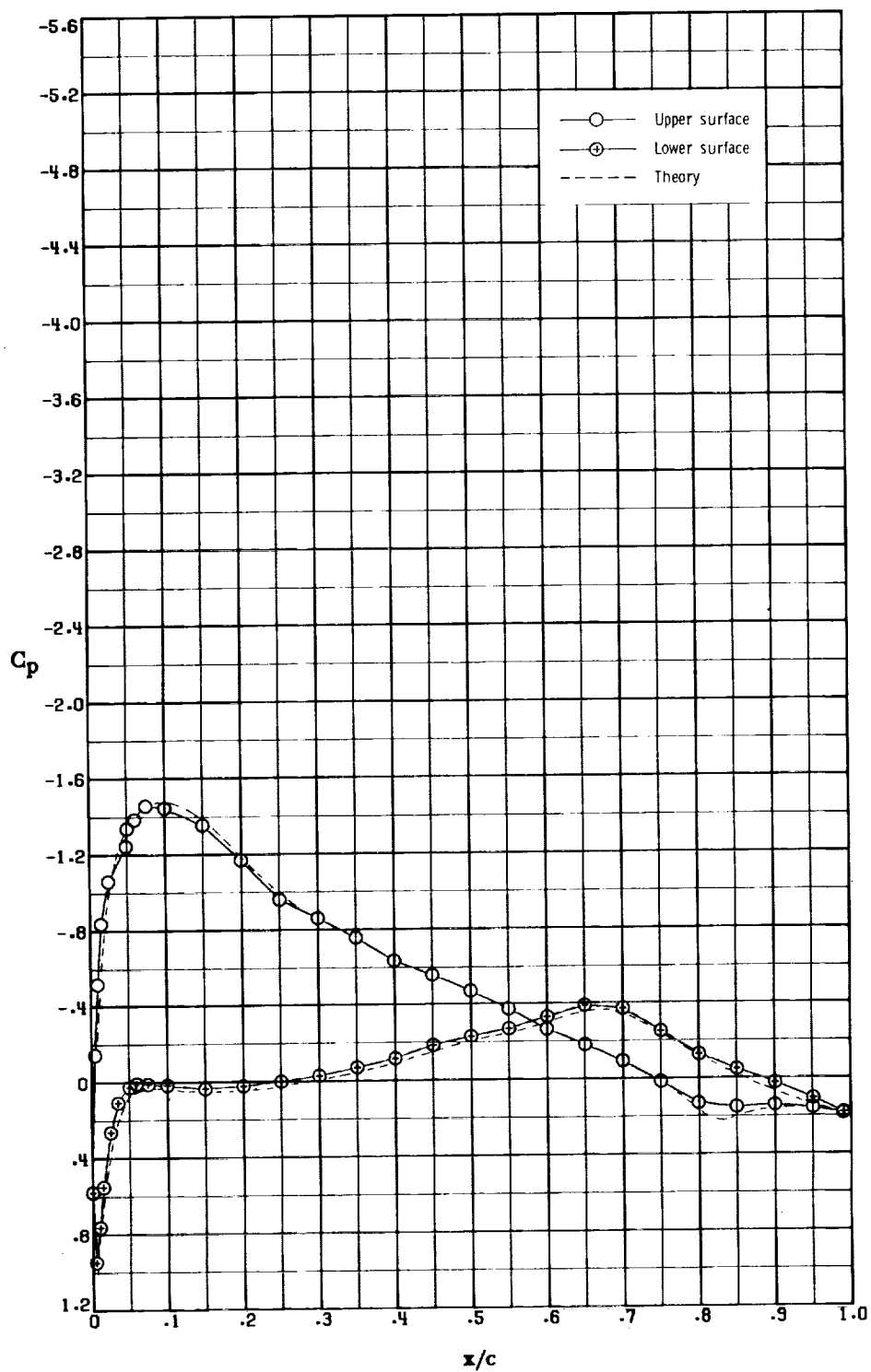(b) $R \approx 4.0 \times 10^6$.

Figure 29.- Continued.

70

(c) $R \approx 6.0 \times 10^6$.

Figure 29.- Concluded.

(a) Climb configuration. $\alpha = 5.9°$; $R \approx 4.0 \times 10^6$.

Figure 30.- Comparison of experimental and theoretical pressure distributions. Transition fixed at x/c = 0.05; M = 0.15.

(b) Cruise configuration. $\alpha = 6.2^{\circ}$; $R \approx 6.0 \times 10^6$.
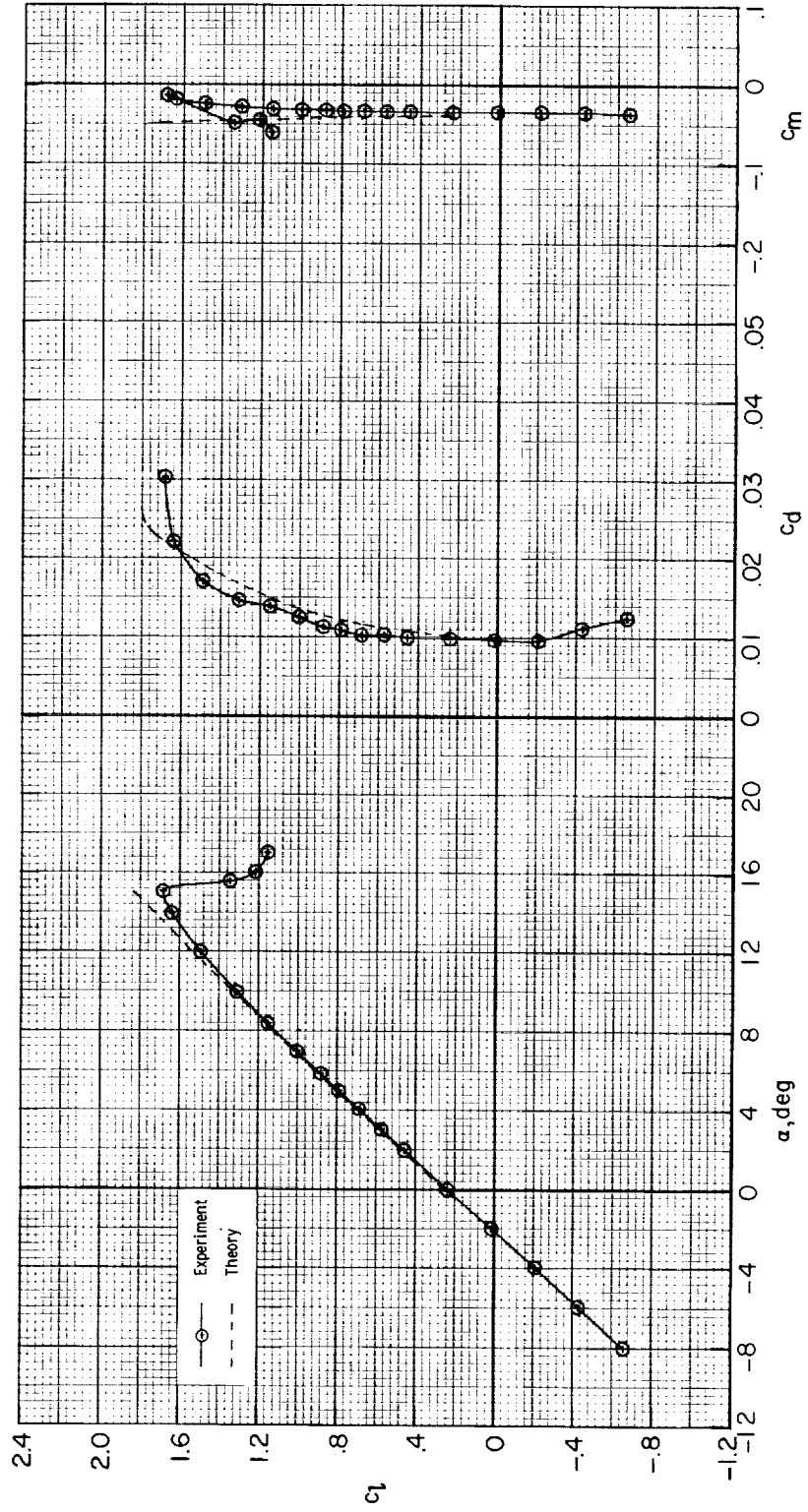
Figure 30.- Concluded.

Figure 31.- Comparison of experimental and theoretical section characteristics of climb configuration. Transition fixed at x/c = 0.05; M = 0.15; R ≈ 4.0 × 10⁶.

74

1. Report No. NASA TP-1324 AVRADCOM TR 78-45	2. Government Accession No.	3. Recipient's Catalog No.
4. Title and Subtitle LOW-SPEED AERODYNAMIC CHARACTERISTICS OF A 16-PERCENT-THICK VARIABLE-GEOMETRY AIRFOIL DESIGNED FOR GENERAL AVIATION APPLICATIONS		5. Report Date December 1978
		6. Performing Organization Code
7. Author(s) Richard W. Barnwell, Kevin W. Noonan, and Robert J. McGhee		8. Performing Organization Report No. L-12107
9. Performing Organization Name and Address NASA Langley Research Center and Structures Laboratory AVRADCOM Research and Technology Laboratories Hampton, VA 23665		10. Work Unit No. 505-06-33-10
		11. Contract or Grant No.
		13. Type of Report and Period Covered Technical Paper
12. Sponsoring Agency Name and Address National Aeronautics and Space Administration Washington, DC 20546 and U.S. Army Aviation Research and Development Command St. Louis, MO 63166		
		14. Army Project No. 1L161102AH45

15. Supplementary Notes

Richard W. Barnwell and Robert J. McGhee: Langley Research Center
Kevin W. Noonan: Structures Laboratory, AVRADCOM Research and
    Technology Laboratories

16. Abstract

Tests were conducted in the Langley low-turbulence pressure tunnel to determine the aerodynamic characteristics of climb, cruise, and landing configurations of a 16-percent-thick variable-geometry airfoil designed for general-aviation applications (NASA GA(PC)-1). These tests were conducted over a Mach number range from 0.10 to 0.35, a chord Reynolds number range from 2.0×10^6 to 20.0×10^6, and an angle-of-attack range from -8° to 20°. Test results show that the maximum section lift coefficients increased in the Reynolds number range from 2.0×10^6 to 9.0×10^6 and reached values of approximately 2.1, 1.8, and 1.5 for the landing, climb, and cruise configurations, respectively. Stall characteristics, although of the trailing-edge type, were abrupt. The section lift-drag ratio of the climb configuration with fixed transition near the leading edge was about 78 at a lift coefficient of 0.9, a Mach number of 0.15, and a Reynolds number of 4.0×10^6. Design lift coefficients of 0.9 and 0.4 for the climb and cruise configurations were obtained at the same angle of attack, about 6°, as intended. Generally, good agreement was obtained between experimental results and the predictions of a viscous, attached-flow theoretical method.

17. Key Words (Suggested by Author(s)) Low-speed airfoil section Reynolds number effects Experimental-theoretical comparison General aviation aircraft GA(PC)-1 airfoil	18. Distribution Statement Unclassified - Unlimited Subject Category 02

19. Security Classif. (of this report) Unclassified	20. Security Classif. (of this page) Unclassified	21. No. of Pages 74	22. Price* $5.25